


1992

# Characterization of self-assembled carboxylate monolayers and multilayers at copper and silver

Earl Laird Smith  
*Iowa State University*

Follow this and additional works at: <https://lib.dr.iastate.edu/rtd>

 Part of the [Analytical Chemistry Commons](#), [Condensed Matter Physics Commons](#), and the [Physical Chemistry Commons](#)

## Recommended Citation

Smith, Earl Laird, "Characterization of self-assembled carboxylate monolayers and multilayers at copper and silver " (1992). *Retrospective Theses and Dissertations*. 10389.  
<https://lib.dr.iastate.edu/rtd/10389>

This Dissertation is brought to you for free and open access by the Iowa State University Capstones, Theses and Dissertations at Iowa State University Digital Repository. It has been accepted for inclusion in Retrospective Theses and Dissertations by an authorized administrator of Iowa State University Digital Repository. For more information, please contact [digirep@iastate.edu](mailto:digirep@iastate.edu).

## INFORMATION TO USERS

This manuscript has been reproduced from the microfilm master. UMI films the text directly from the original or copy submitted. Thus, some thesis and dissertation copies are in typewriter face, while others may be from any type of computer printer.

**The quality of this reproduction is dependent upon the quality of the copy submitted.** Broken or indistinct print, colored or poor quality illustrations and photographs, print bleedthrough, substandard margins, and improper alignment can adversely affect reproduction.

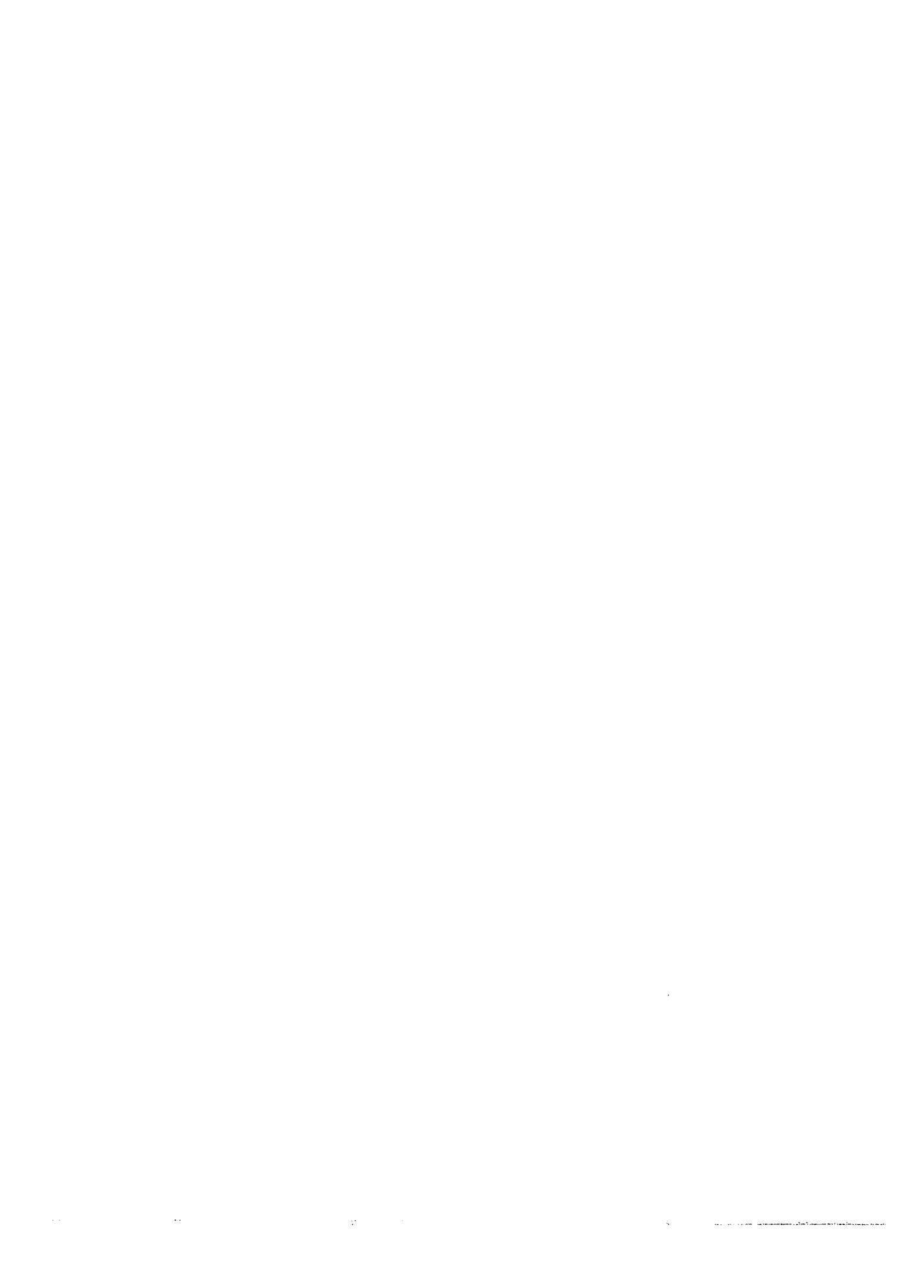
In the unlikely event that the author did not send UMI a complete manuscript and there are missing pages, these will be noted. Also, if unauthorized copyright material had to be removed, a note will indicate the deletion.

Oversize materials (e.g., maps, drawings, charts) are reproduced by sectioning the original, beginning at the upper left-hand corner and continuing from left to right in equal sections with small overlaps. Each original is also photographed in one exposure and is included in reduced form at the back of the book.

Photographs included in the original manuscript have been reproduced xerographically in this copy. Higher quality 6" x 9" black and white photographic prints are available for any photographs or illustrations appearing in this copy for an additional charge. Contact UMI directly to order.

# U·M·I

University Microfilms International  
A Bell & Howell Information Company  
300 North Zeeb Road, Ann Arbor, MI 48106-1346 USA  
313/761-4700 800/521-0600



**Order Number 9302017**

**Characterization of self-assembled carboxylate monolayers and  
multilayers at copper and silver**

Smith, Earl Laird, Ph.D.

Iowa State University, 1992

**U·M·I**

300 N. Zeeb Rd.  
Ann Arbor, MI 48106



**Characterization of self-assembled carboxylate monolayers and multilayers  
at copper and silver**

by

**Earl Laird Smith**

**A Dissertation Submitted to the  
Graduate Faculty in Partial Fulfillment of the  
Requirements for the Degree of  
DOCTOR OF PHILOSOPHY**

**Department: Chemistry  
Major: Analytical Chemistry**

**Approved:**

Signature was redacted for privacy.

**In Charge of Major Work**

Signature was redacted for privacy.

**For the Major Department**

Signature was redacted for privacy.

**For the Graduate College**

**Iowa State University  
Ames, Iowa**

**1992**

**DEDICATION**

**This thesis is dedicated to my wife and best friend, Dr. Susannah Scott.**

**TABLE OF CONTENTS**

LIST OF FIGURES .....	viii
LIST OF TABLES .....	xiii
LIST OF SCHEMES .....	xv
GENERAL INTRODUCTION .....	1
Explanation of dissertation format .....	2
PAPER I. SCANNING TUNNELING MICROSCOPY OF EVAPORATED COPPER FILMS AND COMPOSITION AND STRUCTURE OF SPONTANEOUSLY ADSORBED MONOLAYERS OF n- ALKANOIC ACIDS .....	3
INTRODUCTION .....	4
EXPERIMENTAL SECTION .....	6
Sample preparation .....	6
Copper film preparation .....	6
Monolayer preparation .....	6
Instrumentation .....	7
Contact angle measurements .....	7
Ellipsometric measurements of film thickness .....	7
Infrared spectroscopy .....	7
Scanning tunneling microscopy .....	8
RESULTS AND DISCUSSION .....	9
General observations .....	9
Characterization with optical ellipsometry .....	10
Characterization with contact angle measurements .....	13



Characterization with infrared spectroscopy .....	16
Scanning tunneling microscopy (STM) of the native oxide of copper .....	23
Proposed adsorbate structure .....	29
CONCLUSIONS .....	33
REFERENCES .....	34
PAPER II. SERENDIPITOUS DISCOVERY OF MULTILAYER FILMS OF SHORT CHAIN <i>n</i> -ALKANOIC ACIDS ASSEMBLED FROM THE GAS PHASE AT COPPER .....	38
INTRODUCTION .....	39
EXPERIMENTAL SECTION .....	41
Sample preparation .....	41
Instrumentation .....	42
Contact angle measurements .....	42
Infrared spectroscopy .....	42
RESULTS AND DISCUSSION .....	43
Ellipsometry .....	43
Contact angle measurements for <i>n</i> -alkanoic acids/Cu .....	43
IR spectra of multilayers of <i>n</i> -alkanoic acids/Cu .....	45
General observations and mode assignments .....	45
Methyl modes .....	51
Ordering of the polymethylene chain .....	54
Vibrations of the polymethylene alkyl chain .....	54
Perfluoro and multicomponent multilayer films .....	57
CONCLUSIONS .....	60

REFERENCES.....	61
PAPER III. FORMATION, STRUCTURE AND WETTABILITY OF SHORT CHAIN <i>n</i> -ALKANOIC ACIDS ASSEMBLED FROM THE GAS PHASE AT SILVER .....	
INTRODUCTION .....	64
EXPERIMENTAL SECTION .....	67
Sample preparation .....	67
Instrumentation .....	68
Contact angle measurements.....	68
Infrared spectroscopy .....	68
RESULTS AND DISCUSSION .....	69
Contact angle measurements for <i>n</i> -alkanoic acids/Ag .....	69
IR spectra of <i>n</i> -alkanoic acids/Ag .....	71
General observations and mode assignments.....	71
Methyl modes.....	78
Orientation of the polymethylene chain.....	80
Vibrations of the polymethylene alkyl chain .....	80
Discussion of the general utility of the technique.....	86
<i>n</i> -Alkylthiols at Ag.....	86
<i>n</i> -Alkylthiols at Au.....	86
<i>n</i> -Alkanoic acids and <i>n</i> -alkylthiols at Cu .....	87
CONCLUSIONS.....	88
REFERENCES.....	91

PAPER IV. DEPOSITION OF METAL OVERLAYERS AT END-GROUP FUNCTIONALIZED THIOLATE MONOLAYERS ADSORBED AT AU. SURFACE AND INTERFACIAL CHEMICAL CHARACTERIZATION OF DEPOSITED COPPER OVERLAYERS AT CARBOXYLIC ACID- TERMINATED STRUCTURES .....	93
INTRODUCTION .....	94
EXPERIMENTAL SECTION .....	97
Sample preparation .....	97
Instrumentation .....	98
Contact angle measurements .....	98
Ellipsometric measurements of film thickness .....	98
Infrared spectroscopy .....	99
X-ray photoelectron spectroscopy .....	99
Atomic force microscopy .....	100
RESULTS AND DISCUSSION .....	101
General physical and structural characteristics of MHA/Au and MUA/Au .....	101
Wettability and ellipsometric thicknesses .....	101
Infrared spectroscopic characterization .....	102
Monolayers of MUA/Au and MHA/Au with Cu overlays .....	111
Infrared spectroscopic characterization .....	111
X-ray photoelectron spectroscopy results .....	114
AFM characterization .....	117
CONCLUSIONS .....	122
REFERENCES AND NOTES .....	124

GENERAL SUMMARY.....	129
ACKNOWLEDGEMENTS .....	131

## LIST OF FIGURES

## Paper I

- Figure 1. Ellipsometric film thicknesses for monolayers of *n*-alkanoic acids ( $\text{CH}_3(\text{CH}_2)_n\text{COOH}$ ) adsorbed at Cu. Uncertainties are standard deviations of measurements on 5-12 different samples. .... 11
- Figure 2. Advancing contact angles for monolayers of *n*-alkanoic acids ( $\text{CH}_3(\text{CH}_2)_n\text{COOH}$ ) adsorbed at Cu. ....14
- Figure 3. Infrared spectra (low energy region) for (a) stearic acid ( $n=16$ ) dispersed in KBr, (b) Cu(II) stearate, (c) a self-assembled monolayer of stearic acid adsorbed at Cu. The inset shows the progression of  $\text{CH}_2$  wags for stearic acid at Cu, magnified by four. .... 17
- Figure 4. Infrared spectra (high energy region) for (a) stearic acid ( $n=16$ ) dispersed in KBr, (b) Cu(II) stearate, (c) a self-assembled monolayer of stearic acid adsorbed at Cu. .... 21
- Figure 5a. STM image of the bare  $\text{Cu}_2\text{O}$  surface, as removed from the evaporator and imaged immediately. .... 24
- Figure 5b. STM image of the bare  $\text{Cu}_2\text{O}$  surface, stored and imaged under mineral oil. .... 25
- Figure 5c. STM image of the  $\text{Cu}_2\text{O}$  surface with an adsorbed stearate monolayer. 26
- Figure 6. Schematic of the  $\text{Cu}_2\text{O}(111)$  surface. Filled circles represent Cu atoms. .... 28

- Figure 7. Relationship between chain tilt angle and van der Waals chain thickness for *n*-alkanoic acids self-assembled at Cu..... 31
- Figure 8. Arrangement of alkyl chains tilted 15° on a Cu<sub>2</sub>O surface. The proposed unit cell is a (3/2 x 3/2)..... 32
- Paper II
- Figure 1. Infrared reflection spectra (high energy region) of (a) *n*-nonanoate multilayer, CH<sub>3</sub>(CH<sub>2</sub>)<sub>7</sub>COOH, self-assembled from the gas-phase at Cu, (b) Cu(II) nonanoate in KBr, and (c) liquid nonanoic acid. .... 46
- Figure 2. Infrared reflection spectra (high energy region) of multilayers of deuterium labeled alkanolic acids self assembled from the gas phase at Cu. (a) Nonanoic acid-d<sub>17</sub> (CD<sub>3</sub>(CD<sub>2</sub>)<sub>7</sub>COOH). No hydrocarbon contamination can be discerned. (b) Hexanoic acid-methyl-d<sub>3</sub> (CD<sub>3</sub>(CH<sub>2</sub>)<sub>4</sub>COOH). The major hydrocarbon modes are the methylene stretches. A trace of impurity can be seen in the methyl region of the d<sub>3</sub>-labeled hexanoate film..... 49
- Figure 3. Infrared reflection spectra (low energy region) of (a) *n*-nonanoate multilayer, CH<sub>3</sub>(CH<sub>2</sub>)<sub>7</sub>COOH, self-assembled from the gas-phase at Cu, (b) Cu(II) nonanoate in KBr, and (c) liquid nonanoic acid. .... 50
- Figure 4. Infrared reflection spectra (low energy region) of multilayers of deuterium labeled alkanolic acids self assembled from the gas phase at Cu. (a) Nonanoic acid-d<sub>17</sub> (CD<sub>3</sub>(CD<sub>2</sub>)<sub>7</sub>COOH). No peaks due to

hydrocarbon modes can be seen. (b) Hexanoic acid-methyl-d<sub>3</sub> ( $\text{CD}_3(\text{CH}_2)_4\text{COOH}$ ). No peaks attributable to methyl modes are seen. 52

- Figure 5. Peak positions for d(CH<sub>3</sub>) in multilayers of *n*-alkanoic acids,  $\text{CH}_3(\text{CH}_2)_n\text{COOH}$ , self-assembled from the gas-phase at Cu..... 53
- Figure 6. Array of methylene wagging modes and C-C stretching modes for *n*-alkanoic acid multilayers self-assembled from the gas phase at Cu. .... 56
- Figure 7. Infrared reflection spectra for (a) perfluorononanoate acid multilayer at Cu, (b) two component multilayer film of perfluorononanoate acid and *n*-nonanoate acid at Cu, formed by gas-phase self assembly of perfluorononanoic acid onto an *n*-nonanoate acid multilayer film at Cu. .... 59

### Paper III

- Figure 1. Advancing contact angles for *n*-alkanoic acids self-assembled from the gas-phase at Ag, with the probe liquids hexadecane, methylene iodide, glycerol, and water. .... 70
- Figure 2. Infrared reflection spectra (high energy region) of *n*-alkanoic acids,  $\text{CH}_3(\text{CH}_2)_n\text{COOH}$ , self-assembled from the gas-phase at Ag. ....72
- Figure 3. Infrared reflection spectra (high energy region) of deuterium labeled alkanolic acids self-assembled from the gas phase at Ag. (a) Nonanoic acid-d<sub>17</sub> ( $\text{CD}_3(\text{CD}_2)_7\text{COOH}$ ). No hydrocarbon contamination can be discerned. (b) 6,6,6-trideuterohexanoic acid ( $\text{CD}_3(\text{CH}_2)_4\text{COOH}$ ).

The major hydrocarbon modes are the methylene stretches. A trace impurity can be seen in the methyl region. .... 75

- Figure 4. Infrared reflection spectra (low energy region) of (a) nonanoic acid self-assembled from the gas-phase at Ag, (b) nonanoic acid self-assembled from hexadecane solution at Ag, (c) perdeuteranonanoic acid,  $\text{CD}_3(\text{CD}_2)_7\text{COOH}$ , self-assembled from the gas-phase at Ag, (d) bulk liquid nonanoic acid. The bulk liquid shows localized vibrations associated with short sequences of bonds having a specific conformation ..... 76
- Figure 5. Model of carboxylate monolayers on Ag for chains with an even (right) or odd (left) number of methylene groups, accounting for the odd-even effect in  $n(\text{CH}_3)$  intensities. .... 77
- Figure 6. IR peak intensities for monolayers of *n*-alkanoic acids ( $\text{CH}_3(\text{CH}_2)_n\text{COOH}$ ) self-assembled from the gas phase at Ag .....79
- Figure 7. Infrared reflection spectra (low energy region) of *n*-alkanoic acids,  $\text{CH}_3(\text{CH}_2)_n\text{COOH}$ , self-assembled from the gas-phase at Ag. For clarity, the spectrum for  $n=0$  is plotted at 2/3 intensity. .... 82
- Figure 8. Array of methylene wagging modes and C-C stretching modes for *n*-alkanoic acids self-assembled from the gas phase at Ag..... 85



## Paper IV

- Figure 1. Infrared spectra in the low frequency region for (a) MHA in KBr, (b) MHA/Au/Si, and (c) MUA/Au/Si ..... 103
- Figure 2. Infrared spectrum in the high frequency region for (a) MHA in KBr , (b) MHA/Au/Si , and (c) MUA/Au/Si . ..... 104
- Figure 3. Infrared spectra in the low frequency region after deposition of a 5 nm Cu overlayer. (a) Cu/MHA/Au/Si (b) Cu/MUA/Au/Si ..... 109
- Figure 4. Infrared spectra in the high frequency region after deposition of a 5 nm Cu overlayer. (a) Cu/MHA/Au/Si (b) Cu/MUA/Au/Si..... 112
- Figure 5. Infrared reflection spectrum of 0.2 nm Cu overlayer at MHA/Au/Si ..... 115
- Figure 6. Cu ( $2p_{3/2}$ ,  $2p_{1/2}$ ) photoemission spectra for a 0.2 nm Cu overlayer. (a) Cu/HDT/Au/Si (b) Cu/Au (c) Cu/MHA/Au/Si. The data were not smoothed during or after acquisition ..... 118
- Figure 7. (a) A 0.5 mm x 0.5 mm lowpass filtered AFM image of uncoated Au/mica. The z-range is 5 nm. The arrow points to a grain boundary. (b) A cross-section of the image taken along the black line drawn in (a). ..... 119
- Figure 8. (a) A 0.5 mm x 0.5 mm lowpass filtered AFM image of Cu/MHA/Au/mica. The z-range is 5 nm. (b) A cross-section of the image taken along the black line drawn in (a). ..... 120

**LIST OF TABLES****Paper I**

Table 1.	Mode assignments and peak positions for stearic acid and Cu(II) stearate in KBr .....	18
----------	---	----

**Paper II**

Table 1.	Advancing contact angles for multilayer systems.....	44
Table 2.	Assignments of peak positions for spontaneously adsorbed multilayers of n-alkanoic acids from the gas phase at Cu.....	47

**Paper III**

Table 1.	Assignments of peak positions for spontaneously adsorbed monolayers of acids from the gas phase .....	73
----------	---	----

**Paper IV**

Table 1.	Mode assignments and peak positions (cm <sup>-1</sup> ) for 16-mercaptohexadecanoic acid (MHA) and 11-mercaptoundecanoic acid (MUA) dispersed in KBr, as monolayers at Au, and as monolayers at Au after deposition of ~ 5 nm overlayer of Cu.....	105
----------	--	-----

Table 2.	Binding energies (eV) and compositional assignments for XPS spectra of ~0.2 nm Cu overlayers deposited at uncoated Au (Cu/Au), a hexadecanethiolate monolayer at Au (Cu/HDT/Au), and a monolayer of 16-mercaptohexadecanoic acid at Au (Cu/MHA/Au) .....	116
----------	--	-----

**LIST OF SCHEMES**

## Paper IV

Scheme 1. Schematic representation of self-assembled thiolate at Au .....	95
Scheme 2. Derivatized polymer surface .....	95
Scheme 3. Dimeric form of hydrogen-bonded carboxylic acids .....	107
Scheme 4. Polymeric form of hydrogen-bonded carboxylic acids .....	107
Scheme 5. Proposed structure of hydrogen-bonding in carboxylic-acid terminated monolayers .....	110

## GENERAL INTRODUCTION

The first documented study of monomolecular thin films, or monolayers, was made over 200 years ago by Benjamin Franklin, who observed that a droplet of oil applied to the surface of a pond altered the surface characteristics of the water. Since then, the field has been defined by the pioneering work of Langmuir and Blodgett, who studied monolayer films on water and their transfer to solid substrates. The discovery of the phenomenon of monolayer self-assembly by Zisman was a singularly important advance in thin film construction. Recently, there has been much interest in studies of molecules consisting of a polar head group such as an amine, alcohol, carboxylic acid or thiol, and a long polymethylene alkyl chain.

Classical techniques, such as wettability (pioneered by Zisman and co-workers), were historically used to characterize monomolecular films. However, it was not until the advent of modern vibrational spectroscopies, such as Fourier transform Infrared and Raman, that detailed information about interfacial phenomena became accessible. For example, the frequencies and relative intensities of vibrational modes of surface-bound molecules indicate mode of binding to the surface, orientation and degree of crystallinity. The oxidation state of surface species can be obtained from X-ray photoelectron spectroscopy (XPS). Recently, the development of the scanning tunnelling microscope (STM) and atomic force microscope (AFM) has permitted direct observation of atoms and molecules arranged on surfaces.

A classic monolayer system is formed by the self-assembly of *n*-alkanoic acids at a variety of metal surfaces. Many early studies were published on this system; however, the conclusions were extremely varied and sometimes even contradictory. A detailed, self-consistent reexamination by ellipsometry, contact angle and infrared spectroscopy of the self-assembly of  $\text{CH}_3(\text{CH}_2)_n\text{COOH}$  ( $n = 0 - 20$ ) at Cu is presented in Section I. A detailed examination of the native oxide of Cu, including STM images, is also included. As an

offshoot of this work, arising from the desire to optimize solvent-interface interactions during self-assembly, the serendipitous discovery of gas-phase self-assembled multilayer films of *n*-alkanoic acids and perfluoroalkanoic acids is described in Section II. In Section III, the gas phase is shown to be an ideal medium for self-assembly of *n*-alkanoic acids at Ag, resulting in monomolecular films of unusual crystallinity. It had been previously thought that a long alkyl chain of 10-12 CH<sub>2</sub> units was required for crystalline monolayer formation, but these two works demonstrated crystalline film formation down to 5 CH<sub>2</sub> units. Isotopic substitution experiments enabled the full assignment for the first time of the methylene wagging modes of monolayer films in the IR. A fuller understanding of a variety of monolayer assemblies such as the *n*-alkanethiolates at Au, as well as the monolayer chemisorption of *n*-alkanoic acids at Cu, enabled the design of a metal overlayer structure. The results, presented in Section IV, describe the properties of a thin Cu film vapor-deposited onto a monolayer of acid-terminated thiolate at Au. The reactive chemistry was found to be the same as that found during alkanoate monolayer formation at Cu.

Explanation of dissertation format. This dissertation contains four papers, with Papers I, II and IV written for publication in *Langmuir* and Paper III for publication in *The Journal of Chemical Physics*. All experimental work presented in this dissertation was performed by Earl L. Smith, with the following exceptions: the STM experiments were done by Joseph Franek, the XPS measurements were performed by James Anderegg, and the AFM images were obtained by Carla Alves.

**PAPER I**

**SCANNING TUNNELING MICROSCOPY OF EVAPORATED COPPER  
FILMS AND COMPOSITION AND STRUCTURE OF SPONTANEOUSLY  
ADSORBED MONOLAYERS OF *n*-ALKANOIC ACIDS**

## INTRODUCTION

Self-assembly of organic monolayer films on metal surfaces is well-known and has been studied for many years<sup>1</sup>. Interest in organic monolayer films arises from their use as probes for adhesion studies at interfaces, as models for biological membranes, and their possible adaptation as chemical sensors. These monolayers may also potentially be used to construct interfaces with unusual properties, e.g. non-linear optical devices, better solar cells, or modified electrodes. Planned structures exhibiting order may be assembled by successive deposition of compressed monolayers formed at the water-air interface by Langmuir-Blodgett techniques. In this work, our interest in monolayers stems from their applicability as models for adhesion at the polymer-metal interface. By systematically examining the conditions that control the formation and structure of these monomolecular films, the interactions critical to the chemistry of adhesion can be delineated.

Adsorption of acids, thiols and their derivatives on metal surfaces yields closely packed monomolecular films which are not wetted by a variety of probe liquids and give relatively low-free energy surfaces. Advantages of these simple monolayer systems are that the adsorbate precursors are easy to purify, adsorbate precursor concentration is readily varied, the functional group which interacts with the surface is easy to vary, and the length of the alkyl chain can be changed.

Many workers have studied adsorption of fatty acids on Cu; various studies of specific longer chain acids ( $n \geq 14$ ) give conflicting results on whether submono-, mono-, and/or multilayer coverages are obtained for ambient metal surfaces such as copper<sup>2-4</sup> and aluminum. For example, multilayer coverages<sup>3</sup>, bilayer coverages<sup>2</sup>, and submonolayer coverages<sup>4</sup> have been reported for stearic acid ( $n=16$ ). Further contrasts are noted between work which gives films which do not reject solvent<sup>3</sup> and those which do<sup>5</sup>. The literature is replete with such discrepancies despite an impressive array of experimental techniques which have been brought



to bear upon this problem. Thus, while many comparisons can be made, no general conclusions can be drawn. The present state of affairs reflects the need for a detailed self-consistent study of this chemisorption system. Techniques applied to this system include electron diffraction<sup>6</sup> and radiochemistry using both radioactive Cu<sup>7</sup> to investigate the interfacial chemistry and radiolabeled acids<sup>2,4,8</sup> to estimate coverage. Ellipsometry has also been used to estimate coverage<sup>2</sup>. Contact angles and contact potential were used in some very limited studies<sup>5</sup>. The role of pH and the length of the alkyl chain in aqueous solution on the surface of copper carbonates has also been examined by IR<sup>9</sup> and by electrochemistry<sup>10</sup>. Amino acid adsorption onto Cu from aqueous solution has been studied by infrared reflectance spectroscopy<sup>11</sup>. The first infrared reflection spectroscopy studies of carboxylate monolayers at Cu were of lauric acid (n=10) using multiple reflectance<sup>12,13</sup>. An experimental source of variability is that all of this work was conducted on mechanically polished Cu.

This work describes the first systematic self-consistent study of the *n*-alkanoic acids (CH<sub>3</sub>(CH<sub>2</sub>)<sub>n</sub>COOH, where n=0-19) monolayers self-assembled at evaporated copper films to yield closely packed monolayer structures. Several issues are addressed: whether or not the acids form ordered closest-packed structures, the wettability of the monolayers formed and the important experimental conditions which can be controlled to yield consistent monolayer films. Infrared spectroscopic, ellipsometric and contact angle data are presented to show that the monolayers form by reactive chemisorption to yield the Cu(II) carboxylate salt with a fully extended hydrocarbon chain giving a low-energy surface. The similarities and differences between other monolayer systems self-assembled from solution are briefly presented. Comparisons are made to interaction of short-chain *n*-alkanoic acids with copper single crystal surfaces studied under ultra high vacuum (UHV)<sup>14</sup>. Since the importance of experimental variables on formation of the equilibrium monolayer structure cannot be overemphasized, the necessity for tightly controlling experimental conditions is also discussed.

## EXPERIMENTAL SECTION

### Sample preparation

#### Copper film preparation

The substrates were prepared by the resistive evaporation of 300 nm of Cu onto either silicon (Montco Silicon Inc. Royersford, PA) or mica (Asheville-Schoonmaker, Newport News, VA) using an Edwards 306A cryopumped evaporator. The Cu-coated silicon substrates were prepared by cutting 4 inch Si(100) wafers into 1 x 3 inch<sup>2</sup> plates and rinsing thoroughly with absolute ethanol before placing into the evaporator. The silicon was primed with a ~10 nm adhesive layer of Cr prior to Cu deposition. The mica substrates were prepared from freshly cleaved pieces of green mica. During deposition, the temperature of the samples increased to ~50°C because of radiative heating by the evaporation source. The pressure during all depositions was less than  $1 \times 10^{-6}$  torr. The Cu and Cr deposition rates were 0.3 and 0.2 nm/s, respectively.

#### Monolayer preparation

The monolayers were formed by immersing freshly evaporated copper films into a 1.0 mM solution of the *n*-alkanoic acids (Aldrich) in anhydrous hexadecane (Aldrich 99+%). The hexadecane was stored and handled under nitrogen. Hexadecane handled in this manner always passed the Zisman test, i.e. did not spread on pH 10.5 water<sup>15</sup>. Gentle warming was usually required to dissolve the long-chain acids in the hexadecane as had been noted in an earlier study<sup>16,17</sup>. Immersion times varied from a few minutes for the highly reactive short chain acids to a few hours for the more slowly reacting long chain acids, as discussed below.

For purposes of clarity, we indicate the composition of these multicomponent structures by writing their abbreviations with the topmost layer on the left; *e.g.* a monolayer film of stearic acid ( $n=16$ ) at Cu is written as stearate/Cu.

## **Instrumentation**

### **Contact angle measurements**

Advancing and receding contact angles ( $\theta_a$  and  $\theta_r$ , respectively) were measured in air using a Ramé-Hart Model 100-00 115 goniometer<sup>18</sup>. Hexadecane, methylene iodide, glycerol and deionized water were used as probe liquids. For these measurements, a 2  $\mu\text{L}$  droplet was formed on the substrate with the needle of the syringe in the droplet. The value of  $\theta_a$  was determined as the volume of the droplet was slowly increased and  $\theta_r$  as the volume of the droplet was slowly decreased.

### **Ellipsometric measurements of film thickness**

The thicknesses of the monolayers were determined by optical ellipsometry at 632.8 nm in two steps with a computer-interfaced Gaertner Model L-116B ellipsometer as described previously<sup>18</sup>. After monolayer formation, each sample was again analyzed and the film thickness calculated from a three-phase parallel layer model, using the average complex refractive index of the individual sample and a real refractive index of 1.45 for the film. A value of 1.45, which is representative of the adsorbate precursors<sup>19</sup>, facilitates comparison with thickness data that have been reported for a variety of monolayers<sup>20-25</sup>.

### **Infrared spectroscopy**

Infrared spectra were acquired with a Nicolet 740 FT-IR interferometer. Monolayer spectra were obtained using p-polarized light incident at 80° with respect to the surface normal.

These spectra are reported as  $-\log(R/R_0)$ , where  $R$  is the reflectance of the sample and  $R_0$  is the reflectance of a reference octadecanethiolate-d<sub>37</sub> monolayer at Au. A home-built sample holder was used to position the substrates in the spectrometer<sup>26</sup>. Both sample and reference reflectances are the average of 1024 scans. Spectra of the bulk Cu(II) stearate (K&K Laboratories, Cleveland, Ohio), Cu(II) nonanoate<sup>27</sup>, Cu(II) butyrate (Strem Chemicals, Newburyport, MA), Cu(II) acetate (Fisher), and stearic acid (Aldrich) were obtained by their dispersion in KBr. All spectra were collected at 2 cm<sup>-1</sup> resolution (zero filled) with Happ-Genzel apodization. Liquid N<sub>2</sub> cooled HgCdTe and InSb detectors were used. The spectrometer and sample chamber were purged with boil-off from liquid N<sub>2</sub>. Further details of these methods as well as the preparation of the reference substrates are given elsewhere<sup>18,28</sup>.

#### Scanning tunneling microscopy

All images were acquired with a Digital Instruments Nanoscope II STM (Santa Barbara, CA). The instrument was equipped with a 450 nm x 450 nm scanning head and was operated in the laboratory ambient. With this instrument, the images are displayed as though the tip moves from right to left across the computer monitor; the figures in this paper maintain this presentation.

For atomically resolved images, conditions for constant height imaging were found more useful (the "current" mode of the Nanoscope II). In this mode, the vertical position of the tip is held constant with variations in the tunneling current recorded as the tip moves across the sample surface. Images were obtained under a range of bias voltages (-200 to +200 mV) and tunneling currents (1-10 nA). Tips were fabricated by etching electrolytically a 0.010 in. diameter tungsten wire in a solution of 1 M KOH at 30 V A. C.

## RESULTS AND DISCUSSION

### General observations

In contact with air, freshly deposited copper films readily oxidize. The native cuprous oxide ( $\text{Cu}_2\text{O}$ ) surface is mainly composed of adsorbed oxygen and some carbon<sup>29,30</sup> with a high diffusivity of oxygen through the copper, leading to redistribution of oxygen throughout the Cu matrix<sup>29</sup>. Ellipsometric measurements required manipulation in air to obtain the substrate optical constants for subsequent film thickness measurements; we minimized this exposure by measuring the substrate optical properties as quickly as possible and by immersing the substrates immediately. The subsequently formed monolayers still showed small hystereses in contact angle (10-12° for the longer chain acids); the peak positions of the hydrocarbon stretches in the IR were consistent with crystalline packing and arrangement of the alkyl chains.

The resultant monolayer structure depended on a variety of factors such as solvent, immersion times, and manipulation of the bare metal substrate. There are many poorly controlled experimental parameters which may vary between different laboratories. These include humidity, different trace contaminants in the ambient or under vacuum, variations in evaporation rate and ambient temperature. (There may be other, as yet undefined experimental parameters.) One easily identified variable is the self-assembly solution. For our exploratory work we used ethanolic solutions. As was observed for the *n*-alkanoic acids self-assembling from ethanol on silver<sup>31</sup>, visible corrosion of the copper substrate occurred after ~10 minutes, with formation of a greenish precipitate in the solution after 1-2 hours. Hexadecane solutions showed no corrosion of the long chain monolayers at very long immersion times, even up to two weeks. Solvents tested were acetone, chloroform, methylene iodide, hexane, hexadecane, ethanol, methanol, benzene, toluene and water, of which hexadecane proved to be optimum in providing a balance between ability to dissolve the least soluble *n*-alkanoic acids without

dissolving the monolayer. However, monolayers formed from short chain acids showed some corrosion after long immersion times (greater than a few minutes), no matter what the solvent. Generally these immersion times varied between a few minutes to a few hours, with less time being required to form monolayers from the shorter chain length acids. The optimum immersion time was determined by selecting the samples which gave the highest contact angles. These typically showed lowest contact angle hysteresis, and "best" IR spectra. (The criteria for IR spectra are discussed below.) For a given acid, the same sample was evaluated as "best" from any series of measurements. The same results were obtained with ethanol and hexadecane solutions of *n*-alkanethiols to form thiolate monolayers at Cu, *i.e.*, of the solvents evaluated for self-assembly of either acids or thiols, hexadecane gives the best reproducibility and least corrosion of the substrate. Using these methods, good quality monolayers were usually obtained.

#### Characterization with optical ellipsometry

Optical ellipsometry is a convenient means of determining average thickness of a monolayer film<sup>16</sup>. The ellipsometric data in Figure 1 indicate that the thickness of the *n*-carboxylic acid monolayers tends to increase with increasing *n*. The line drawn through the data in Figure 1 has a slope of 1.4 Å per CH<sub>2</sub> group and an intercept of 5 Å. To compare these data to a simple structural model, thicknesses were calculated for idealized *n*-carboxylate monolayers with the chain axis perpendicular to the surface. The thicknesses of these model structures were estimated from tabulations of covalent and van der Waals radii<sup>32</sup>. The theoretical slope and intercept for a perpendicular orientation are 1.26 Å/CH<sub>2</sub> and 5.2 Å respectively. This intercept corresponds to the length of a *n*-alkanoic acid minus the length of the methylene groups, *i.e.*, the length of the carboxylate and terminal methyl groups. If the data in Figure 1 are bracketed by the highest and lowest lines which can plausibly be fitted to the data, (1.25-1.6) the slope is comparable to that obtained experimentally. The difference in

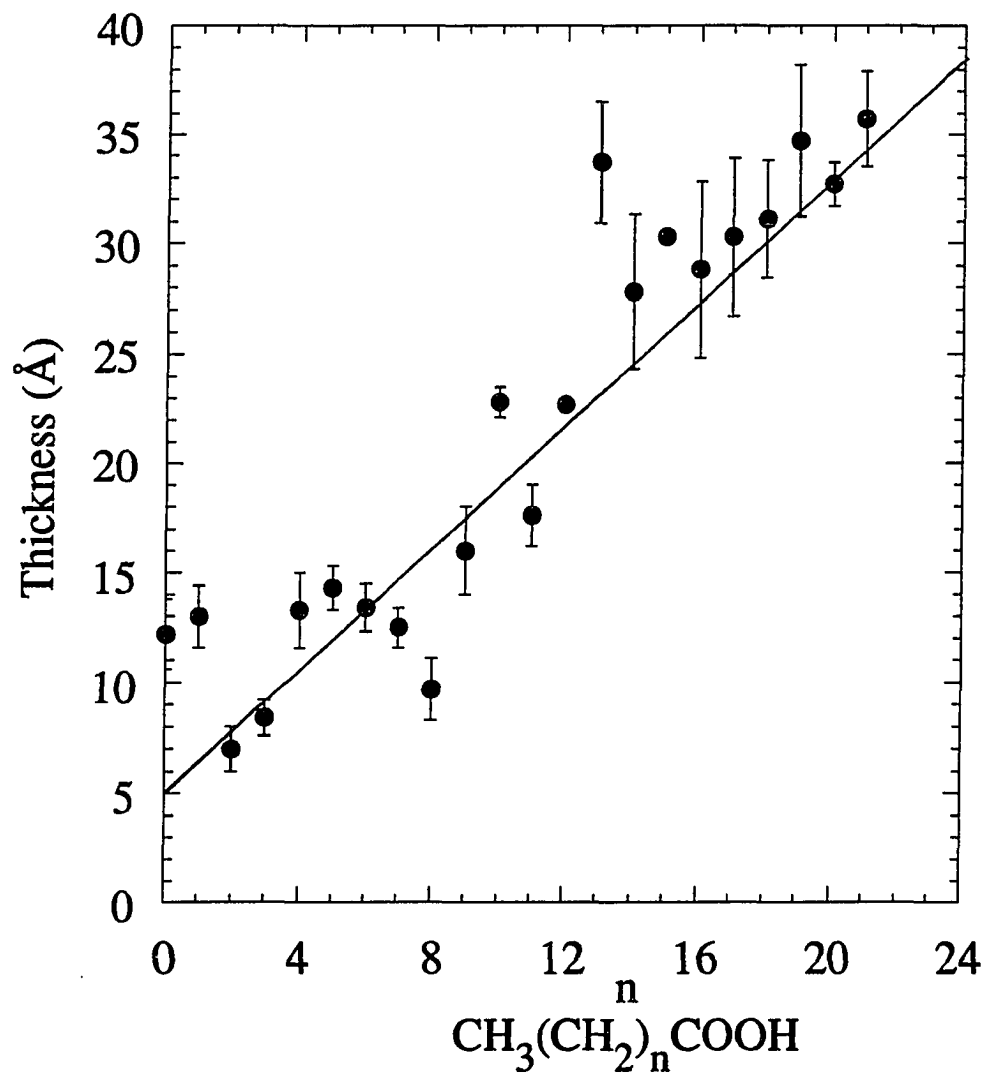


Figure 1. Ellipsometric film thicknesses for monolayers of *n*-alkanoic acids ( $\text{CH}_3(\text{CH}_2)_n\text{COOH}$ ) adsorbed at Cu. Uncertainties are standard deviations of measurements on 5-12 different samples.

intercept may be due to a variety of factors including changes of the optical constants at the interface due to the chemisorptive chemistry of the monolayer, the inclusion of a copper atom or copper oxide in the film thickness measurement, or adsorbed contaminants.

The thickness values measured are consistently *greater* than those for an ideal limiting structure. This discrepancy is not adequately accounted for by the experimental precision. The same type of discrepancy also appears in studies of the adsorption of organo sulfides on gold<sup>33</sup>, *n*-alkanoic acids on silver<sup>31</sup> and thiols on gold<sup>22</sup> and silver<sup>18</sup>, and contrasts with the good agreement between ideal and experimental film thickness reported for the adsorption of carboxylic acids on aluminum oxides<sup>16</sup>. Two factors which we cannot accurately evaluate stand out as possible contributors. First, the chemisorption may induce changes in the optical response of the gold substrate relative to the bare, unreacted substrate. Such effects could be coverage dependent. Second, as the chain length increases and the packing of the monolayer becomes more dense, the real refractive index of the monolayer is expected to increase. For example, the value of the refractive index of the most densely packed chain should be  $\sim 1.50$ , which is the value for polyethylene<sup>34</sup>, compared to the average value of 1.45 assigned to the films for the thickness calculation. If the value for the  $n=16$  monolayer approached 1.50, the corresponding thickness value would approach 24.8 Å, with the experimental line in Figure 1 approaching the hypothetical line. We cannot accurately evaluate this effect because single-wavelength ellipsometric measurements cannot be easily adapted to independently determine both the refractive index and film thickness for monolayer film<sup>22</sup>, other analysis techniques are needed to address the issue of film thickness in detail.

Unlike the results for alkanethiolates at Au<sup>22</sup>, the biphasic line shows much greater film thickness for the shorter chains. This observation may lead to insight about the ability of the monolayer films to impart corrosion resistance to the metal surface. Ellipsometric thicknesses less than the length of a fully extended molecule may be attributed to less densely packed monolayers, which occur if the underlying surface is unreactive (for example, Au). For a



reactive metal such as Cu, instead of reducing film thickness, corrosion protection of the underlying Cu is reduced, leaving the metal open to continuing oxidation. Apparent film thickness increases as a result. This increased build-up of surface oxide for shorter chains compared to longer chains has been observed for alkanolic acid monolayers on Cu by XPS<sup>30</sup>. Further evidence that the long chain monolayer films impart corrosion resistance is given by the fact that monolayer coated evaporated Cu films remain mirror-like for many months (at least 2 years over the course of these experiments).

To summarize, the results strongly imply the formation of monolayer films, which are more densely packed at longer chain lengths. This conclusion is consistent with the results presented below.

#### Characterization with contact angle measurements

The wetting properties of the carboxylic acid monolayers were examined with various liquids by contact angle measurement. The results are given as a function of chain length in Figure 2 for the probe liquids hexadecane, methylene iodide, glycerol and water. These provide a range of surface tensions and intermolecular interactions with the monolayer surface. Error bars, calculated as the standard deviation for at least 5 samples for each  $n$ , were only slightly larger than the points and are omitted for clarity. Two observations from the data in Figure 2 are immediately apparent. First, advancing contact angles ( $\theta_a$ ) for each liquid increase as the chain length increases, and reach limiting values that are comparable to the low free energy surfaces formed by other hydrocarbon monolayers<sup>20</sup>. For hexadecane,  $\theta_a$  is zero on monolayers of  $n$ -alkanoates with  $n < 4$ . By comparison,  $\theta_a$  for water at the stearic acid monolayer is approximately the same as for a pure  $\text{CH}_3$  terminated alkyl chain<sup>35</sup>. All probe liquids' contact angles reach a limiting value at  $n \geq 10$ . Second, the  $\theta_a$  values for the short-chain structures also exhibit a dependence on whether there are an even or odd number of methylene

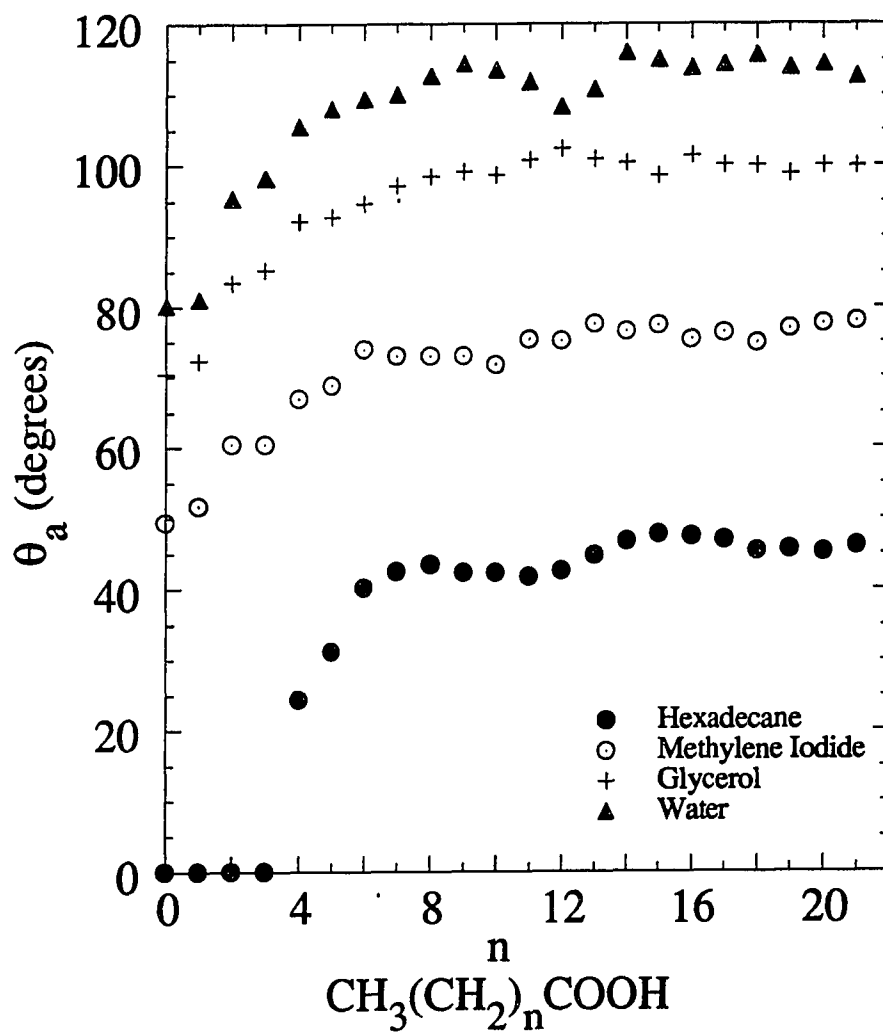


Figure 2. Advancing contact angles for monolayers of  $n$ -alkanoic acids ( $\text{CH}_3(\text{CH}_2)_n\text{COOH}$ ) adsorbed at Cu.

groups in the alkyl chain. For simplicity, we refer to a chain with an even number of methylene groups as an “even chain” and a chain with an odd number of methylene groups as an “odd chain”. Even chain monolayers have  $\theta_{as}$  which are markedly greater than those that are composed of chains with one less methylene group. This variation suggests the orientation of the terminal methyl group is different for chains with odd and even numbers of methylene groups<sup>28</sup>. Possible reasons for the “washing out” of the trend for long chains are not well understood and have been discussed previously<sup>18</sup>. We note that this odd-even effect for our short chain *n*-alkanoate monolayers at Cu is the same as for *n*-alkanethiolate monolayers at Ag, suggesting similarities in the environment of the terminal methyl group.

The contact angle hysteresis, which is the difference between the advancing and receding contact angles, can be used to estimate the surface coverage. The calculation is based on the premise that contact angle hysteresis is caused by heterogeneities in the surface. These consist of regions where the monolayer is completely perfect and smaller regions where it is completely imperfect, at virtually no coverage. The advancing contact angles may be associated with the high contact angle regions (the perfect monolayer) and the receding contact angle with the low contact angle regions (the defects, or areas of no coverage). Hence, the Cassie equation, where  $\sigma$  is the fraction of a surface with a particular  $\theta$ ,

$$\cos \phi = \sigma_1 \cos \theta_1 + \sigma_2 \cos \theta_2 \quad (1)$$

can be used to estimate the surface coverage where 1 represents the monolayer and 2 represents the defects. The advancing contact angle is  $\theta_1$ . The angle  $\theta_2$  is zero, because a probe liquid will tend to spread on a bare metal or metal oxide<sup>36</sup>. Making these substitutions and given that  $\sigma_1 + \sigma_2 = 1$ , we obtain

$$\cos \phi = (1 - \cos \theta_{rec}) / (1 - \cos \theta_{adv})$$

Using this method, fractional coverage of ca. 0.8-0.9 monolayer was estimated from the hysteresis between the advancing and receding contact angles<sup>37,38</sup> for the long-chain ( $n > 5$ ) for the *n*-alkanoic acids self-assembled at Cu. We have made the analogous measurements for

*n*-octadecanethiolate/Cu, indicating a structure of similar  $\theta_a$  but lower  $\theta_r$ , implying lower coverage.

#### Characterization with infrared spectroscopy

The molecular composition and orientation of the carboxylic acid monolayers were probed with IR spectroscopy. The assignment of the carboxylate modes raises the issue of the nature of the interaction between the canted carboxylate group and the copper surface. This interaction has been assigned in the literature as either an ester-like species in the UHV<sup>39</sup> and for a glycine monolayer<sup>11</sup>, by analogy to the bulk Cu(glycinato)<sub>2</sub> species in which the acid-metal interaction is ester-like due to chelation of the Cu with the amino group<sup>40,41</sup>, or an asymmetrically bound carboxylate<sup>14,16,17,42</sup>. We have formally assigned the structure as the carboxylate salt. This is based on consideration of sample preparation, literature precedents, and comparison of the spectra obtained to the spectra of analogous bulk Cu(II) *n*-alkanoate salts. Figure 3A is a low energy region IR spectrum for a monolayer of stearic (*n*=16) acid at copper.

Transmission IR spectra of Cu(II) stearate, Cu[O<sub>2</sub>C(CH<sub>2</sub>)<sub>16</sub>]<sub>2</sub> and bulk stearic acid are given in Figures 3B and 3C, respectively. Peak positions and vibrational mode assignments are shown in Table 1. The IR spectrum of bulk stearic acid (Figure 3B) has an absorption near 1703 cm<sup>-1</sup> for  $\nu(\text{C=O})$  of the carboxylic acid dimer, whereas the corresponding copper stearate monolayer has a broad band centered at 1565 cm<sup>-1</sup> for  $\nu_a(\text{COO}^-)$  and a band at 1443 cm<sup>-1</sup> for  $\nu_s(\text{COO}^-)$  (Figure 3). The bulk Cu(II) stearate has  $\nu_a(\text{COO}^-)$  at 1586 cm<sup>-1</sup> and  $\nu_s(\text{COO}^-)$  at 1440 cm<sup>-1</sup>. The bulk spectrum of the copper carboxylate salt also shows a peak at 1708 cm<sup>-1</sup>, probably due to the carbonyl mode of unreacted stearic acid. The spectrum of Cu(II) nonanoate prepared in our laboratory has no discernible peak in the region of 1703 cm<sup>-1</sup>, but the sample does have a slight odor of nonanoic

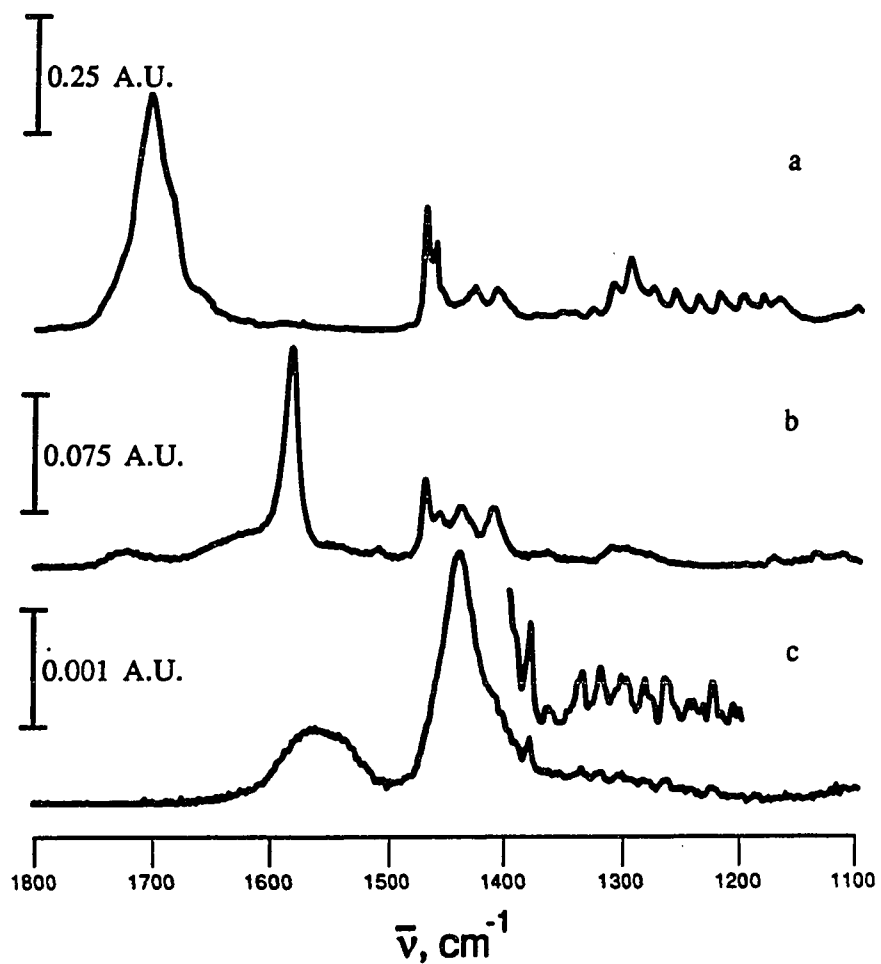


Figure 3. Infrared spectra (low energy region) for (a) stearic acid ( $n=16$ ) dispersed in KBr, (b) Cu(II) stearate, (c) a self-assembled monolayer of stearic acid adsorbed at Cu. The inset shows the progression of CH<sub>2</sub> wags for stearic acid at Cu, magnified by four.

Table 1. Mode assignments and peak positions for stearic acid and Cu(II) stearate in KBr matrix, and for a monolayer of stearic acid adsorbed at copper

Assignment	Peak position (cm <sup>-1</sup> )		
	Stearic acid in KBr	Cu(II) stearate in KBr	Monolayer of stearate/Cu
$\nu_a(\text{CH}_3, \text{ip})$	–	–	2965
$\nu_a(\text{CH}_3)$	2954	2956	–
$\nu_s(\text{CH}_3, \text{FR}_1)$	–	–	2938
$\nu_a(\text{CH}_2)$	2917	2915	2918
$\nu_s(\text{CH}_3, \text{FR}_2)$	2871(weak)	2873(weak)	2879
$\nu_s(\text{CH}_2)$	2849	2849	2850
$\nu(\text{C}=\text{O})$	1703	(1708) <sup>a</sup>	–
$\nu_a(\text{COO}^-)$	–	1586	1566
$\nu_s(\text{COO}^-)$	–	1440	1443
$\delta(\text{CH}_2)$	1472, 1464	1471	–
$\nu(\text{C}-\text{O}) + \delta(\text{O}-\text{H})$	1431	–	–
$\delta(\alpha\text{-CH}_2)$	1412	1414	–
$\text{CH}_2$ wagging fundamental	–	–	1382
$\delta(\text{CH}_3)$	–	1367	–
$\omega(\text{CH}_2)^b$	1331, 1313, 1298, 1279, 1261, 1241, 1223	–	1356, 1338, 1322, 1302, 1281, 1265, 1245, 1225
Disordered $\omega(\text{CH}_2)^c$	–	1315	–
$\nu(\text{C}-\text{C})$	1202, 1187, 1172	1176, 1138, 1115	1187

a Trace unreacted stearic acid.

b The IR selection rules for a polymethylene alkyl chain with 16 CH<sub>2</sub> units predict 8 wagging modes<sup>44</sup>.

c This mode is slightly higher in energy than the disordered *n*-alkanes CH<sub>2</sub> wagging mode<sup>45</sup>. This is probably due to effects of the polar end group.

acid<sup>43</sup>. The position of  $\nu_a(\text{COO}^-)$  depends on the cation and is in this case is consistent with that expected for a copper carboxylate<sup>13,17</sup>.

A diagnostic IR feature for an ester-like species is the free carbonyl mode. There is evidence in the literature for asymmetrically bound adsorbed carboxylate species on copper oxide surfaces, including *n*-alkanoates<sup>14,17,41,46-50</sup> and acetylacetonate<sup>47</sup>. The comparison of the monolayer spectra to those of the analogous bulk compounds is even more convincing. If an ester-like species were present, the C-O stretching frequency would be shifted to higher frequency ( $>1600\text{ cm}^{-1}$ ) and the low energy mode would be shifted to lower energy ( $<1425\text{ cm}^{-1}$ ) as has been observed for Cu *bis*  $\beta$ -diketonates and  $\text{Cu}(\text{oxalate})_2$ <sup>41,48,49</sup>. However, the spectral features for the interfacial Cu-carboxylate interactions are in fact *lower* than the same peak positions in the bulk Cu(II) salts of alkanolic acids which are chelated through both oxygen atoms of the carboxylate.

The  $\nu(\text{C=O})$  is absent in the monolayer spectrum (Figure 3C). This fact, as well as the presence of  $\nu_s(\text{COO}^-)$  at  $1435\text{ cm}^{-1}$ , indicates that the chemisorption process results in the formation of a carboxylate salt. Further, the detection of  $\nu_a(\text{COO}^-)$  near  $1585\text{ cm}^{-1}$  suggests that the carboxylate head group is asymmetrically bound at the copper substrate as a bridging or bidentate ligand<sup>51</sup>. This conclusion is based on the "IR surface selection rule" which gives rise to a preferential excitation of vibrational modes with dipoles normal to highly reflecting metallic surfaces<sup>50</sup>. X-ray crystallographic studies of bulk copper carboxylate salts support a bridging structure<sup>52-54</sup>. A comparison of the positions of the asymmetric and symmetric carboxylate modes, while not always rigidly correct, can be useful to suggest the structure of the carboxylate. Therefore, if one defines a value  $\Delta = \nu_a(\text{COO}^-) - \nu_s(\text{COO}^-)$ , this value can be correlated with known carboxylate complexes' structures. Generally, for values of  $\Delta > 180\text{ cm}^{-1}$ , a unidentate complex is formed. For values  $< 80\text{ cm}^{-1}$ , a bidentate complex is formed, and for intermediate values of  $\Delta$ , one finds a bridging complex. For the monolayers of *n*-

alkanoic acids on copper,  $\Delta$  is  $122\text{ cm}^{-1}$ . As for the bulk Cu(II) carboxylate salts<sup>52-54</sup>, this value implies a bridging coordination chemistry at the interface, where each carboxylate anion is directly attached to two copper sites on the oxide surface.

The IR spectrum between  $3100$  and  $2700\text{ cm}^{-1}$  for a monolayer of stearic acid on Cu is shown in Figure 4C. Based on previous studies<sup>55,56</sup>, the bands at  $2917\text{ cm}^{-1}$  and  $2851\text{ cm}^{-1}$  are attributed to  $\nu_a(\text{CH}_2)$  and  $\nu_s(\text{CH}_2)$ , respectively. The band at  $2965\text{ cm}^{-1}$  is assigned to  $\nu_a(\text{CH}_3, \text{ip})$  and the bands at  $2938\text{ cm}^{-1}$  and  $2879\text{ cm}^{-1}$ , which are split due to Fermi resonance interactions with lower-energy modes, are  $\nu_s(\text{CH}_3, \text{FR1})$  and  $\nu_s(\text{CH}_3, \text{FR2})$ , respectively.

In addition to probing molecular composition, IR spectroscopy was also used to determine the average orientation of the monolayers. Orientation was determined by a comparison of the measured absorbances with those calculated for an isotropic monolayer using classical electromagnetic theory and including considerations of the "IR surface selection rule"<sup>16,50,57</sup>. The results of the calculations with the  $\nu_a(\text{CH}_2)$  and  $\nu_s(\text{CH}_2)$  indicate an average tilt of the molecular axis of the long carbon chains ( $n \geq 16$ ) of  $\sim 15^\circ$ . Defects would give rise to disordered chain packing, and hence, larger IR absorbances yielding larger calculated chain tilts. We can thus conclude that the long-chain monolayers are highly ordered. The structures of the monolayers of shorter carbon chains are different from the longer chain monolayers. The shorter chain monolayers ( $n < 16$ ) have IR spectra which are not as well resolved. The  $\nu_a(\text{CH}_2)$  mode at  $2920\text{ cm}^{-1}$  could not be resolved from the  $\nu_s(\text{CH}_3, \text{FR1})$  mode, and the  $\nu_s(\text{CH}_2)$  could not be resolved from the  $\nu_s(\text{CH}_3, \text{FR2})$ . Because these modes are qualitative indicators of the packing of the alkyl chain<sup>55,56</sup>, we interpret the peak positions of  $\nu_s(\text{CH}_2)$  of the long-chain monolayers as indicative of crystalline-like packing of the alkyl chains, while the short chain monolayers are liquid-like. These differences imply an increase in disorder, inferred from poorer resolution of the hydrocarbon peaks for the shorter chains compared to the IR spectra of the longer chain analogs.



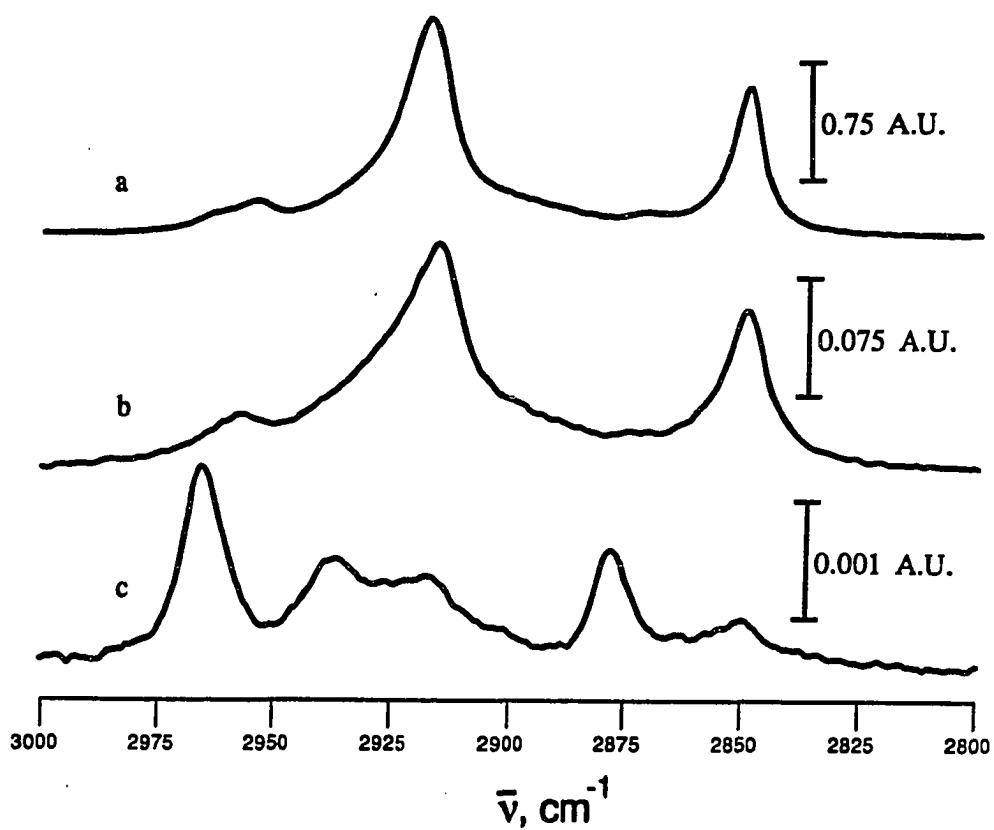


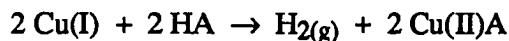
Figure 4. Infrared spectra (high energy region) for (a) stearic acid ( $n=16$ ) dispersed in KBr, (b) Cu(II) stearate, (c) a self-assembled monolayer of stearic acid adsorbed at Cu.

The surface selection rule also can be applied to gain insight into the orientation of the asymmetric and symmetric carboxylate stretching modes, because they arise from dipole transitions that are mutually perpendicular. The asymmetric mode is parallel to the O-C-C axis, while the symmetric mode is parallel to the  $\alpha$ -C-C axis. The intensity of  $\nu_s(\text{COO}^-)$  at 1435  $\text{cm}^{-1}$  is greater than  $\nu_a(\text{COO}^-)$  at 1585  $\text{cm}^{-1}$ . The observation of both modes reveals that the carboxylate head group is itself bound asymmetrically. Note that this is consistent with a tilt from the surface normal of 15°.

The observation of the  $\nu_a(\text{COO}^-)$  mode demonstrates that the carboxylate bound to the surface is canted (surface effect, see above). However, a comparison of the relative intensities of the  $\nu_a(\text{COO}^-)$  and  $\nu_s(\text{COO}^-)$  modes for the monolayers vs. the bulk salts reveals that the intensity of the  $\nu_a(\text{COO}^-)$  mode is greatly reduced in the monolayers. This qualitatively indicates that the carboxylate is oriented only slightly away from the surface. A more detailed orientational analysis of the carboxylate orientation is precluded by the lack of a reference optical function for the monolayer structure.

The fairly good agreement of  $\nu_a(\text{COO}^-)$  and  $\nu_s(\text{COO}^-)$  peak positions with the structure of the bulk Cu(II) salt suggests that the monolayer is bound to the Cu in the +2 oxidation state. Because Cu(I) alkanoate salts are known to be extremely air and moisture sensitive<sup>58</sup>, we believe that the Cu at the monolayer exists as the cupric ion. XPS has been used to show that before monolayer formation, the clean Cu oxide surface exists as Cu metal and Cu(I), but that after monolayer formation, Cu(II) can be detected<sup>30,42</sup>.

The presence of Cu(II) provides further insight into the reaction chemistry which occurs upon monolayer formation. The Cu(I), bound in the  $\text{Cu}_2\text{O}$  matrix, may reduce the proton of the acid to hydrogen.



Attempts to measure the very small amounts of  $\text{H}_2$  that would be evolved were unsuccessful<sup>59</sup>. Another possibility for the interfacial reaction chemistry is reaction of the acid with a surface-

bound hydroxide. This hydroxide could be formed by reaction of  $\text{Cu}_2\text{O}$  with trace water in the solvent. However, while it has been known for some time that oxidation of  $\text{Cu}^0$  films to  $\text{Cu(I)}$  promotes monolayer formation<sup>14,60</sup>, the role of water has not been clearly demonstrated. Furthermore, acid-base reactivity would not cause the manifestation of  $\text{Cu(II)}$  observed upon monolayer formation.

The spectra also show a series of bands between  $1200\text{-}1360\text{ cm}^{-1}$ , attributed to the methylene wagging modes,  $\omega(\text{CH}_2)$ . Their presence indicates that the chains are fully extended in an all-trans zig-zag conformation. The  $\omega(\text{CH}_2)$  modes in monolayers have recently been discussed in detail<sup>44</sup>; assignments for a monolayer of stearate/ $\text{Cu}$  are given in Table 1.

In conclusion, analysis of the IR spectra reveals: 1) binding of the carboxylate salt to a copper cation, 2) the absence of unionized acid molecules on the metal surface, and 3) the presence of progression bands between  $1200$  and  $1360\text{ cm}^{-1}$ .

#### Scanning tunneling microscopy (STM) of the native oxide of copper

Images of metal surfaces with atomic scale resolution has previously been achieved with a variety of metal surfaces<sup>61,62</sup>. Here we report the first observation of atomic scale images of  $\text{Cu}_2\text{O}$ . To develop a detailed understanding of the factors that lead to the formation of a canted carboxylate head group for alkanolic acid monolayers at copper<sup>14</sup>, STM was used to image the microstructure of the native oxide at the copper surface.  $\text{Cu}$  films deposited under these conditions are predominantly (111) textured<sup>11,63-65</sup>, and upon exposure to air, react to give  $\text{Cu}_2\text{O}$  films that are also predominantly (111) textured<sup>65-68</sup>. Atomically resolved images were found for evaporated  $\text{Cu}$  films, directly revealing for the first time the arrangement of individual atoms in the native oxide (i.e.  $\text{Cu}_2\text{O}$ ) lattice. The (111) face of the  $\text{Cu}_2\text{O}$  is the structure in which the copper atoms have the highest density per unit area.

Three atomically resolved STM images of  $\text{Cu}$  films are shown in Figure 5a-c. The images encompass an area slightly less than  $3\text{ nm}$  by  $3\text{ nm}$  each, and are given in a

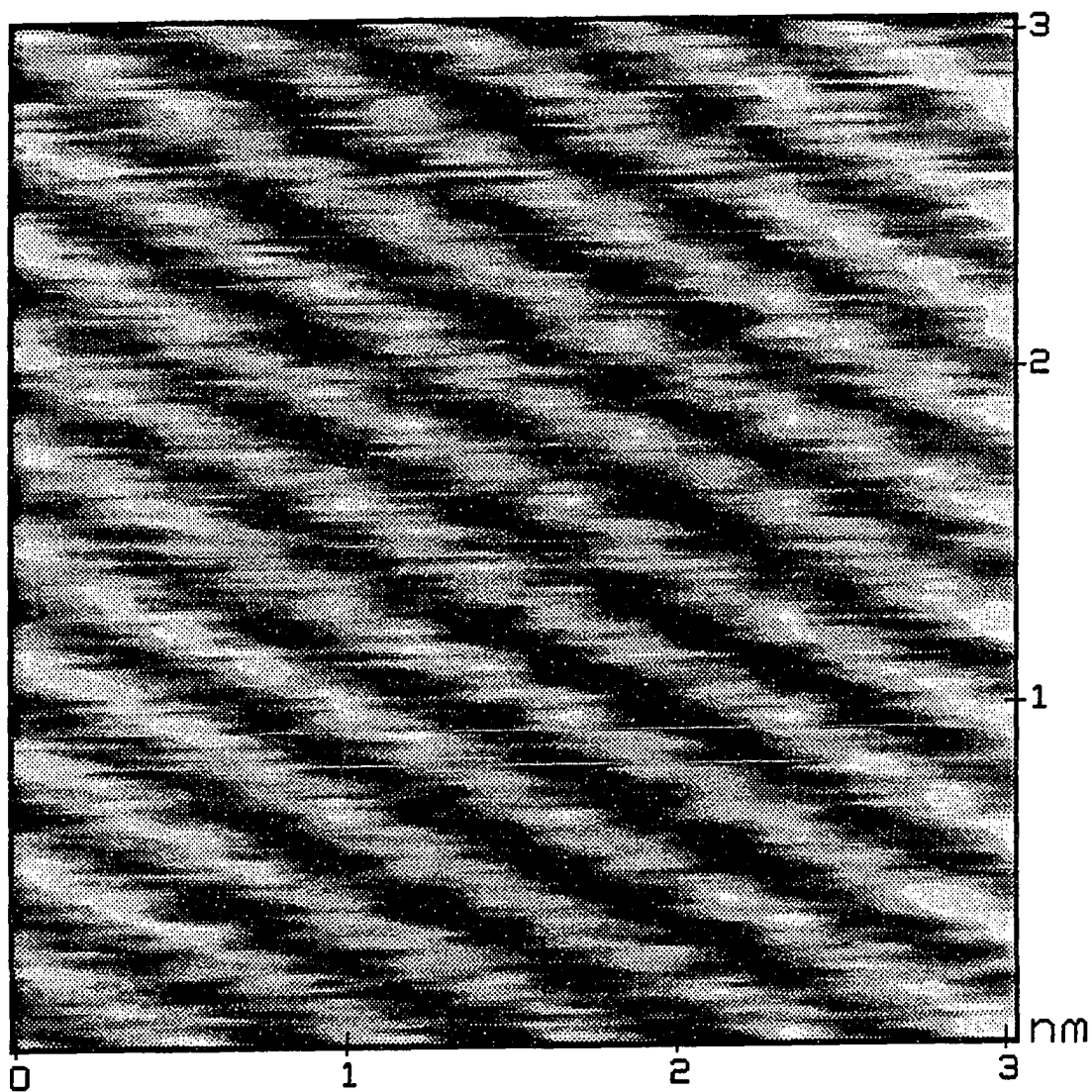


Figure 5a. STM image of the bare  $\text{Cu}_2\text{O}$  surface, as removed from the evaporator and imaged immediately.

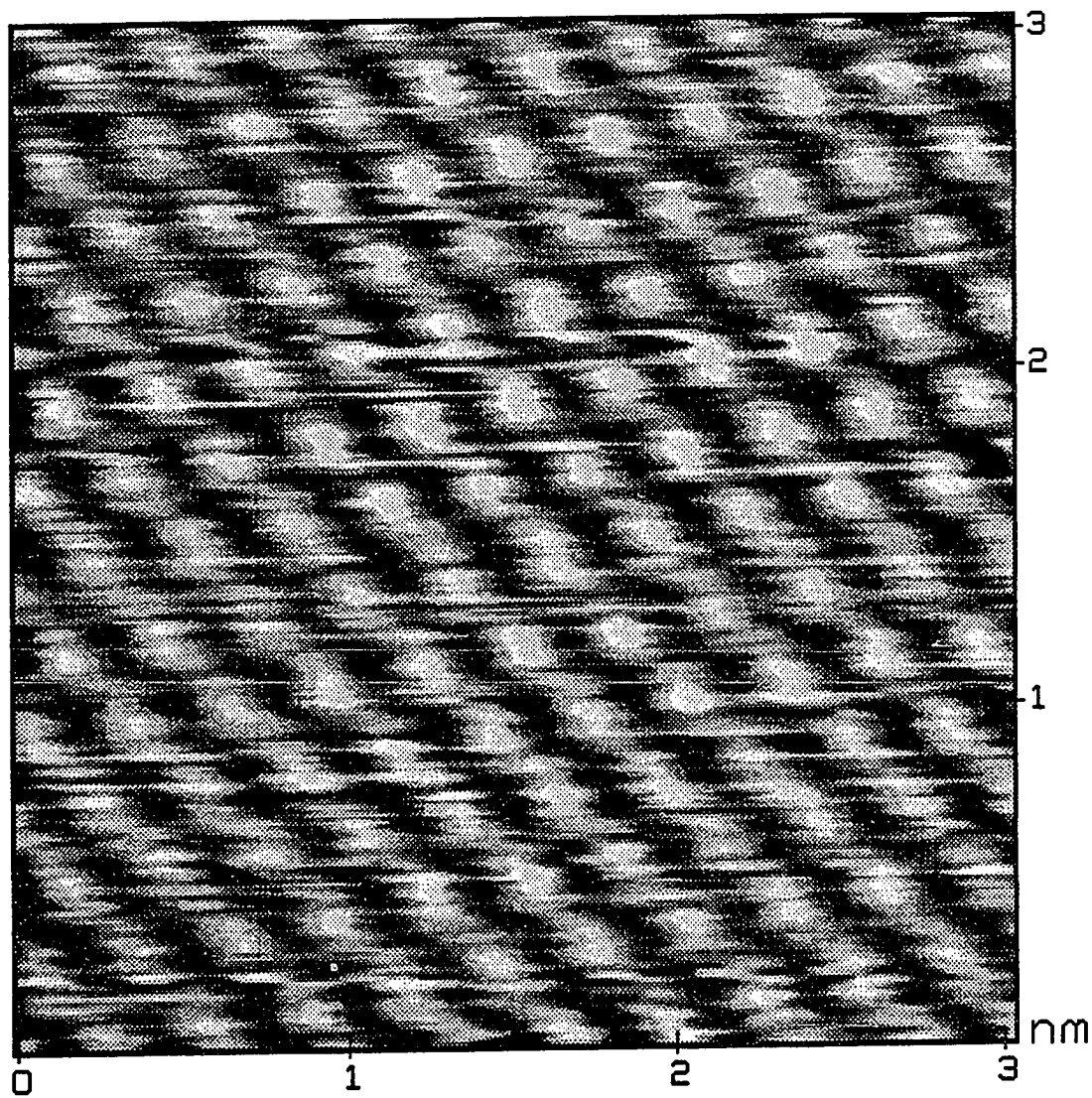


Figure 5b. STM image of the bare  $\text{Cu}_2\text{O}$  surface, stored and imaged under mineral oil.

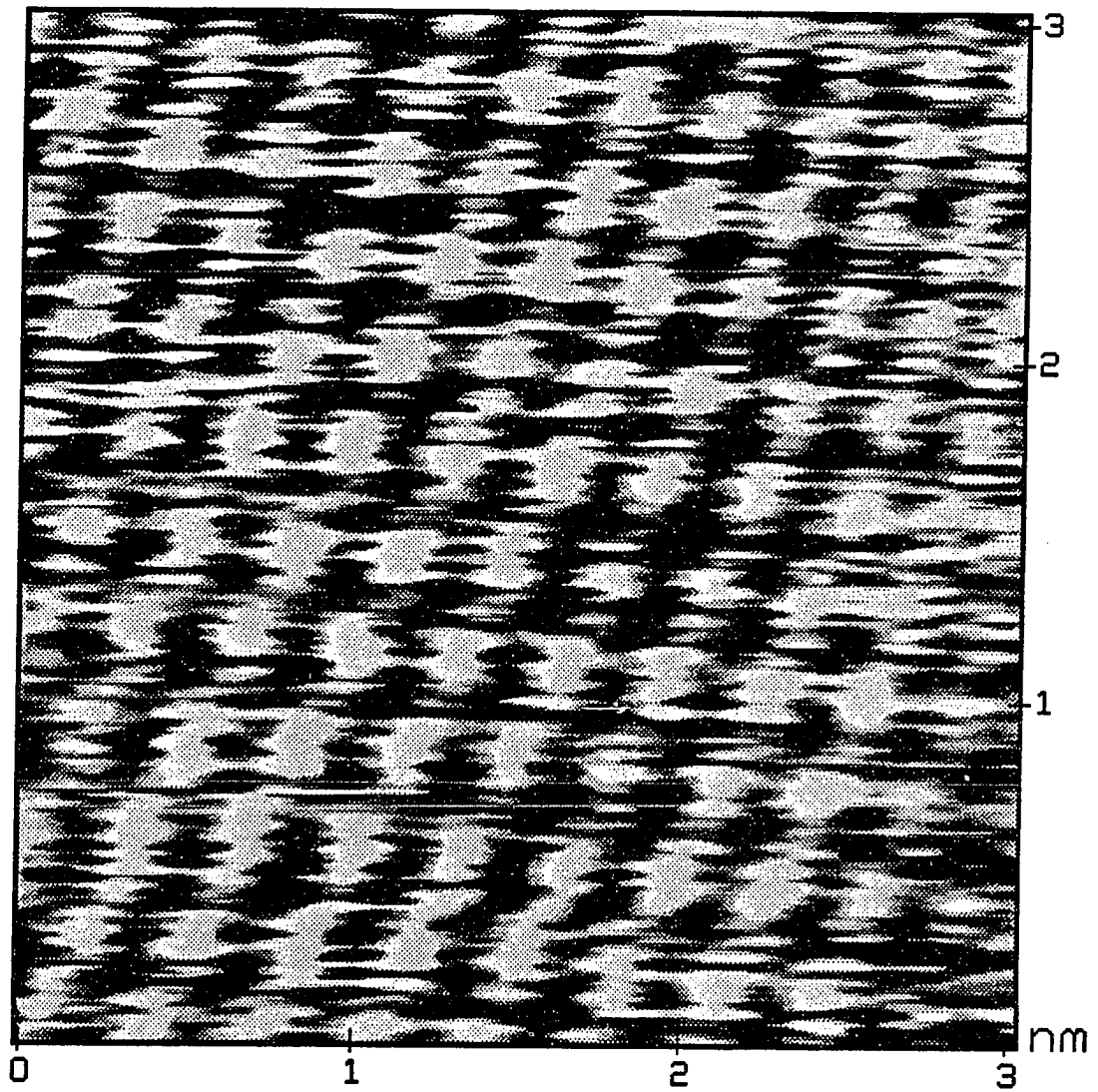


Figure 5c. STM image of the  $\text{Cu}_2\text{O}$  surface with an adsorbed stearate monolayer.

top-view presentation with the lighter portions of the gray vertical scale corresponding to higher regions of the surface and the darker portions to lower regions of the surface. The images in Figures 5a-c are composed of a hexagonal pattern of spots of uniform brightness; this is the only periodic feature that we have found to date on such samples. Such uniform brightness generally arises from atoms with a similar work function, arguing that there is only one type of atom being imaged. We have measured the nearest neighbor and next-nearest neighbor spacings to be  $2.9 \pm 0.2 \text{ \AA}$  and  $5.1 \pm 0.4 \text{ \AA}$  for bare Cu films (Figure 5a),  $2.9 \pm 0.1 \text{ \AA}$  and  $5.1 \pm 0.2 \text{ \AA}$  for mineral-oil covered Cu films (Figure 5b), and  $3.0 \pm 0.2 \text{ \AA}$  and  $5.1 \pm 0.4 \text{ \AA}$  for monolayer-covered Cu films (Figure 5c), respectively. The images are attributed to tunneling at the Cu atoms of the native  $\text{Cu}_2\text{O}$  surface oxide. For  $\text{Cu}_2\text{O}$ , the bulk structure consists of a face-centered cubic arrangement of oxygen atoms. The structure consists of a face-centered cube of copper atoms intermeshed with a body centered cube of oxygen atoms. The planes of copper atoms are interleaved with two planes of oxygen atoms. The cell constant,  $a$ , of  $\text{Cu}_2\text{O}$  has been determined to be  $4.2696 \text{ \AA}$ <sup>54</sup>. For the (111) face of  $\text{Cu}_2\text{O}$ , this gives a Cu-Cu spacing of  $3.0 \text{ \AA}$  and an O-O spacing of  $6.0 \text{ \AA}$ , consistent with our findings and those of earlier electron transmission<sup>11</sup> and diffraction studies<sup>65</sup>. A schematic of the  $\text{Cu}_2\text{O}$  surface structure is given in Figure 6.

It is also important to note that the images with the highest periodic definition were obtained for samples prepared by the room temperature deposition of Cu. With our evaporation system, such a procedure leads to an increase in the temperature of the substrates to  $\sim 50 \text{ }^\circ\text{C}$ , a consequence of radiative heating by the Cu deposition source. After cooling in the evaporator, bare Cu samples were removed immediately and loaded for imaging (Figure 5a). Images with good definition were also found for samples that were stored under mineral oil (Figure 5b). The uncoated samples generally gave no satisfactory images a few hours after removal from the evaporator. The inability to image substrates handled in the latter fashion is attributed to the formation of a thick passive oxide that inhibits electron tunneling.

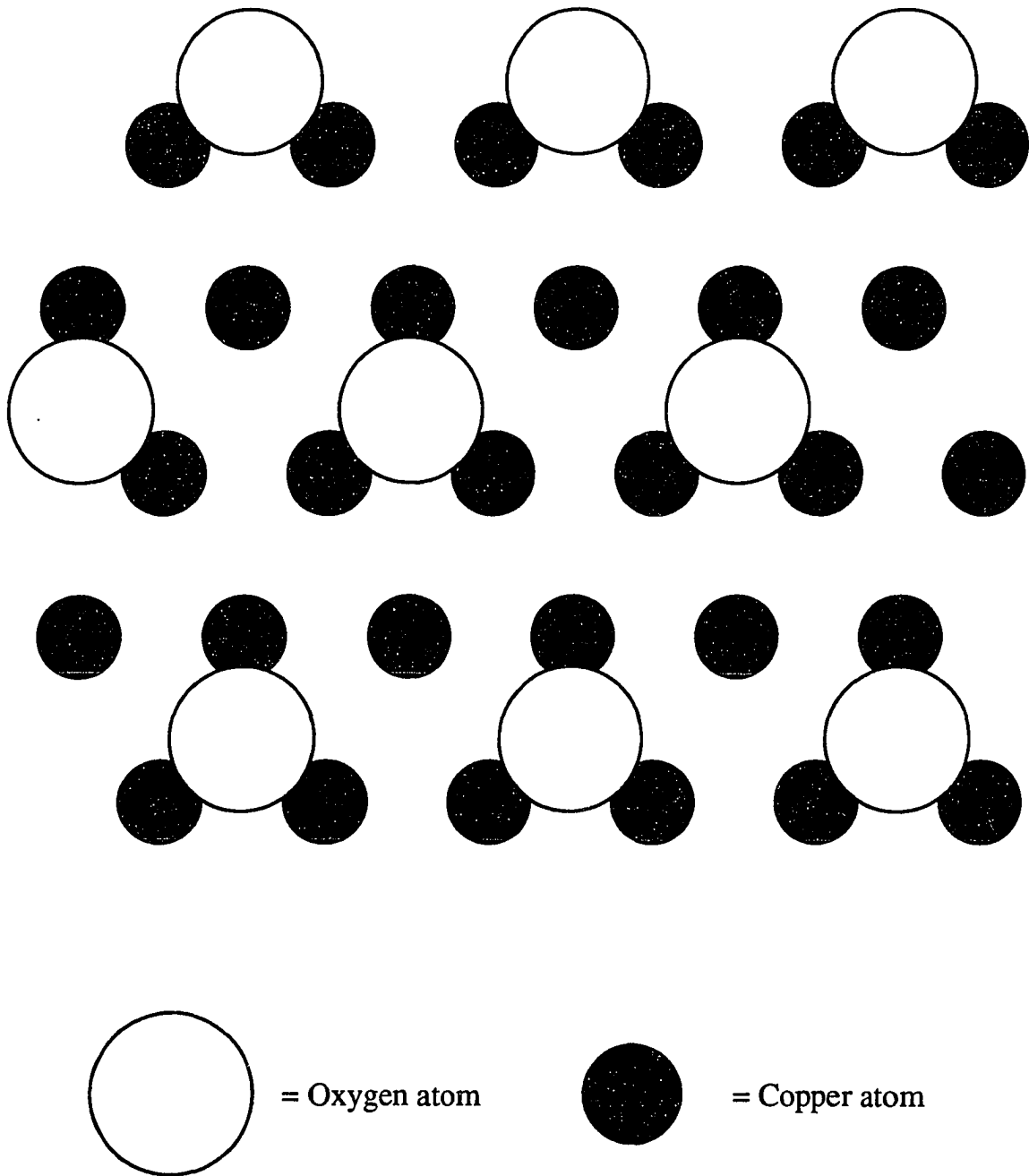


Figure 6. Schematic representation of the  $\text{Cu}_2\text{O}(111)$  surface. Filled circles represent Cu atoms; white circles are oxygen atoms.



The ability to image for prolonged periods of time under mineral oil and after monolayer formation (see below), which would reduce the rate of oxide growth, is consistent with the above contention. Attempts to image bare samples using Cu deposited onto heated ( $>100^{\circ}\text{C}$ ) mica substrates, in a deposition process similar to that used for Au films<sup>61-63</sup>, have not yet been successful.

We also scanned stearic acid monolayer coated  $\text{Cu}_2\text{O}$  substrates using STM (Figure 5c). These samples show the same arrangement and spacings as were obtained from bare Cu films and those stored under mineral oil. The acquisition of images was actually easier for monolayer coated samples, with images being obtained even on samples that were up to two weeks old.

To attempt to obtain a different image which could potentially be ascribed to the adsorbate, tunneling currents and bias voltage were varied from 0.75 nA to 2.0 nA, and from -200 to +300 mV, respectively. With bias voltages at the extreme ends, no images were found; at intermediate values, only structures similar to those in Figure 5 were obtained.

Images of both the bare underlying metal and the adsorbed monolayer have been observed previously for alkanethiolates at Au(111). We attribute our inability to observe the adsorbate in this case to the greater ionicity of the adsorbate-metal linkage, i.e., Au-S is a covalent bond, whereas Cu-carboxylate is ionic. A lack of tunneling current through the O-Cu linkage may arise from one of two causes: (1) tunneling currents do not pass readily through ionic bonds, or (2) the STM tip is abrading the monolayer, until only the bare  $\text{Cu}_2\text{O}$  image is seen. However, these results suggest that STM of other reactive metals may be aided by the oxidation protection (*i.e.*, corrosion resistance) imparted by a monolayer film.

#### Proposed adsorbate structure

The direct confirmation that the surface of evaporated Cu films consists of  $\text{Cu}_2\text{O}(111)$ , as well as the knowledge of the alkyl chain conformation, enabled us to propose a structure for

the two-dimensional arrangement of the monolayer. Only if the substrate spacing allows the adsorbed molecules to be closest-packed can the chains interact and be stabilized in a perpendicular orientation. If the substrate spacing prohibits close-packing, the chains will tilt to maximize interchain interactions. This is represented schematically in Figure 7. It has been shown that the nearest-neighbor spacings can be used as a predictor of alkyl chain tilt<sup>61</sup>. Based on the experimentally determined tilt for the  $\text{CH}_3(\text{CH}_2)_n\text{CO}_2/\text{Cu}$  monolayers and the van der Waals chain diameter of 4.24 Å, the calculated nearest neighbor spacing is ~4.4 Å. (Given the qualitative nature of the tilt calculation, this number is of course approximate.) However, 4.4 Å is 3/2x the Cu-Cu nearest neighbor spacing. This suggests a (3/2 x 3/2) unit cell, indicated in Figure 8.

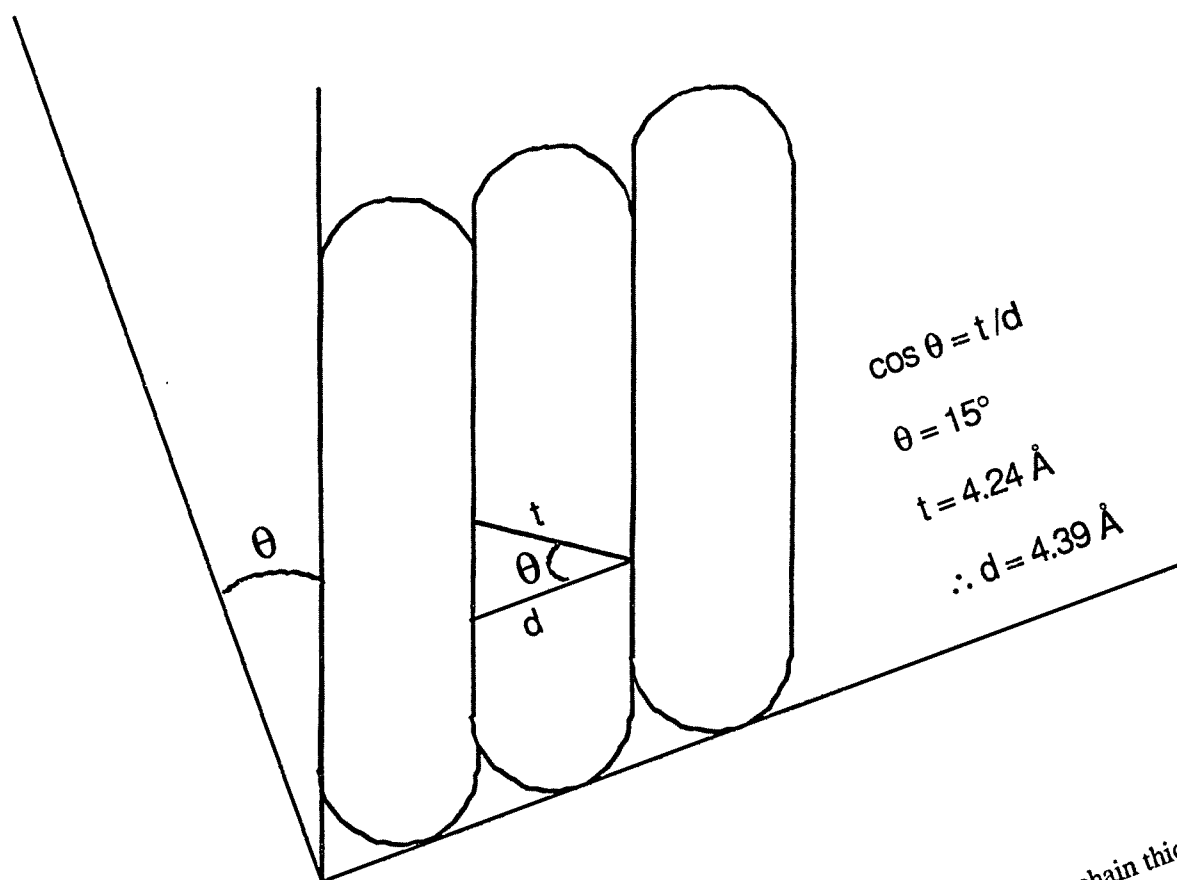


Figure 7. Relationship between chain tilt angle and Van der Waals chain thickness for n-alkanoic acids self-assembled at Cu.

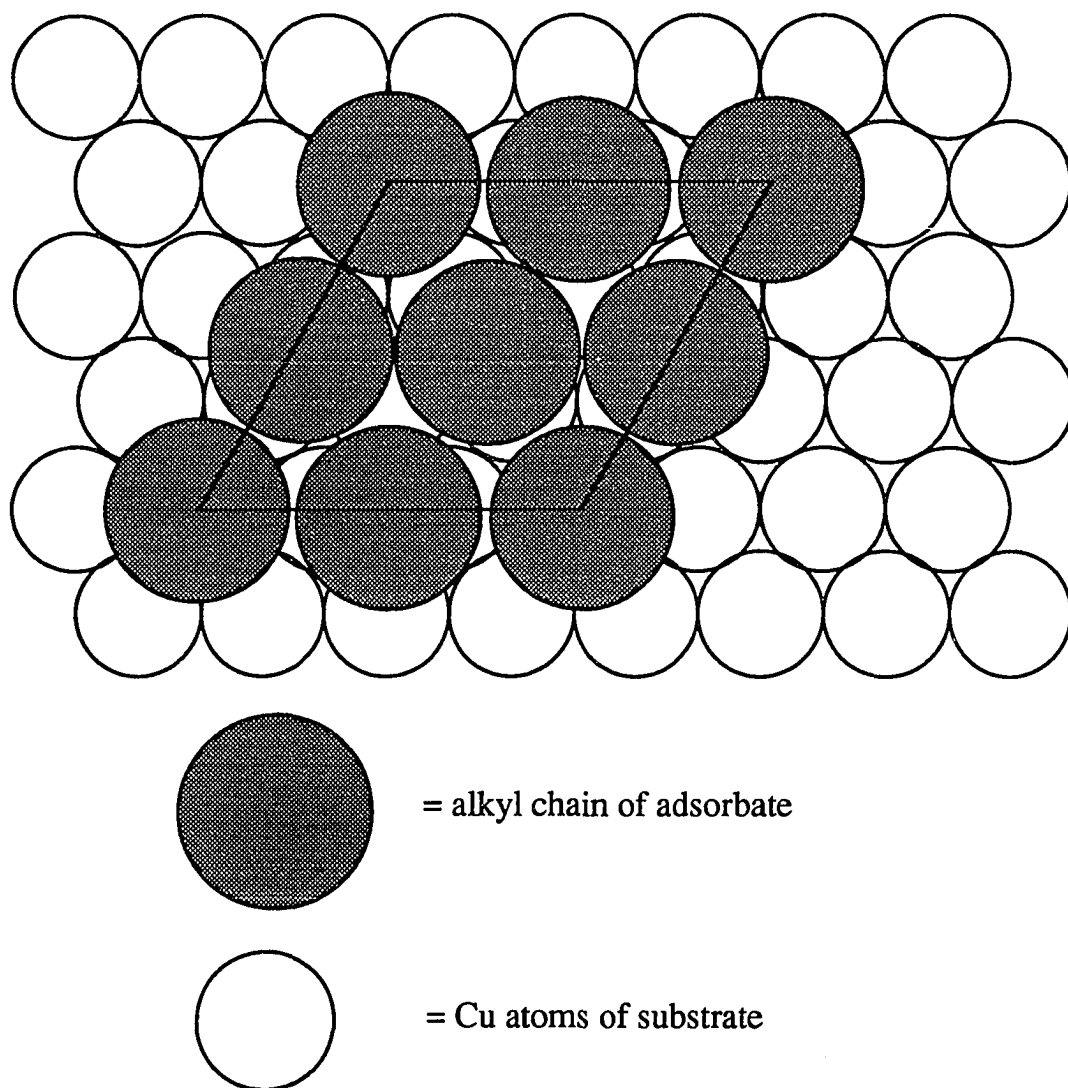


Figure 8. Arrangement of alkyl chains tilted  $15^\circ$  on a  $\text{Cu}_2\text{O}$  surface. The proposed unit cell is a  $(3/2 \times 3/2)$ .

## CONCLUSIONS

Infrared reflection spectroscopy, optical ellipsometry, and contact angle measurements indicate that *n*-carboxylic acids adsorb at evaporated polycrystalline copper substrates to form monolayer films. The IR data indicate that monolayer formation results in the transformation of the carboxylic acid to an asymmetrically bound carboxylate salt. These monolayer structures form low-free energy surfaces as indicated by contact angle (wetting) studies.

The surface chemist's arsenal of monolayer chemistries as probes of adhesion at the molecular level is expanding to enable the rational design of monolayers<sup>42</sup>. These monolayer studies<sup>18,23,25,42,44</sup> give further information as to what is the best adhesive for a particular metal. For example, the chemistry of chemisorption to give highest quality monolayers in terms of crystallinity and surface coverage can be controlled by judicious choice of functional head group and solvent. To date, thiols have been shown to pack well to form well-ordered structures on gold. On silver and copper, both acids and thiols react to form tightly packed monolayer structures. On copper, however, the acids form monolayers with higher surface coverage than do the thiols.

Extensive studies concerning the packing, surface coverage, and dynamics of film formation are currently in progress. Further information will be yielded by STM, AFM, XPS as well as the above techniques.

## REFERENCES

- (1) Bigelow, W. C.; Pickett, D. L.; Zisman, W. A. *J. Colloid Sci.* **1946**, *1*, 513.
- (2) Babik, A. N.; Zaichenko, L. P.; Gromov, V. K. *Vsesoyuznyy Institut Nauchnay i Tekhnicheskoy Informatsii* **1984**, *94*, 1-19. *Chem. Abs.* 102(6):49646d.
- (3) Gaines, G. L. *J. Colloid Sci.* **1960**, *15*, 321-89.
- (4) Walker, D. C.; Ries, H. E. J. *J. Colloid Sci.* **1962**, *17*, 789-800.
- (5) Timmons, C. O.; Zisman, W. A. *J. Phys. Chem.* **1965**, *69*, 984-90.
- (6) Brockway, L. O.; Karle, J. *J. Colloid Sci* **1947**, *2*, 277-87.
- (7) Bowden, F. P.; Moore, A. C. *Trans. Farad. Soc.* **1951**, 900-908.
- (8) Young, J. E. *Austr. J. Chem.* **1955**, *8*, 173-93.
- (9) Prédali, J. J. *Trans. Inst. Mining & Metallurgy* **1969**, C140-7.
- (10) Chu, A. K. P.; Sukava, A. J. *J. Electrochem. Soc.: Electrochem. Sci.* **1969**, *116*, 1188-93.
- (11) Ihs, A.; Liedberg, B.; Uvdal, K.; Törnkvist, C.; Bodö, P.; Lundstrom, I. *J. Coll. Int. Sci.* **1990**, *140*, 192-206 and references therein.
- (12) Boerio, F. J.; Chen, S. L. *J. Coll. Int. Sci.* **1979**, *73*, 176-85.
- (13) Scowen, R. V.; J., L. *Can. J. Chem.* **1967**, *45*, 2829-2835.
- (14) Dubois, L. H.; Zegarski, B. R.; Nuzzo, R. G. *Langmuir* **1986**, *2*, 412-7.
- (15) Bigelow; Glass; Zisman *J. Colloid Sci.* **1947**, *2*, 563.
- (16) Allara, D. L.; Nuzzo, R. G. *Langmuir* **1985**, *1*, 45-52.
- (17) Allara, D. L.; Nuzzo, R. G. *Langmuir* **1985**, *1*, 52-66.
- (18) Walczak, M. M.; Chung, C.; Stole, S. M.; Widrig, C. A.; Porter, M. D. *J. Am. Chem. Soc* **1991**, *113*, 2370-8.
- (19) *Handbook of Chemistry and Physics*; 72nd. ed.; Lide, D. R., Ed.; Chemical Rubber Co.: Boca Raton, FL, 1991-1992.
- (20) Bain, C. D.; Troughton, E. B.; Tao, Y.-T.; Evall, J.; Whitesides, G. M.; Nuzzo, R. G. *J. Am. Chem. Soc.* **1989**, *111*, 321-35.
- (21) Finklea, H. O.; Avery, S.; Lynch, M.; Furtsch, T. *Langmuir* **1987**, *3*, 409- 13.

- (22) Porter, M. D.; Bright, T. B.; Allara, D. L.; Chidsey, C. E. D. *J. Am. Chem. Soc.* **1987**, *109*, 3559-68.
- (23) Whitesides, G. M.; Laibinis, P. E. *Langmuir* **1990**, *6*, 87-96 and references therein.
- (24) Bain, C. D.; Biebuyck, H. A.; Whitesides, G. M. *Langmuir* **1989**, *5*, 723-7.
- (25) Ulman, A. *J. Mater. Educ.* **1989**, *11*, 205-80.
- (26) Stole, S. M.; Porter, M. D. *Appl. Spectrosc.* **1990**, *49*, 1418-20.
- (27) Cu(II) nonanoate was prepared by the reaction of Cu(CO<sub>3</sub>) with nonanoic acid in ether, and was recrystallized from ether.
- (28) Nuzzo, R. G.; Dubois, L. H.; Allara, D. L. *J. Am. Chem. Soc.* **1990**, *112*, 558-69.
- (29) Lefakis, H.; Ho, P. S. *Thin Solid Films* **1986**, *136*, L31-34.
- (30) Johnson, R.; Gardella, J.; Smith, E. L.; Walczak, M. M.; Porter, M. D. in preparation.
- (31) Chau, L.-K.; Smith, E. L.; Wolff, K.; Porter, M. D. in preparation.
- (32) Pauling, L. *The Nature of the Chemical Bond*; Cornell University: Ithaca, NY, 1960.
- (33) Nuzzo, R. G.; Allara, D. L. *J. Am. Chem. Soc.* **1983**, *105*, 4481-83.
- (34) Swalen, J. D.; Santo, R.; Take, M.; Fischer, J. *IBM J. Res. Dev.* **1977**, *21*, 169-175.
- (35) Fox, H. W.; Zisman, W. A. *J. Colloid Sci.* **1952**, *7*, 428.
- (36) Fox, H. W.; Hare, E. F.; Zisman, W. A. *J. Phys. Chem.* **1955**, *59*, 1097.
- (37) Dettre, R. H.; Johnson, R. E., Jr. *J. Phys. Chem.* **1965**, *69*, 1507.
- (38) Cassie, A. B. O. *Discuss. Faraday Soc.* **1948**, *3*, 11.
- (39) Czanderna, A. W.; King, D. E.; Spaulding, D. J. *Vac. Sci. Technol.* **1991**, *A9*, 2607-13.
- (40) Condrate, R. J.; Nakamoto, K. *J. Chem. Phys.* **1965**, *42*, 2590-8.
- (41) Nakamoto, K. *Infrared and Raman Spectra of Inorganic and Coordination Compounds*; Third ed.; Wiley: New York, NY, 1978, pp 269.
- (42) Smith, E. L.; Alves, C. A.; Anderegg, J. W.; Porter, M. D.; Siperko, L. M. *Langmuir* **1992**, submitted.
- (43) The spectra of the bulk salts were run *immediately* after purification by recrystallization. The amounts of unreacted acid, as measured by intensity of the carbonyl, decreased but never disappeared. Given that the association constants for *n*-alkanoic acids with

$\text{Cu}^{2+}_{(\text{aq})}$  are only  $\sim 10^2$  (Martell, A. E. *Stability Constants of Metal-Ion Complexes. II. Organic Ligands*. Metcalfe: London, 1964), it does not seem unreasonable to expect some decomposition.

- (44) Smith, E. L.; Porter, M. D. *J. Chem. Phys.* in preparation.
- (45) Maroncelli, M.; Qi, S. P.; Strauss, H. L.; Snyder, R. G. *J. Am. Chem. Soc.* **1982**, *104*, 6237-6247.
- (46) Tompkins, H. G.; Allara, D. L. *J. Coll. Interface Science* **1974**, *47*, 697.
- (47) Allara, D. L. In *Vibrational Spectroscopies for Adsorbed Species*; A. T. Bell and M. L. Hair, Ed.; American Chemical Society: Washington, D.C., 1980; Vol. 137; pp 37-49.
- (48) Bellamy, L. J.; Branch, R. F. *J. Chem. Soc.* **1954**, 4491-9.
- (49) Fujita, J.; Martell, A. E.; Nakamoto, K. *J. Chem. Phys.* **1962**, *36*, 324-31.
- (50) Greenler, R. G. *J. Chem. Phys.* **1966**, *44*, 310-15.
- (51) Canning, N. D. S.; Madix, R. J. *J. Phys. Chem.* **1984**, *88*, 2437-46.
- (52) Doedens, R. J. *Prog. Inorg. Chem.* **1976**, *21*, 209.
- (53) Oldham, C. *Prog. Inorg. Chem.* **1968**, 223-258.
- (54) Wyckoff, R. W. G. *Crystal Structures*; second ed.; Wiley: New York, 1963; Vol. 1.
- (55) Snyder, R. G.; Hsu, S. L.; Krimm, S. *Spectrochim. Acta, Part A* **1978**, *34A*, 395-406.
- (56) Snyder, R. G.; Strauss, H. L.; Elliger, C. A. *J. Phys. Chem.* **1982**, *86*, 5145-50.
- (57) Greenler, R. G. *J. Chem. Phys.* **1966**, *44*, 310.
- (58) Mounts, R. D.; Ogura, T.; Fernando, Q. *Inorg. Chem.* **1974**, *13*, 802-805.
- (59) Lamp, B. D.; Porter, M. D. Unpublished results.
- (60) Tingle, E. D. *Trans. Faraday Soc.* **1950**, *46*, 93-102.
- (61) Widrig, C. A.; Alves, C. A.; Porter, M. D. *J. Am. Chem. Soc.* **1991**, *113*, 2805-10 and references therein.
- (62) Hallmark, V. M.; Chiang, S.; Rabolt, J. F.; Swalen, J. D.; Wilson, R. *J. Phys. Rev. Lett.* **1987**, *59*, 2879-82.
- (63) Borges, G. L.; Samant, M. G.; Ashley, K. *J. Electrochem. Soc.* **1992**, *139*, 1565-1568.



- (64) Kim, H. S.; Zheng, Y. C.; Bryant, P. J. *J. Vac. Sci. Technol. A* **1990**, *8*, 314-316.
- (65) Vook, R. W.; Ho, J. H. *SAMPE Quarterly* **1978**, 7-13.
- (66) Preston, G. D.; Bircumshaw, L. L. *Phil. Mag.* *vii* **1935**, *20*, 706-20.
- (67) Heinemann, K.; Rao, D. B.; Douglass, D. L. *Oxid. Met.* **1975**, *9*, 379.
- (68) Ling, D. T.; Miller, J. N.; Pianetta, P.; Weissman, D. L.; Lindau, I.; Spicer, W. E. *J. Vac. Sci. Technol.* **1982**, *21*, 47-49 and references therein.

**PAPER II**

**SERENDIPITOUS DISCOVERY OF MULTILAYER FILMS OF SHORT  
CHAIN *n*-ALKANOIC ACIDS ASSEMBLED FROM THE GAS PHASE AT  
COPPER**

## INTRODUCTION

Over the previous decades, one of the most widely-studied adsorbate-surface systems has been the *n*-alkanoic acids on the coinage metals (Cu and Ag)<sup>1</sup>. Multilayers of *n*-alkanoic acids can be made by the Langmuir-Blodgett method. This technique is capable of producing crystalline structures for the long chain alkanolic acids ( $\geq 12$  methylene groups, e.g., stearic acid ( $\text{CH}_3(\text{CH}_2)_{16}\text{COOH}$ )), but does not work well for  $n < 12$ , due to failure to form a condensed monolayer film on the water during compression<sup>2</sup>. In spontaneous adsorption techniques, which usually involve a dilute homogeneous solution of the acid under equilibrium conditions, highly ordered crystalline monolayers have been obtained only with the long chain alkanolic acids.

Our interest in organic thin films stems from their applicability to adhesion modeling at the polymer-metal interface. By systematically examining the conditions that control the formation and structure of these films, the interactions critical to the chemistry of adhesion can be delineated<sup>3</sup>. However, with more reactive metals such as Ag and Cu, self-assembly of long-chain *n*-alkanoic acids from ethanolic solution leads to corrosion of the metal surface before a good quality monolayer can form.

We recently embarked on a series of gas phase self-assembly experiments of polar, amphiphobic molecules at a variety of metal surfaces. Potential advantages of this technique are: ease of use, elimination of the need for vigorous rinsing after emersion, and no worries about solvent impurities. To date, gas phase self-assembly at Cu has been studied in ultrahigh vacuum (UHV)<sup>4,5</sup> but at ambient pressures monolayer formation has only just begun to be explored fully<sup>3,6-8</sup>. Studies of the reaction chemistry upon adsorption are particularly important to ensure that monolayer formation, and not bulk deposition, is occurring. Also, the possibility of using gas-phase adsorption to make assemblages not accessible from solution has

not yet been developed. This work presents the discovery of ordered, easily characterized self-assembled multilayer structures on the native oxide of copper.

This study includes optical ellipsometry, contact angle and grazing incidence reflection infrared (IR) spectroscopic evidence for the spontaneous adsorption of multilayer films of *n*-alkanoic acids,  $(\text{CH}_3(\text{CH}_2)_n\text{COOH}, n=0-9)$  assembled as gas phase molecules from the laboratory ambient, on copper substrates. Because of their relevance to adhesion studies at the metal-fluoropolymer interface, we have also studied multilayer films formed by perfluorononanoic acid at Cu, and multicomponent films formed from mixtures of *n*-alkanoic acids and perfluoroacids at Cu. The IR spectra show that, as in solution self assembly, the films spontaneously adsorbed from the gas phase form by reactive chemisorption to yield a carboxylate salt. The IR spectra also indicate a high degree of order in these films, by the intensity of the progression bands for methylene wags, as well as by the low relative absorbance of the symmetric and asymmetric methylene stretches ( $\nu_s(\text{CH}_2)$  and  $\nu_a(\text{CH}_2)$ , respectively). Assignments of the IR modes are made by isotope studies and comparisons to literature precedents. Comparisons are made to the gas phase self-assembly of monolayers of *n*-alkanoic acids at Ag and the solution assembly of monolayers of *n*-alkanoic acids at Cu.

Self-assembly from the gas phase of both *n*-alkanoic acids and *n*-perfluoroalkanoic acids give multilayer structures which are on the order of tens of monolayers thick, as demonstrated by IRS and ellipsometry. Contact angle (wettability) results show that these films are comparable in surface free energy to their monomolecular analogues. Further, oleophobic multilayers containing more than one component (mixed multilayers) can be produced by adsorption of one type of acid followed by adsorption of a second acid, resulting in a film with highly ordered structure but surprisingly low wettability.

## EXPERIMENTAL SECTION

### Sample preparation

The substrates were prepared by the resistive evaporation of 300 nm of Cu onto silicon using an Edwards 306A cryopumped evaporator. The Cu-coated silicon substrates were used for optical ellipsometry, IRS and wettability characterizations, and were prepared by cutting 4 inch Si(100) wafers into 1 x 3 inch plates. The substrates were rinsed thoroughly with absolute ethanol before loading into the coating system. The silicon substrates were primed with a ~10 nm layer of Cr prior to Cu deposition. The pressure during all depositions was less than  $1 \times 10^{-6}$  torr. The Cu and Cr deposition rates were 0.3 and 0.2 nm/s, respectively.

Monolayers were formed for comparative purposes by self-assembly from solution. They were prepared by immersion of freshly evaporated Cu substrates into 1 mM hexadecane solutions of the monolayer precursor (all *n*-alkanoic acids Aldrich, hexanoic acid-methyl-d<sub>3</sub>, Cambridge Isotope Laboratories, nonanoic acid-d<sub>17</sub>, MSD Isotopes, perfluorononanoic acid, Columbia Organic Chem.). The solid acids were recrystallized once in methanol; the liquid acids were used as received. Immersion times varied from a few minutes for the shortest chains to a few hours for the longest. Upon removal from solution, the samples were rinsed thoroughly with hexane and dried on a spin coater.

Multilayers were formed from the gas phase by placing freshly evaporated Cu substrates into a glass petri dish containing 1-2 drops (or a few hundred milligrams if solid) of the acid of interest. Samples were removed every few hours or days and characterized by IRS to monitor the course of the reaction; fresh acid was added as needed to replenish that lost by evaporation. Hence, the samples were continuously exposed to the vapor phase acid. No special effort was made to control humidity or temperature. Upon removal from the vapor-phase reaction chamber, the samples were allowed to air for a few minutes before characterization in order to ensure evaporation of any unreacted acid.

## **Instrumentation**

### **Contact angle measurements**

Advancing contact angles ( $\theta_a$ ) in air were measured with a Ramé-Hart Model 100-00 115 goniometer. Hexadecane, methylene iodide, glycerol and water were used as probe liquids. For these measurements, a 2  $\mu$ L droplet was formed on the substrate with the needle of the syringe in the droplet. The value of  $\theta_a$  was determined as the volume of the droplet was slowly increased. Full details of this measurement have been given previously<sup>9</sup>.

### **Infrared spectroscopy**

Infrared spectra were acquired with a Nicolet 740 FT-IR interferometer. Monolayer and multilayer spectra were obtained using p-polarized light incident at 80° with respect to the surface normal, and are reported as  $-\log(R/R_0)$ , where  $R$  is the reflectance of the sample and  $R_0$  is the reflectance of a reference octadecanethiolate-d<sub>37</sub> monolayer at Au. A home-built sample holder was used to position the substrates in the spectrometer<sup>10</sup>. Both sample and reference reflectances are the average of 1024 scans. Monolayer and multilayer reflectance spectra were collected at 2  $\text{cm}^{-1}$  resolution (zero filled) with Happ-Genzel apodization. Spectra of the bulk liquid *n*-alkanoic acids were collected at 4  $\text{cm}^{-1}$  resolution using a ZnSe internal reflectance (ATR) cell (Harrick), as the average of 64 scans. Liquid N<sub>2</sub> cooled HgCdTe and InSb detectors were used, depending on the spectral region of interest. The spectrometer and sample chamber were both purged with boil-off from liquid N<sub>2</sub>. Further details of these methods as well as the preparation of the reference substrates are given elsewhere<sup>9</sup>.

## RESULTS AND DISCUSSION

### Ellipsometry

The ellipsometric data indicate that film thicknesses increase with increased assembly time. Film thicknesses were typically a few hundred Å. Film thicknesses varied greatly across the substrate, with greatest thickness obtained for regions of the sample which were closest to the acid droplet or powder, *i.e.*, the areas which experienced the greatest gas phase acid molecule flux. This result implies that the gas phase in the reaction vessels was not saturated with acid molecules, since if the gas phase above the samples were saturated, a uniformly thick film would be obtained.

### Contact angle measurements for *n*-alkanoic acids/Cu

The advancing contact angles ( $\theta_a$ ) for the *n*-nonanoic acid multilayer self-assembled at Cu from the gas phase are given in Table 1 for the probe liquids hexadecane, methylene iodide, glycerol, and water. The uncertainty in these data is  $\pm 2^\circ$ .  $\theta_a$  values were  $\sim 110^\circ$  for water and  $\sim 45^\circ$  for hexadecane, higher than their solution-formed analogues and comparable to values obtained for long-chain methyl-terminated *n*-alkyl monolayers at a variety of metal surfaces<sup>9,11,12</sup>.

The perfluorononanoic acid multilayer gave advancing contact angle values which were, within experimental error, the same as for a perfluorononanoic acid monolayer at copper. All data were consistent with previously published reports of perfluoroacid monolayers<sup>13</sup>. The advancing contact angles could not be measured for water for any multilayer structure containing a perfluoroacid. This is attributed to the more highly ionic character of the Cu-perfluorononanoate bond, leading to dissolution of the films. The advancing contact angle for glycerol on the perfluorononanoate multilayer film is lower than the advancing contact angle for the analogous monolayer. This may be due to the defective nature of the multilayer film, reflecting only partial

Table 1. Advancing contact angles for multilayer systems: comparison with monolayers

Sample	Probe Liquid			
	Hexadecane	CH <sub>2</sub> I <sub>2</sub>	Glycerol	Water
<i>n</i> -Nonanoic acid monolayer	38.2	72.1	96.2	107.3
<i>n</i> -Octadecanoic acid monolayer	47.4	80.3	101.4	113.8
Perfluorononanoic acid monolayer	75.0	109.5	118.4	119.5
<i>n</i> -Nonanoic acid multilayer	44.7	74.2	99.7	110.3
Perfluorononanoic acid multilayer	76.2	113.2	108.3	a
<i>n</i> -acid after Perfluoroacid multilayer	78.4	106.6	111.4	a
Perfluoroacid after <i>n</i> -acid multilayer	83.9	104.5	114.8	a

<sup>a</sup>Could not be measured - see text.



dissolution. We attempted to measure receding contact angles but they were generally very low and poorly reproducible, as seen for gas phase self-assembled monolayers at Ag<sup>3</sup>.

### IR spectra of multilayers of *n*-alkanoic acids/Cu

#### General observations and mode assignments

The infrared spectra are shown in Figures 1 to 4. The peak positions and mode assignments are presented in Table 2. Absorbances vary from sample to sample, and increased with increasing reaction time, confirming the trend suggested by ellipsometry of continuous film formation. The spectra contain several important structural signatures of the monolayer assembly that are relevant to molecular orientation, interfacial chemistry, alkyl chain conformation, and crystallinity. From the spectra we conclude that (1) the alkyl chains are in a crystalline environment oriented approximately 14° from the surface normal; (2) there are no detectable hydrocarbon impurities incorporated in the longer chain films; (3) the acid head group dissociatively chemisorbs at the surface to form a carboxylate species with a specific orientation; and (4) the alkyl chains are extended planar zig-zag structures. Detailed discussions of these points are presented below.

The infrared reflection spectrum in the C-H stretching region between 3000 and 2800 cm<sup>-1</sup> for the nonanoic acid multilayer self assembled from the gas phase at Cu is shown in Figure 1a. Peak positions for all the *n*-alkanoic acid multilayers at Cu are tabulated in Table 2. For  $n \geq 5$ , five bands are observed and are ascribed, in order of descending energy, to  $\nu_a(\text{CH}_3, \text{ip})$ ,  $\nu_s(\text{CH}_3, \text{FR}_1)$ ,  $\nu_a(\text{CH}_2)$ ,  $\nu_s(\text{CH}_3, \text{FR}_2)$ , and  $\nu_s(\text{CH}_2)$ . For shorter chains  $n \leq 4$ , the  $\nu_s(\text{CH}_3, \text{FR}_1)$  mode is seen as a shoulder on the  $\nu_a(\text{CH}_2)$ . The Fermi-resonance couplet,  $\nu_s(\text{CH}_3, \text{FR}_1)$  and  $\nu_s(\text{CH}_3, \text{FR}_2)$ , is designated by the subscripts 1 and 2, which refer to the higher and lower energy components, respectively. These assignments have been discussed in earlier studies of *n*-alkanethiolate monolayers<sup>14,15</sup> and are based on a number of in-depth

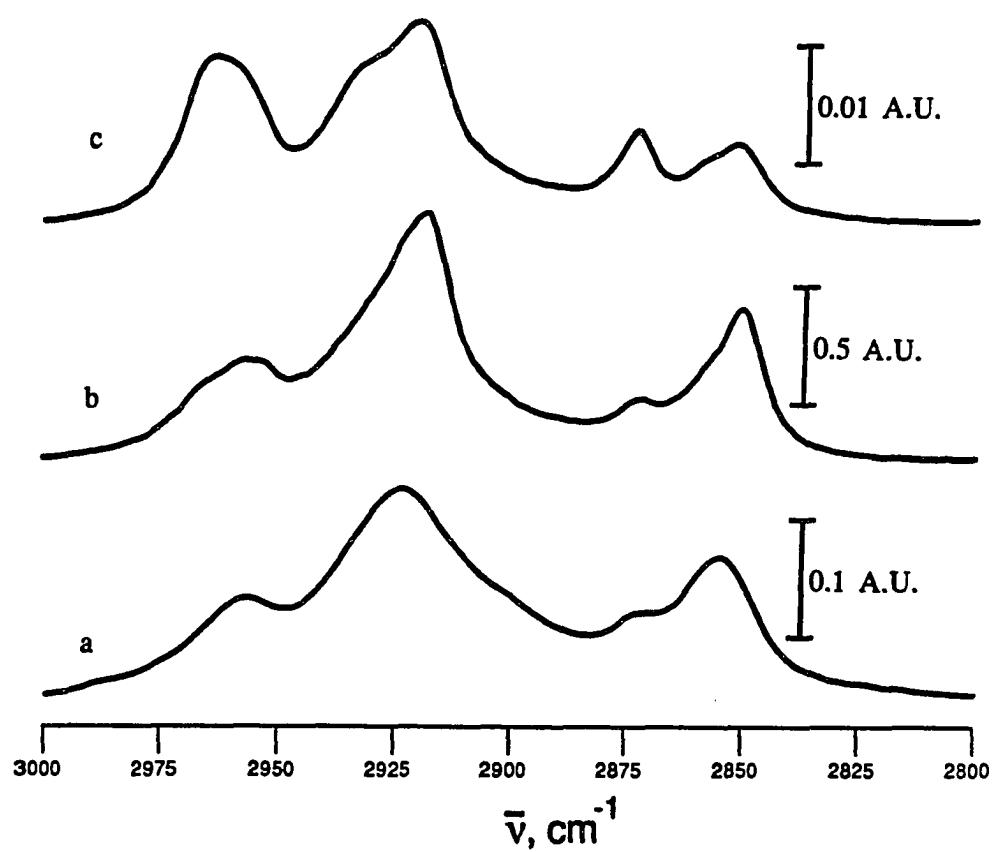


Figure 1. Infrared reflection spectra (high energy region) of (a) *n*-nonanoate multilayer,  $\text{CH}_3(\text{CH}_2)_7\text{COOH}$ , self-assembled from the gas-phase at Cu, (b) Cu(II) nonanoate in KBr, and (c) liquid nonanoic acid.

Table 2. Assignments of peak positions for spontaneously adsorbed multilayers of *n*-alkanoic acids from the gas phase at Cu

Vibrational mode	Gas phase <i>n</i> -alkanoic acid multilayers on Cu, peak position (cm <sup>-1</sup> )									d <sub>17</sub> -Nonanoate	Methyl-d <sub>3</sub> -hexanoate
	n (number of CH <sub>2</sub> units)									on Cu, peak	on Cu, peak position
	n=0	1	2	3	4	5	6	7	8	n=7	n=4
$\nu_a(\text{CH}_3, \text{ip})$	a	a	2968	2966	2964	2957	2961	2964	2963		
$\nu_s(\text{CH}_3, \text{FR}_1)$	a	a	2927	2933	2933	2930	2930	2929	2930sh		
$\nu_a(\text{CH}_2)$	-	2920	-	-	-	2918sh	2922	2920	2919		
$\nu_s(\text{CH}_3, \text{FR}_2)$	-	2879	2873	2874	2878	2873	2872	2873	2873		
$\nu_s(\text{CH}_2)$	-	-	-	-	-	2857	2852	2851	2850		
$\nu_a(\text{COO}^-)$	1570	1589	1586	1582	1588	1588	1588	1588	1587	1580	1589
Unidentified	-	1513	1516	1510	1509	1508	1510	1508	1509	1503	1511
carboxylate mode											
at ~1510 cm <sup>-1</sup>											
$\nu_s(\text{COO}^-)$	1435	1432	1443	1449	1435	1435	1436	1438	1433	1432	1437
$\delta(\text{CH}_2)^b$	-	1462	1464	1470,	1454	1447,	1463	1464	1467	1476	1458
				1460		1464					

Table 2 continued

$\delta(\text{C}_\alpha\text{H}_2)^b$	-	-	-	1417	1410	1418	1416	1417	1418		1419
$\delta(\text{CH}_3)$	-	1373	1381	1373	1378	1373	1378	1370	1379		not observed
Unidentified mode						1406	1407	1403	1404		1419
$\omega(\text{CH}_2)$ k=1		1375	1349	1319	1294	1274	1259	1249	1241		1291
k=3				1363	1346	1324	1306	1287	1276		1346
k=5						1358	1342	1327	1314		
k=7								1353	1341		
$\nu(\text{C}_\alpha\text{-COO}^-)$	1342	1305	1267	1243	1230	1220	1214	1209	1205	1211	1224
Other		1304	1244	1201	1367	1256	1242	1232	1301	1230	1367
skeletal modes		1244		1228	1330	1306	1330	1313	1331	1211	1330
					1272		1366		1362	1161	1312
					1230					1143	1167
					1192						
	1049	1078	1106	1109	1111	1112	1114	1115	1115	1117	1119

<sup>a</sup>For n=0,1, two peaks corresponding to  $\nu_a(\text{CH}_3)$  and  $\nu_s(\text{CH}_3)$  are seen at 2988 and 2942  $\text{cm}^{-1}$ , respectively, for acetic acid, and 2975 and 2942  $\text{cm}^{-1}$ , respectively, for propionic acid multilayers.

<sup>b</sup>Seen as a shoulder on  $\nu_s(\text{COO}^-)$ .

studies of the IR spectroscopy of hydrocarbons<sup>16,17</sup>.

In comparison to spectra of solution assembled monolayers, the multilayer spectra are remarkable in both peak positions and intensities. The peak positions for  $\nu_a(\text{CH}_2)$  and  $\nu_s(\text{CH}_2)$  indicate that the alkyl chains are in a crystalline environment, based on in-depth studies of the IR spectroscopy of hydrocarbons<sup>18</sup>. The solution assembled monolayers have  $\nu_a(\text{CH}_2)$  and  $\nu_s(\text{CH}_2)$  at lower, liquid-like peak positions and these modes are more intense. Both factors reveal that gas phase self-assembly yields a higher proportion of alkyl chains in a crystalline-like environment than does solution phase assembly.

Earlier work on self-assembly from solution demonstrated that no hydrocarbon impurities were incorporated into a monolayer film of arachidic acid self-assembled from dilute hexadecane solution at Ag<sup>19</sup>. We tested for the possible adsorption of hydrocarbon-containing impurities from the gas phase using deuterium labeled alkanolic acids. These labelling studies proved to be very useful in the assignment of the IR bands in the low energy region (see Table 2). The labeled monolayers were prepared in the same manner as the *n*-acid films; the C-H stretching regions for *n*-nonanoic acid-*d*<sub>17</sub> and hexanoic acid-methyl-*d*<sub>3</sub> are shown in Figure 2. CD<sub>3</sub>-labeled hexanoic acid and perdeuterononanoic acids were used. For perdeuterononanoic acid/Cu, the absence of C-H stretches in the labeled film indicates that, within detection limits, no hydrocarbon impurity was incorporated in the gas phase assembled nonanoic acid monolayer. Thus at the longer chain lengths, the predominant species is the one of interest.

The IR spectra between 1800 cm<sup>-1</sup> and 1100 cm<sup>-1</sup> for the gas phase adsorbed multilayer of nonanoic acid is shown in Figure 3. Bulk nonanoic acid shows an absorption band near 1705 cm<sup>-1</sup> due to the hydrogen-bonded carboxylic acid group. In the multilayer spectrum, the bands at 1438 and 1588 cm<sup>-1</sup> are attributed to the  $\nu_s(\text{COO}^-)$  and  $\nu_a(\text{COO}^-)$  modes for a carboxylate salt bound to Cu. Comparison must be made to the bulk Cu(II) salt, where it is

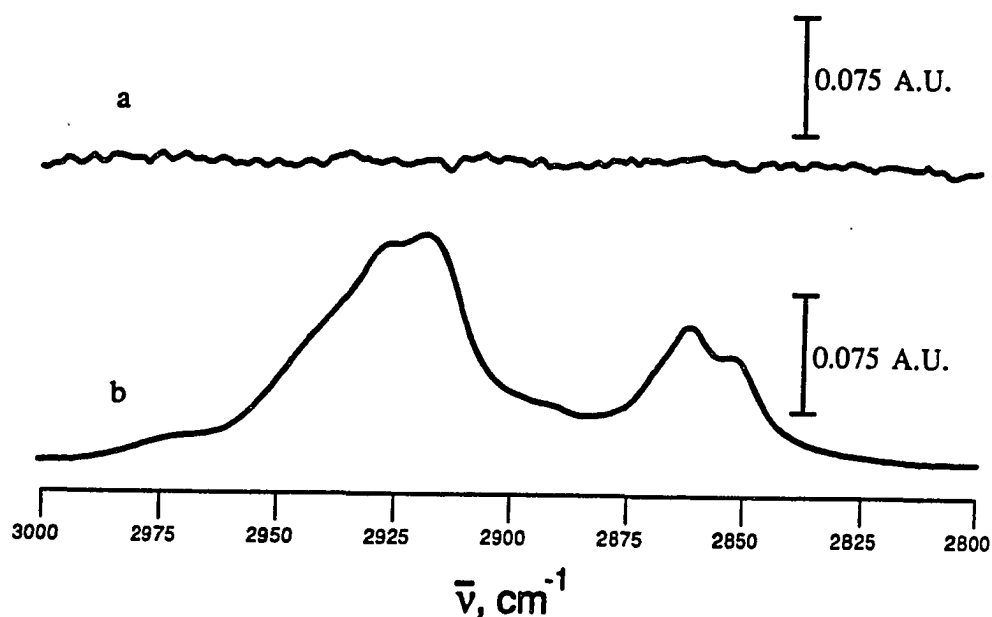


Figure 2. Infrared reflection spectra (high energy region) of multilayers of deuterium labeled alkanolic acids self assembled from the gas phase at Cu. (a) Nonanoic acid-d<sub>17</sub> ( $\text{CD}_3(\text{CD}_2)_7\text{COOH}$ ). No hydrocarbon contamination can be discerned. (b) Hexanoic acid-methyl-d<sub>3</sub> ( $\text{CD}_3(\text{CH}_2)_4\text{COOH}$ ). The major hydrocarbon modes are the methylene stretches. A trace of impurity can be seen in the methyl region of the d<sub>3</sub>-labeled hexanoate film.

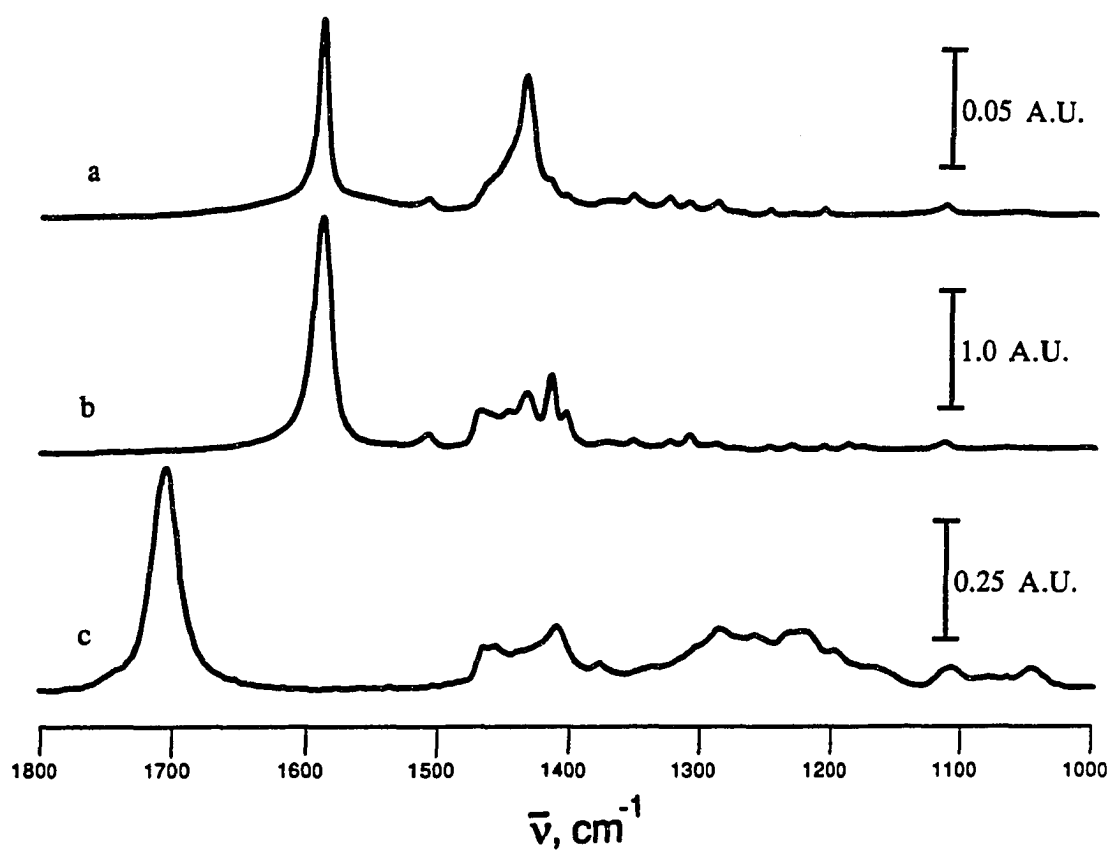


Figure 3. Infrared reflection spectra (low energy region) of (a) *n*-nonanoate multilayer,  $\text{CH}_3(\text{CH}_2)_7\text{COOH}$ , self-assembled from the gas-phase at Cu, (b) Cu(II) nonanoate in KBr, and (c) liquid nonanoic acid.

seen that the  $\nu_a(\text{COO}^-)$  mode is much stronger than the  $\nu_s(\text{COO}^-)$  mode. Because the relative intensity of the  $\nu_a(\text{COO}^-)$  is greatly reduced in the multilayer spectrum, the carboxylate group must be oriented partially towards the surface parallel<sup>20</sup>.

Reactive chemisorption with proton dissociation at the surface is consistent with the mechanism proposed for solution phase self-assembled monolayers of alkanolic acids<sup>21</sup>. The  $\nu_s(\text{COO}^-)$  mode appears at  $1393\text{ cm}^{-1}$  for nonanoic- $\text{d}_{17}$  acid/Cu, indicating that increasing mass of the alkyl chain attached to the carboxylate decreases the energy of the  $\nu_s(\text{COO}^-)$  mode. The mode at  $1510\text{ cm}^{-1}$  is attributable to either the CC skeleton or a carboxylate mode. It is known not to be a hydrocarbon mode because it is present in both the hydrido and perdeutero spectra, Figure 4. Based on its position, it is more probably an asymmetric carboxylate mode. No such mode is observed in the monolayers of *n*-acids at Cu; in those spectra, the  $\nu_a(\text{COO}^-)$  band is much broader, obscuring any weak modes in that region.

### Methyl modes

Once the polymethylene wagging modes were assigned (see below), we looked for a spectral feature at  $1370\text{ cm}^{-1}$ , which could be assigned to the methyl umbrella mode. As shown in Figure 5, a peak is observed between  $1370$  and  $1380\text{ cm}^{-1}$ . This mode alternates between high and low energy. This trend is not manifested in the spectra of the bulk compounds. The variation may be due to the highly ordered nature of the multilayer structure formed. The zig-zagging may arise from different crystal structures for the odd and even chains, as occurs in the bulk *n*-alkanes<sup>22</sup>. Its assignment is confirmed by its absence from the spectrum of  $\text{CD}_3$ -labelled *n*-hexanoate/Cu (Figure 4b).



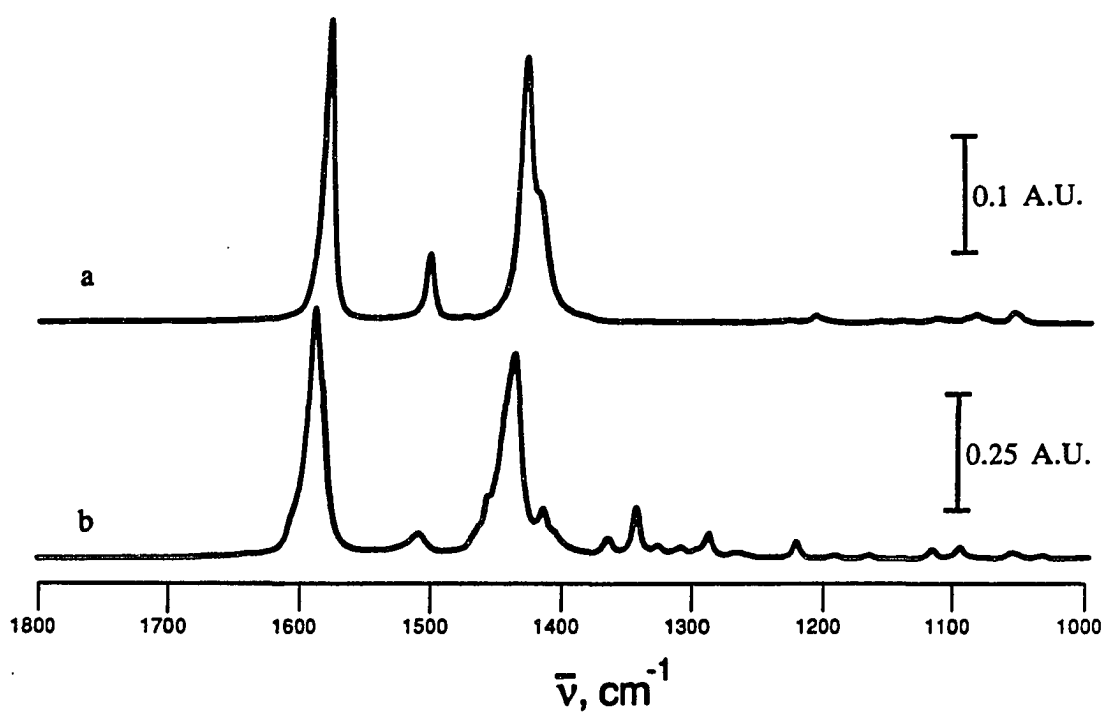


Figure 4. Infrared reflection spectra (low energy region) of multilayers of deuterium labeled alkanolic acids self assembled from the gas phase at Cu. (a) Nonanoic acid- $\text{d}_{17}$  ( $\text{CD}_3(\text{CD}_2)_7\text{COOH}$ ). No peaks due to hydrocarbon modes can be seen. (b) Hexanoic acid-methyl- $\text{d}_3$  ( $\text{CD}_3(\text{CH}_2)_4\text{COOH}$ ). No peaks attributable to methyl modes are seen.

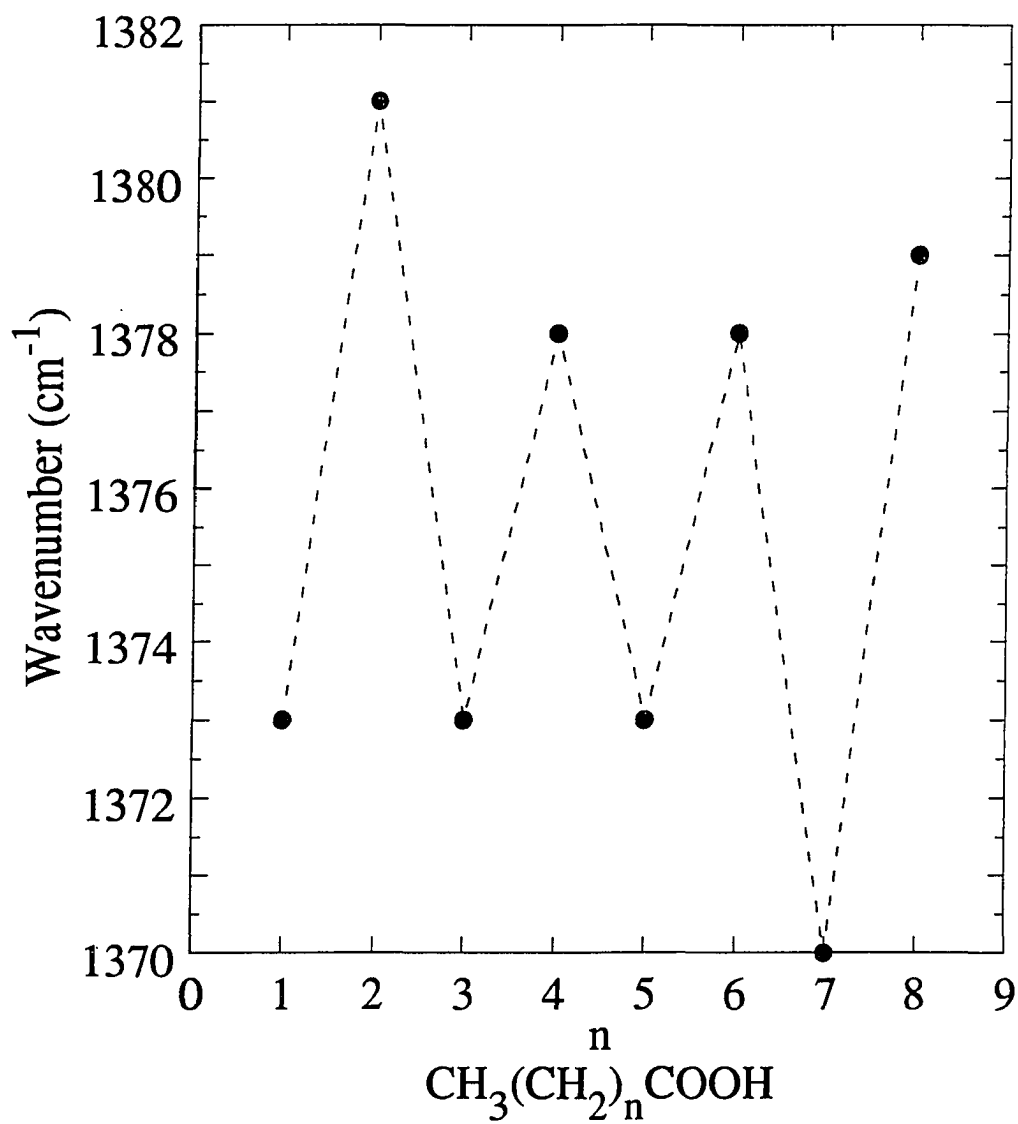


Figure 5. Peak positions for  $\delta(\text{CH}_3)$  in multilayers of *n*-alkanoic acids,  $\text{CH}_3(\text{CH}_2)_n\text{COOH}$ , self-assembled from the gas-phase at Cu.

### Ordering of the polymethylene chain

The weak intensities of both the  $\nu_a(\text{CH}_2)$  and  $\nu_s(\text{CH}_2)$  stretching modes indicate a near normal orientation of the chain axis to the Cu surface. This conclusion is based on the "surface selection rule"<sup>20</sup>, which causes a preferential excitation of vibrational modes with dipoles normal to highly reflecting metallic surfaces. A chain axis exactly normal to a smooth metallic surface plane with no defects in the polymethylene chain has surface-forbidden (zero intensity) methylene C-H modes. The low relative intensities observed for  $\nu_a(\text{CH}_2)$  and  $\nu_s(\text{CH}_2)$  indicate there are very few disordered chains, i.e., most of the monolayer is organized into crystalline domains where the chains have small average tilts. The trend is most pronounced for  $\nu_s(\text{CH}_2)$ , which is more intense than  $\nu_a(\text{CH}_3)$  in the spectra of both the bulk salt and the bulk acid, but is less intense than  $\nu_a(\text{CH}_3)$  in the spectrum of the multilayer film.

### Vibrations of the polymethylene alkyl chain

A spectral feature at  $1467\text{ cm}^{-1}$  attributable to  $\delta(\text{CH}_2)$  or "scissors" mode is seen as a shoulder on high energy side of the  $\nu_s(\text{COO}^-)$  band. The intensity of this mode is weak for a perpendicular surface-chain geometry because the orientation of the transition moment is parallel to the surface (see above). A spectral feature attributable to the polymethylene wagging fundamental<sup>23</sup> was observed as a shoulder at  $1380\text{-}1382\text{ cm}^{-1}$ . A shoulder was also observed at  $1412\text{ cm}^{-1}$ , attributable to the  $\alpha\text{-CH}_2$  deformation,  $\delta(\text{C}_\alpha\text{H}_2)$ . Both the  $\delta(\text{C}_\alpha\text{H}_2)$  and  $\delta(\text{CH}_2)$  modes are readily observed in the bulk salt spectra.

The series of progression bands observed between  $1345\text{-}1220\text{ cm}^{-1}$  is characteristic of an alkyl chain fully extended in an all trans zig-zag conformation. Thus the series of bands between  $1375$  and  $1241\text{ cm}^{-1}$  in Figure 3, which are assigned to the  $\omega(\text{CH}_2)$  (wagging) modes, indicates that the multilayer assembly exhibits this extended conformation. Disordered chains would show end gauche or kink modes at  $1469\text{ cm}^{-1}$ ,  $1366\text{ cm}^{-1}$ ,  $1353\text{ cm}^{-1}$ ,  $1341\text{ cm}^{-1}$ , and  $1300\text{ cm}^{-1}$ <sup>24-26</sup>; no such peaks were observed. This is reasonable as the concentration of

defects approaches zero for short chain alkanes in the bulk<sup>25,26</sup>. The bulk liquid shows localized vibrations associated with short sequences of bonds having a specific conformation<sup>26</sup>, but no specific bands attributable to end gauche modes or kinks. There may be some weak bands between 1380-1200 cm<sup>-1</sup> due to a low concentration of defects, but their detection is precluded by the many wagging modes of the all-*trans* conformer. This region also contains other skeletal modes, *e.g.*, at 1313 cm<sup>-1</sup> for the *n*-nonanoate multilayer.

The assignment of individual peaks and the factors affecting their positions have already been discussed in some detail<sup>3</sup>. For the multilayer assemblies, we observe the intense sharp bands characteristic of the fully extended crystalline alkyl chain. For a particular oscillator mode, methylene wagging modes are slightly higher in energy in this work compared to the monolayers of *n*-acids on Ag. This is attributed to greater polarity of the end group caused by greater ionicity of the carboxylate bound to Cu. We observe the  $\nu(\text{C}_\alpha\text{-COO}^-)$  mode at approximately the same energy on Cu and on Ag. As well, with the improved signal-to-noise ratio obtained for multilayer IR spectra, weak C-C stretches are observed between 1050 and 1350 cm<sup>-1</sup>. As in the earlier alkane studies<sup>23</sup>, there are still some modes that are difficult to assign due to their low intensities.

The selection rules for methylene wagging modes, as derived in previous studies of alkyl chains in *n*-paraffins<sup>18</sup>, and their application to thin *n*-alkanoate films, has recently been discussed<sup>3</sup>. The array of methylene wagging modes is displayed in Figure 6 for the *n*-alkanoic acid multilayers self-assembled from the gas phase at Cu. For both *n*=odd and *n*=even chains at a surface, only the *k*-odd modes are observed. For example, octanoic acid (*n*=6)/Cu has  $6/2 = 3$  modes; nonanoic acid (*n*=7)/Cu has  $(7+1)/2 = 4$  wagging modes.

The assignment of the progression bands was greatly aided by the initial assignment of the C-C<sub>*k*=1</sub> stretching mode. This band, the highest energy band of the C-C stretches, is observed at 1209 cm<sup>-1</sup> for nonanoic acid/Cu. It is assigned to  $\nu(\text{C-C})$  because it is observed in

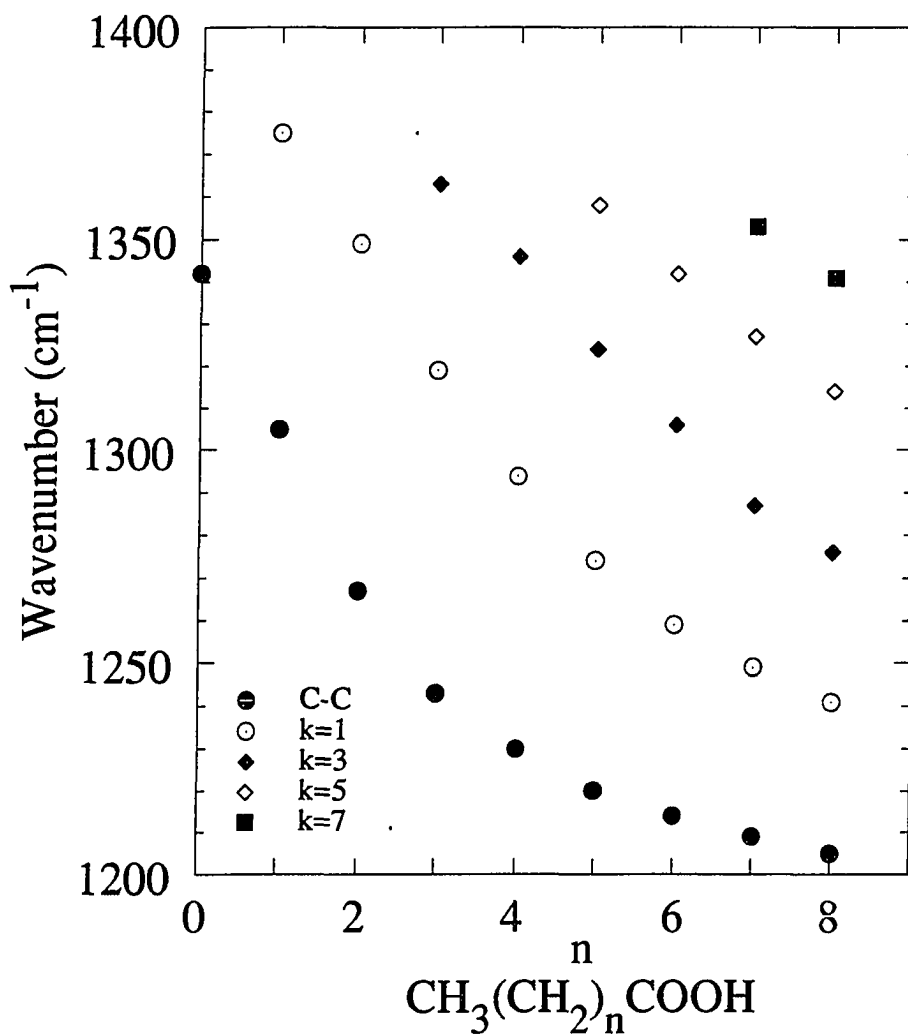


Figure 6. Array of methylene wagging modes and C-C stretching modes for  $n$ -alkanoic acid multilayers self-assembled from the gas phase at Cu.

both the nonanoic acid/Cu and the perdeuterionanoic acid/Cu multilayer, which has no CH<sub>2</sub> modes. The other multilayer studied which has no CH<sub>2</sub> groups is acetic acid/Cu, which has a single peak at 1342 cm<sup>-1</sup>, corresponding to its position as predicted from the trend for  $\nu(\text{C-C})$  as illustrated in Figure 6. The C-C<sub>k=1</sub> mode is observed from 1342 cm<sup>-1</sup> for n=0 to 1205 cm<sup>-1</sup> for n=8. The trend to increasing energy for the C-C mode as chain length decreases is also observed for the C-C<sub>k=1</sub> mode of *n*-alkyl paraffins<sup>23</sup>.

While the progression of wagging modes arises from nonlocalized vibrations, i.e., vibrations involving the entire chain, the C-C<sub>k=1</sub> mode appears to be localized. Because the position of this C-C mode follows a monotonic trend all the way down to acetic acid (n=0), we believe that this relatively high intensity mode is due to vibration of the C-CO<sub>2</sub><sup>-</sup> bond. The carboxylate is a polar end group to the polymethylene chain, and causes energy and intensity of this mode to increase. The band moves to lower energy as the length, i.e., the weight, of the attached alkyl chain increases. Although the spectra suggest other  $\nu(\text{C-C})$  modes at lower energy, these modes are so weak as to be barely distinguishable from the background; no definite assignments could be made.

#### Perfluoro and multicomponent multilayer films

A multilayer film of perfluorononanoate was prepared in the same manner as the *n*-alkanoic acid multilayer films. The ellipsometry results show formation of a film hundreds of Å thick, with the same variability in thickness as the *n*-alkanoic acid films. The IRS peak intensities are also consistent with a film hundreds of Å thick, and show only fluorocarbon chains present at the surface. Assignments of modes are as previously reported<sup>13</sup> with the exception of  $\nu_a(\text{COO}^-)$  at 1667 cm<sup>-1</sup> and 1592 cm<sup>-1</sup> and  $\nu_s(\text{COO}^-)$  at 1430 cm<sup>-1</sup>, consistent with formation of a Cu(II) carboxylate salt. A similar splitting of the  $\nu_a(\text{COO}^-)$  modes was previously observed for metal salts of perfluorocarboxylic acids<sup>27</sup>.

Having demonstrated by ellipsometry, advancing contact angle and IR spectroscopy (see above) the nature of the pure multilayer structures, we attempted to construct a multiple phase multilayer consisting of a perfluorocarbon multilayer on top of a hydrocarbon multilayer, or the reverse. This was done by immersing *n*-nonanoate multilayer films into perfluorononanoic acid vapor; the reverse order experiment placing perfluorononanoate multilayer films into the *n*-nonanoic acid vapor were also performed. It was hoped that such a multiple phase film would yield advancing contact angles characteristic of the film which had been deposited last. The advancing contact angle results, while not reflecting the nature of the uppermost multilayer, gave surprising results nonetheless. In both instances, the advancing contact angles measured are very high,  $\sim 78^\circ$  for *n*-nonanoic acid treatment after formation of perfluorononanoate multilayer film at Cu and  $\sim 84^\circ$  for perfluorononanoic acid treatment after formation of an *n*-nonanoate multilayer film at Cu. To the best of our knowledge, these are the highest contact angles ever measured for hexadecane.

The films prepared from mixtures of perfluorononanoic acid and *n*-nonanoic acid show spectral features for both perfluorocarbon and hydrocarbon features, as shown in Figure 7. The spectra are essentially the same regardless of whether perfluorononanoic acid or *n*-nonanoic acid was deposited first, indicating that similar multilayer films are obtained in both cases. In the high energy region, the appearance of the C-H stretching modes is unchanged by the presence of the perfluorocarbon film. In particular, the peak positions remain unchanged and crystalline, with approximately the same intensity as in the pure *n*-nonanoic acid film. This is consistent with the previously demonstrated irreversibility of Cu-carboxylate film formation<sup>28</sup>.

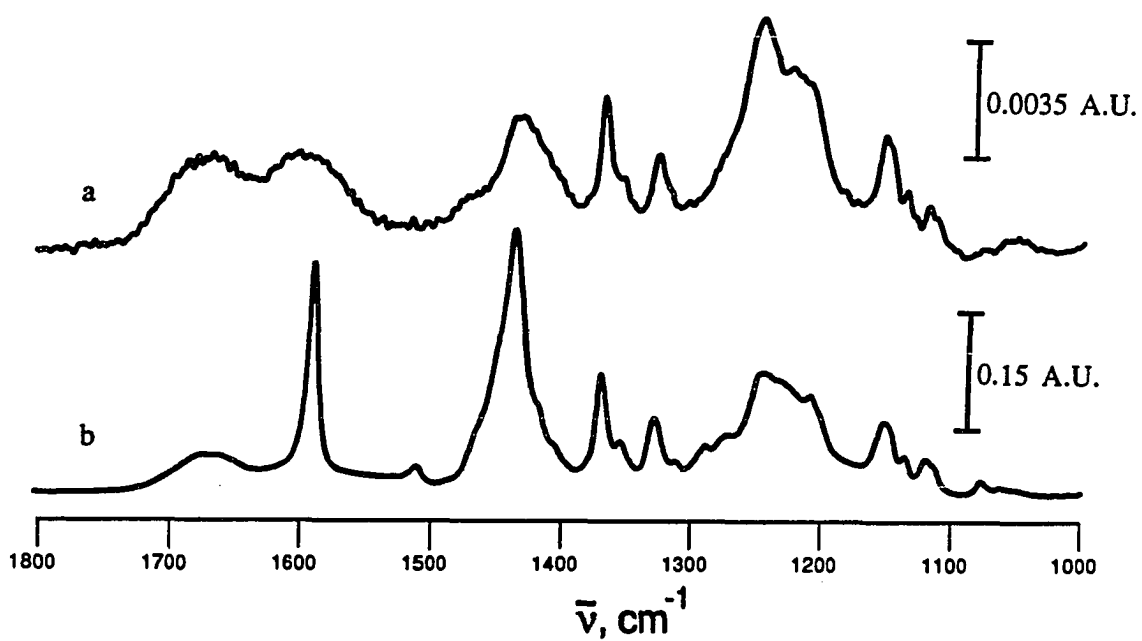


Figure 7. Infrared reflection spectra for (a) perfluorononanoate acid multilayer at Cu, (b) two component multilayer film of perfluorononanoate acid and *n*-nonanoate acid at Cu, formed by gas-phase self assembly of perfluorononanoic acid onto an *n*-nonanoate acid multilayer film at Cu.



## CONCLUSIONS

Ellipsometry, contact angle measurements and infrared reflection spectroscopy indicate that *n*-alkanoic acids adsorb from the gas phase to form multilayer films at Cu. The IR spectra indicate that film formation proceeds via a Cu(II) carboxylate salt, analogous to the bulk compounds. IRS also shows that the multilayers formed are crystalline and ordered. Advancing contact angle data demonstrate that multimolecular films of short chain *n*-alkanoic acids and perfluoroalkanoic acids self-assembled from the gas phase have low wettability, comparable to that of their solution analogs. Further, multicomponent multilayer films in which the crystallinity of the hydrocarbon chains is maintained can be formed with extremely low wettability.

## REFERENCES

- (1) Allara, D. L.; Nuzzo, R. G. *Langmuir* **1985**, *1*, 45-52 and references therein.
- (2) Gaines, G. L. *Insoluble Monolayers at Liquid-Gas Interfaces*; Interscience: New York, 1966.
- (3) Smith, E. L.; Porter, M. D. *J. Chem. Phys.* **1992**, submitted, and references therein.
- (4) Dubois, L. H.; Zegarski, B. R.; Nuzzo, R. G. *Langmuir* **1986**, *2*, 412-7.
- (5) Nuzzo, R. G.; Zegarski, B. R.; Dubois, L. H. *J. Am. Chem. Soc.* **1987**, *109*, 2358.
- (6) Thomas, R. C.; Sun, L.; Crooks, R. M.; Ricco, A. J. *Langmuir* **1991**, *7*, 620-622.
- (7) Schneider, T.; Buttry, D. A. *submitted 1992*,
- (8) Cook, H. D.; Ries, H. E. *J. Phys. Chem.* **1959**, *63*, 226-230.
- (9) Walczak, M. M.; Chung, C.; Stole, S. M.; Widrig, C. A.; Porter, M. D. *J. Am. Chem. Soc.* **1991**, *113*, 2370-8.
- (10) Stole, S. M.; Porter, M. D. *Appl. Spectrosc.* **1990**, *49*, 1418-20.
- (11) Bain, E. D.; Whitesides, G. M. *J. Am. Chem. Soc.* **1989**, *111*, 7164-75.
- (12) Nuzzo, R. G.; Dubois, L. H.; Allara, D. L. *J. Am. Chem. Soc.* **1990**, *112*, 558-69.
- (13) Chau, L.-K.; Porter, M. D. *Chem. Phys. Lett.* **1990**, *167*, 198-204.
- (14) Nuzzo, R. G.; Allara, D. L. *J. Am. Chem. Soc.* **1983**, *105*, 4481-83.
- (15) Porter, M. D.; Bright, T. B.; Allara, D. L.; Chidsey, C. E. D. *J. Am. Chem. Soc.* **1987**, *109*, 3559-68.
- (16) Snyder, R. G.; Hsu, S. L.; Krimm, S. *Spectrochim. Acta, Part A* **1978**, *34A*, 395-406.

- (17) Snyder, R. G.; Strauss, H. L.; Elliger, C. A. *J. Phys. Chem.* **1982**, *86*, 5145-50.
- (18) Snyder, R. G. *J. Molecular Spectroscopy* **1960**, *4*, 411-434.
- (19) Schlotter, N. E.; Porter, M. D.; Bright, T. B.; Allara, D. L. *Chem. Phys. Lett.* **1986**, *132*, 93-98.
- (20) Greenler, R. G. *J. Chem. Phys.* **1966**, *44*, 310-15.
- (21) Smith, E. L.; Franek, J. E.; Porter, M. D. *Langmuir* **1992**, in preparation.
- (22) Smith, A. E. *J. Phys. Chem.* **1953**, *21*, 2229-31.
- (23) Snyder, R. G.; Schachtschneider, J. H. *Spectrochimica Acta* **1963**, *19*, 85-116.
- (24) Hagemann, H.; Strauss, H. L.; Snyder, R. G. *Macromolecules* **1987**, *20*, 2810-2819.
- (25) Maroncelli, M.; Qi, S. P.; Strauss, H. L.; Snyder, R. G. *J. Am. Chem. Soc.* **1982**, *104*, 6237-6247.
- (26) Snyder, R. G. *J. Chem. Phys.* **1967**, *47*, 1316.
- (27) Lines, D.; Sutcliffe, H. *J. Fluorine Chem.* **1984**, *25*, 505-512.
- (28) Young, J. E. *Austr. J. Chem.* **1955**, *8*, 173-93.

**PAPER III**

**FORMATION, STRUCTURE AND WETTABILITY OF SHORT CHAIN  
*n*-ALKANOIC ACIDS ASSEMBLED FROM THE GAS PHASE AT SILVER**

## INTRODUCTION

Ordered monomolecular arrays of polar, amphiphobic molecules supported at metal surfaces have been studied for a long time<sup>1</sup>. In recent years, monolayers of *n*-alkylthiols self-assembled at Au have received a great deal of attention<sup>2,3</sup>, due to the ease of preparing high quality, reproducible Au surfaces which react readily with S-containing molecules and little else, yielding stable monolayers. To a large degree, the adsorbate-metal system that has received the greatest amount of study over the decades has been the *n*-alkanoic acids<sup>4</sup>. Monolayers of *n*-alkanoic acids can be made either by spontaneous adsorption from solution or by the Langmuir-Blodgett method. Both techniques are capable of producing crystalline structures, particularly with the long chain alkanolic acids ( $\geq 12$  methylene groups, e.g., stearic acid ( $\text{CH}_3(\text{CH}_2)_{16}\text{COOH}$ )). In spontaneous adsorption, which usually takes place from a dilute homogeneous solution under equilibrium conditions, solvent effects such as desorption of the monolayer, corrosion of the metal substrate, and the need to remove the solvent by vigorous and potentially destructive techniques such as rinsing with other solvents can degrade the quality of the monolayer formed<sup>5,6</sup>. This is the origin of the requirement for long alkyl chains to form high quality monolayers. Although bulk phase *n*-alkanoic acids are crystalline solids regardless of chain length, highly ordered crystalline monolayers have been obtained only with the long alkyl chain acids.

Our interest in monolayers stems from their applicability to adhesion modeling at the polymer-metal interface. By systematically examining the conditions that control the formation and structure of these monomolecular films, the interactions critical to the chemistry of adhesion can be delineated. In our studies of a variety of monolayer systems self-assembled from solution, we have found that the solvent plays an important role. The nature of the solvent has already been shown to affect the properties of thiolate monolayers on gold<sup>7</sup>. For example, at Au, good quality alkanethiolate monolayers can be obtained from a variety of

solvents such as hexadecane, ethanol, acetonitrile, isooctane, chloroform, acetone and tetrahydrofuran.<sup>5,7-9</sup> However, with more reactive metals such as Ag and Cu, self-assembly of long-chain *n*-alkanoic acids from ethanolic solution leads to corrosion of the metal surface before a good quality monolayer can form. Some solvents, such as benzene, partially dissolve monolayers formed under other solvents<sup>10</sup>. Better quality monolayers of long-chain alkanolic acids can be formed from the nonpolar paraffinic solvent hexadecane than from ethanol. However, corrosion of the metal substrate was still observed for the short chain acids in hexadecane solution. Based on a comparison of the solubilities of their acid precursors (in which the shorter chain monolayers have the greater solubility), we attributed this effect to dissolution of the monolayer. Changing to a solvent even less polar than hexadecane to avoid this corrosion is not feasible due to limited solubility of the monolayer precursors. Hence, the solvent itself presents barriers to effective monolayer formation.

Due to these solvent-related problems, we decided to study the feasibility of using the gas phase for monolayer formation of the short chain alkanolic acids, based on their volatility. Potential advantages of this technique are: ease of use, elimination of the need for vigorous rinsing after immersion, and no worries about solvent impurities. To date, gas phase self-assembly has been studied in ultrahigh vacuum (UHV)<sup>11,12</sup> but at ambient pressures monolayer formation has been explored in only a cursory fashion<sup>5,13,14</sup>. Studies of the reaction chemistry upon adsorption are particularly important to ensure that monolayer formation, and not bulk deposition, is occurring. Also, the possibility of using gas-phase adsorption to make assemblages not accessible from solution has not yet been developed.

This study provides contact angle and grazing incidence reflection infrared (IR) spectroscopic evidence for a close correspondence between the structure of spontaneous adsorption monolayer films of *n*-alkanoic acids,  $(\text{CH}_3(\text{CH}_2)_n\text{COOH}, n=0-9)$  assembled from solution with those assembled as gas phase molecules from the laboratory ambient, on silver substrates. Other systems are also briefly discussed. The IR data show that, as in solution,

the film spontaneously adsorbed from the gas phase forms by reactive chemisorption to yield a carboxylate salt. Monitoring the gas phase self-assembly over the course of time demonstrates growth to an optimum film.

## EXPERIMENTAL SECTION

### Sample preparation

The substrates were prepared by the resistive evaporation of 300 nm of Ag onto silicon using an Edwards 306A cryopumped evaporator. The Ag-coated silicon substrates were used for IRS and wettability characterizations, and were prepared by cutting 4 inch Si(100) wafers into 1 x 3 inch plates. The substrates were rinsed thoroughly with absolute ethanol before loading into the coating system. The silicon substrates were primed with a ~10 nm layer of Cr prior to Ag deposition. The pressure during all depositions was less than  $1 \times 10^{-6}$  torr. The Ag and Cr deposition rates were 0.3 and 0.2 nm/s, respectively.

Monolayers formed by self-assembly from solution were prepared by immersion of freshly evaporated Ag substrates into 1 mM hexadecane solutions of the *n*-alkanoic acid (all acids Aldrich). The solid acids were recrystallized once in methanol; the liquid acids were used as received. Immersion times varied from a few minutes for the shortest chains to a few hours for the longest. Upon removal from solution, the samples were rinsed thoroughly with hexane and dried on a spin coater.

Monolayers were formed from the gas phase by placing freshly evaporated Ag substrates into a glass petri dish containing 1-2 drops of the acid of interest. Samples were removed every few days and characterized by IRS to monitor the course of the reaction; fresh acid was added as needed to replenish that lost by evaporation. Upon removal, the samples were allowed to dry in air for a few minutes before characterization to ensure evaporation of any unreacted acid.



## **Instrumentation**

### **Contact angle measurements**

Advancing contact angles ( $\theta_a$ ) in air were measured with a Ramé-Hart Model 100-00 115 goniometer. Hexadecane and water were used as probe liquids. For these measurements, a 2  $\mu\text{L}$  droplet was formed on the substrate with the needle of the syringe in the droplet. The value of  $\theta_a$  was determined as the volume of the droplet was slowly increased, and  $\theta_r$  as the volume of the droplet was slowly decreased. Full details of this measurement have been given previously<sup>15</sup>.

### **Infrared spectroscopy**

Infrared spectra were acquired with a Nicolet 740 FT-IR interferometer. Monolayer spectra were obtained using p-polarized light incident at  $80^\circ$  with respect to the surface normal, and are reported as  $-\log(R/R_0)$ , where  $R$  is the reflectance of the sample and  $R_0$  is the reflectance of a reference octadecanethiolate- $d_{37}$  monolayer at Au. A home-built sample holder was used to position the substrates in the spectrometer<sup>16</sup>. Both sample and reference reflectances are the average of 1024 scans. Monolayer reflectance spectra were collected at  $2\text{ cm}^{-1}$  resolution (zero filled) with Happ-Genzel apodization. Spectra of the bulk liquid *n*-alkanoic acids were collected at  $4\text{ cm}^{-1}$  resolution using a ZnSe internal reflectance (ATR) cell (Harrick), as the average of 64 scans. Liquid  $\text{N}_2$  cooled HgCdTe and InSb detectors were used, depending on the spectral region of interest. The spectrometer and sample chamber were both purged with boil-off from liquid  $\text{N}_2$ . Further details of these methods as well as the preparation of the reference substrates are given elsewhere<sup>15</sup>.

## RESULTS AND DISCUSSION

### Contact angle measurements for *n*-alkanoic acids/Ag

The results for the advancing contact angles ( $\theta_a$ ) of the *n*-alkanoic acids self-assembled at Ag from the gas phase are shown in Figure 1 for the probe liquids hexadecane, methylene iodide, glycerol, and water. The uncertainty in these data is  $\pm 2^\circ$ . For all probe liquids,  $\theta_a$  increases with *n*. The highest  $\theta_a$  values were measured on monolayers formed from decanoic acid:  $\sim 112^\circ$  for water and  $\sim 47^\circ$  for hexadecane, comparable to long-chain methyl-terminated *n*-alkyl monolayers formed at a variety of metal surfaces<sup>7,15,17</sup>. For simplicity, we refer to a chain with an even number of methylene groups as an "even chain" and a chain with an odd number of methylene groups as an "odd chain". Although the data for the  $\theta_a$  values measured suggest a dependence on whether there is an even or odd number of methylene groups in the alkyl chain (particularly for hexadecane), this effect is within the uncertainty of the measurement. The  $\theta_a$  values measured for monolayers containing even chains are slightly greater than for odd chains, suggesting that the orientation of the terminal methyl group is different for chains with odd and even numbers of methylene groups<sup>7,15,17</sup>. However, the wetting studies do not definitively reveal an odd-even effect. The structure of the monolayer films is discussed further in the IRS section.

The receding contact angles measured were much less reproducible than the advancing contact angles. Receding contact angles were always zero for  $n < 5$ , and were very low and varied greatly for  $n \geq 5$ . This variation was not only from sample to sample but for individual samples as well. This was attributed to dissolution of the monolayer in the probe liquid. These results are probably a reflection of low coverage, which affects the receding contact angle more than the advancing contact angle.

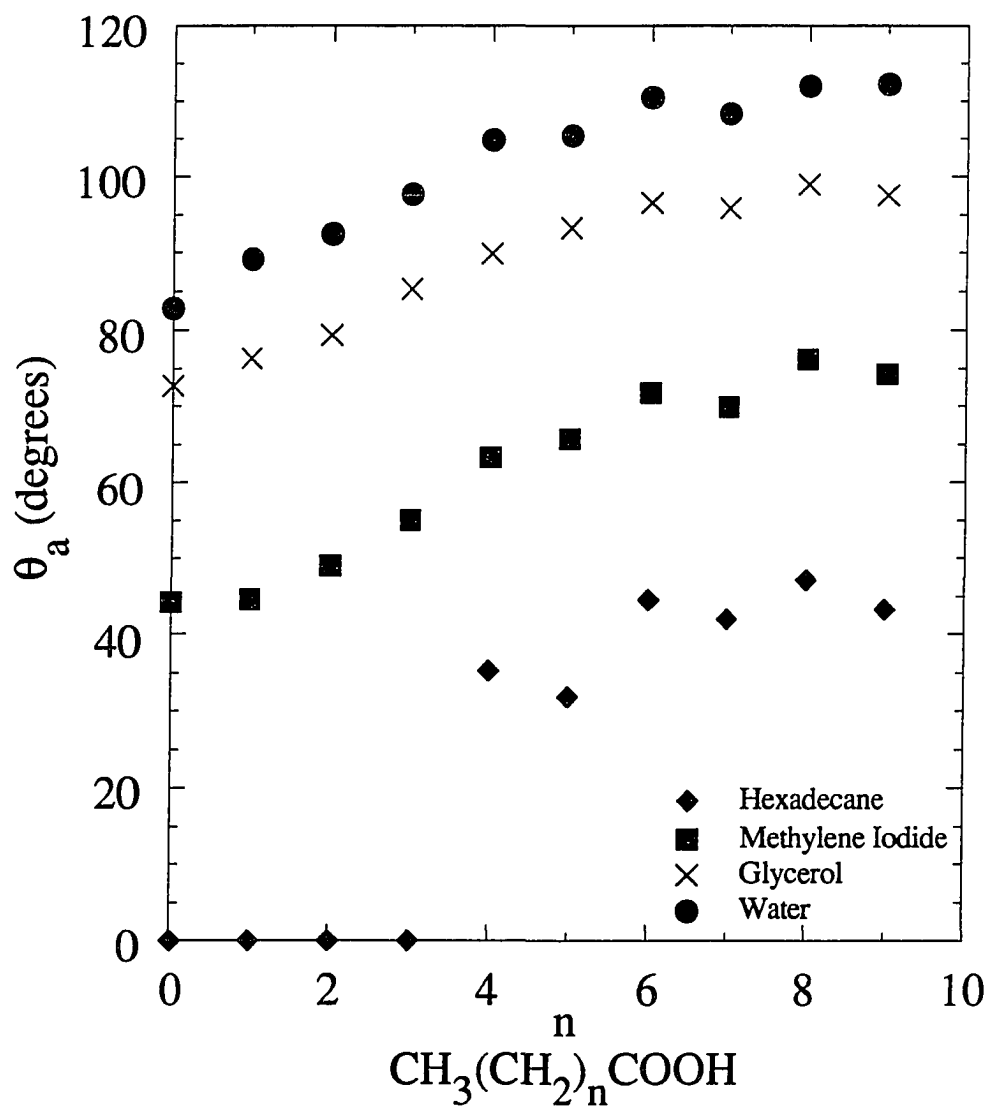


Figure 1. Advancing contact angles for  $n$ -alkanoic acids self-assembled from the gas-phase at Ag, with the probe liquids hexadecane, methylene iodide, glycerol, and water.

## IR spectra of *n*-alkanoic acids/Ag

### General observations and mode assignments

The infrared spectra are shown in Figures 2 to 4 and 7. The peak positions and mode assignments are presented in Table 1. These spectra contain several important structural signatures of the monolayer assembly that are relevant to molecular orientation, interfacial chemistry, alkyl chain conformation, and crystallinity: (1) the alkyl chains are in a crystalline environment oriented approximately  $14^\circ$  from the surface normal; (2) there are no detectable hydrocarbon impurities incorporated in the longer chain films; (3) the acid head group dissociatively chemisorbs at the surface to form a carboxylate species with a specific orientation; and (4) the alkyl chains are extended planar zig-zag structures. Detailed discussions of these points are presented below.

Infrared reflection spectra in the C-H stretching region between  $3000$  and  $2800\text{ cm}^{-1}$  for the *n*-alkanoic acids self assembled from the gas phase at Ag are shown in Figure 2. For  $n \geq 7$ , five bands are observed and are ascribed, in order of descending energy, to  $\nu_a(\text{CH}_3, \text{ip})$ ,  $\nu_s(\text{CH}_3, \text{FR}_1)$ ,  $\nu_a(\text{CH}_2)$ ,  $\nu_s(\text{CH}_3, \text{FR}_2)$ , and  $\nu_s(\text{CH}_2)$ . The Fermi-resonance couplet,  $\nu_s(\text{CH}_3, \text{FR}_1)$  and  $\nu_s(\text{CH}_3, \text{FR}_2)$ , is designated by the subscripts 1 and 2, which refer to the higher and lower energy components, respectively. These assignments have been discussed in earlier studies of *n*-alkanethiolate monolayers<sup>9,18</sup> and are based on a number of in-depth studies of the IR spectroscopy of hydrocarbons<sup>19,20</sup>.

When compared to those of solution assembled monolayers, these spectra are remarkable in both peak positions and intensities. The peak positions for  $\nu_a(\text{CH}_2)$  and  $\nu_s(\text{CH}_2)$  indicate that the alkyl chains are in a crystalline environment, based on in-depth studies of the IR spectroscopy of hydrocarbons<sup>21</sup>. The solution assembled monolayers have  $\nu_a(\text{CH}_2)$  and  $\nu_s(\text{CH}_2)$  with greater intensity at lower, liquid-like peak positions. Both factors

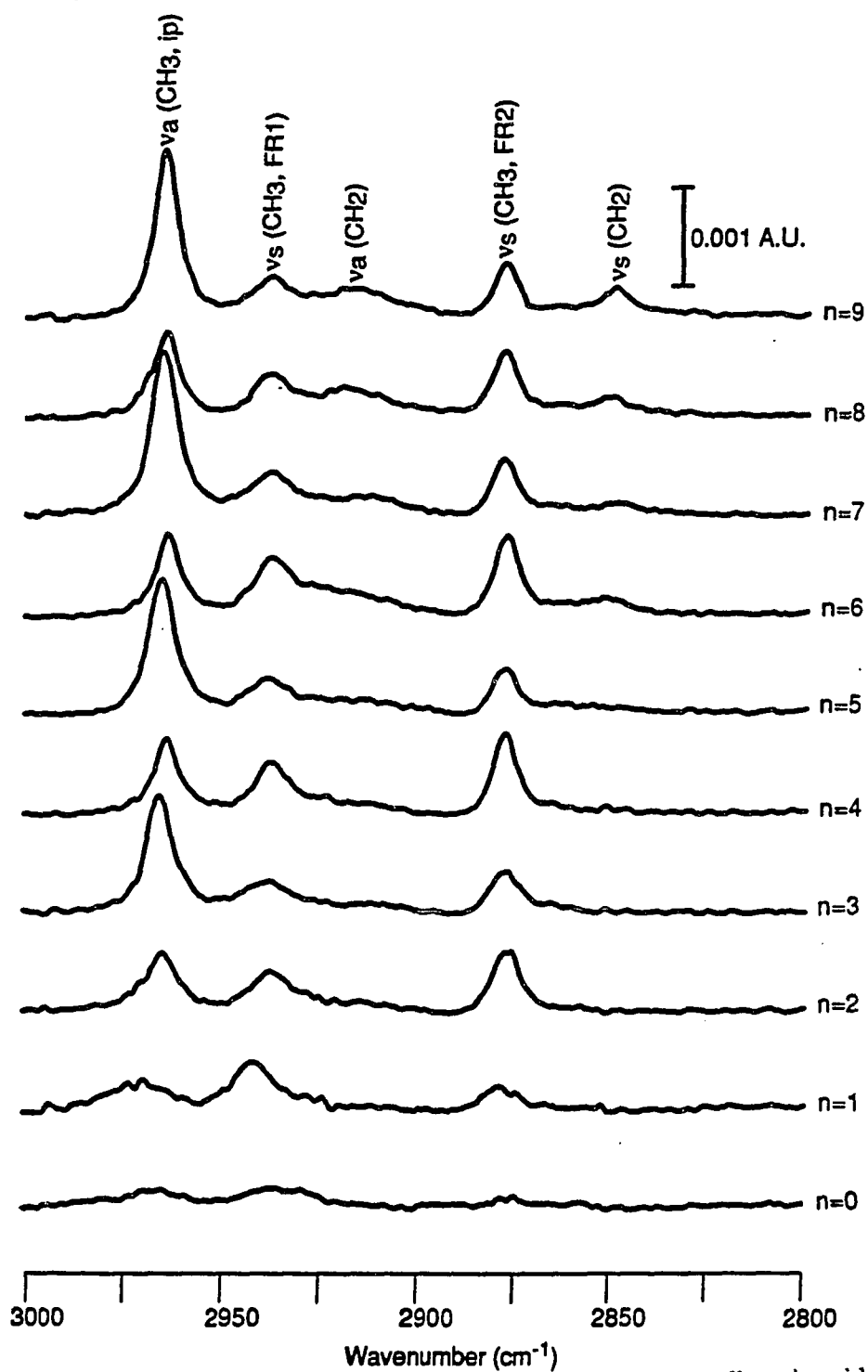


Figure 2. Infrared reflection spectra (high energy region) of  $n$ -alkanoic acids,  $\text{CH}_3(\text{CH}_2)_n\text{COOH}$ , self-assembled from the gas-phase at Ag.

Table 1. Assignments of peak positions for spontaneously adsorbed monolayers of acids from the gas phase<sup>a</sup>

Vibrational mode	Gas phase <i>n</i> -alkanoic acid on Ag, peak position (cm <sup>-1</sup> )										Gas phase d <sub>17</sub> -nonanoic acid on Ag, peak position (cm <sup>-1</sup> )
	n (number of CH <sub>2</sub> units)										
	n=0	1	2	3	4	5	6	7	8	9	n=7
$\nu_a(\text{CH}_3, \text{ip})$	2966	2970	2963	2965	2963	2965	2964	2965	2964	2966	
$\nu_s(\text{CH}_3, \text{FR}_1)$	2937	2941	2936	2938	2937	2938	2937	2937	2938	2938	
$\nu_a(\text{CH}_2)$								2918	2920	2918	
$\nu_s(\text{CH}_3, \text{FR}_2)$	2876	2878	2876	2877	2877	2877	2878	2878	2878	2878	
$\nu_s(\text{CH}_2)$							2851	2851	2850	2849	
$\nu_s(\text{COO}^-)$	1411	1405	1401	1402	1400	1402	1400	1402	1398	1397	1391
$\nu(\text{C-COO}^-)$	1344	1295	1257	1236	1224	1216	1209	1205	1200	1200	1206
Wagging fundamental <sup>b</sup>		1380	1382	1382	1382	1382	1382	1382			
$\delta(\alpha\text{-CH}_2)$ <sup>b</sup>					1412	1415		1415	1416	1416	
$\omega(\text{CH}_2)$ k=1		1371	1340	1311	1287	1268	1254	1245	1237	1230	
k=3				1358	1337	1318	1300	1284	1271	1262	
k=5						1356	1338	1321	1304	1293	
k=7								1350	1335	1322	
k=9										1345	

<sup>a</sup>Band assignments and labelling scheme from refs. 20 and 28.

<sup>b</sup>Seen as a shoulder on  $\nu_s(\text{COO}^-)$ .

reveal that gas phase self-assembly yields films with lower concentrations of defects than the solution phase.

Earlier work on self-assembly from solution demonstrated that no hydrocarbon impurities were incorporated into a monolayer film of arachidic acid self-assembled from dilute hexadecane solution at Ag<sup>22</sup>. We tested for the possible adsorption of hydrocarbon-containing impurities from the gas phase using deuterium labeled alkanolic acids. The labeled monolayers were prepared in the same manner as the *n*-acid films; the C-H stretching region is shown in Figure 3. Deuterium labeled acetic and hexanoic acids revealed trace hydrocarbon contamination. For perdeuteriononanoic acid/Ag, the absence of C-H stretches in the labeled film indicates that, within detection limits, no hydrocarbon impurity was incorporated in the gas phase assembled nonanoic acid monolayer. Thus at the longer chain lengths, the predominant species is the one of interest, and the long chains are capable of isolating the metal surface from contamination. This result implies that either (1) the acids adsorb very quickly, or (2) they irreversibly displace adventitious adsorbents.

The IR spectra between 1800 cm<sup>-1</sup> and 1100 cm<sup>-1</sup> for the gas phase adsorbed monolayer of nonanoic acid, solution adsorbed nonanoic acid, gas phase adsorbed perdeuteriononanoic acid and bulk *n*-nonanoic acids are shown in Figure 4. Bulk nonanoic acid shows an absorption band near 1705 cm<sup>-1</sup> due to the hydrogen-bonded carboxylic acid group, whereas the band at 1402 is attributed to the  $\nu_s(\text{COO}^-)$  for a carboxylate salt bound to Ag. The bulk liquid shows localized vibrations associated with short sequences of bonds having a specific conformation<sup>23</sup>, but no specific bands attributable to end gauche modes or kinks (see below). The observation of only the  $\nu_s(\text{COO}^-)$  mode and no  $\nu_a(\text{COO}^-)$  mode indicates that the carboxylate is bound symmetrically to the surface, as indicated in Figure 5. The  $\nu_a(\text{COO}^-)$  mode, usually much more intense than the  $\nu_s(\text{COO}^-)$  mode, must have its dipole moment parallel to the surface to be unobservable (surface effect, see above). Reactive chemisorption with proton dissociation at the surface is consistent with the mechanism

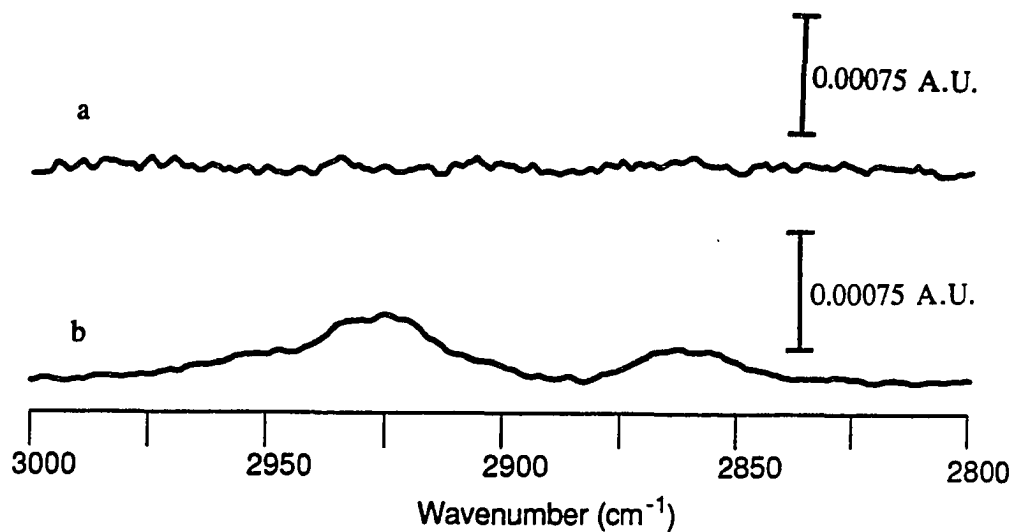


Figure 3. Infrared reflection spectra (high energy region) of deuterium labeled alkanolic acids self-assembled from the gas phase at Ag. (a) Nonanoic acid-d<sub>17</sub> (CD<sub>3</sub>(CD<sub>2</sub>)<sub>7</sub>COOH). No hydrocarbon contamination can be discerned. (b) 6,6,6-trideuterohexanoic acid (CD<sub>3</sub>(CH<sub>2</sub>)<sub>4</sub>COOH). The major hydrocarbon modes are the methylene stretches. A trace impurity can be seen in the methyl region.



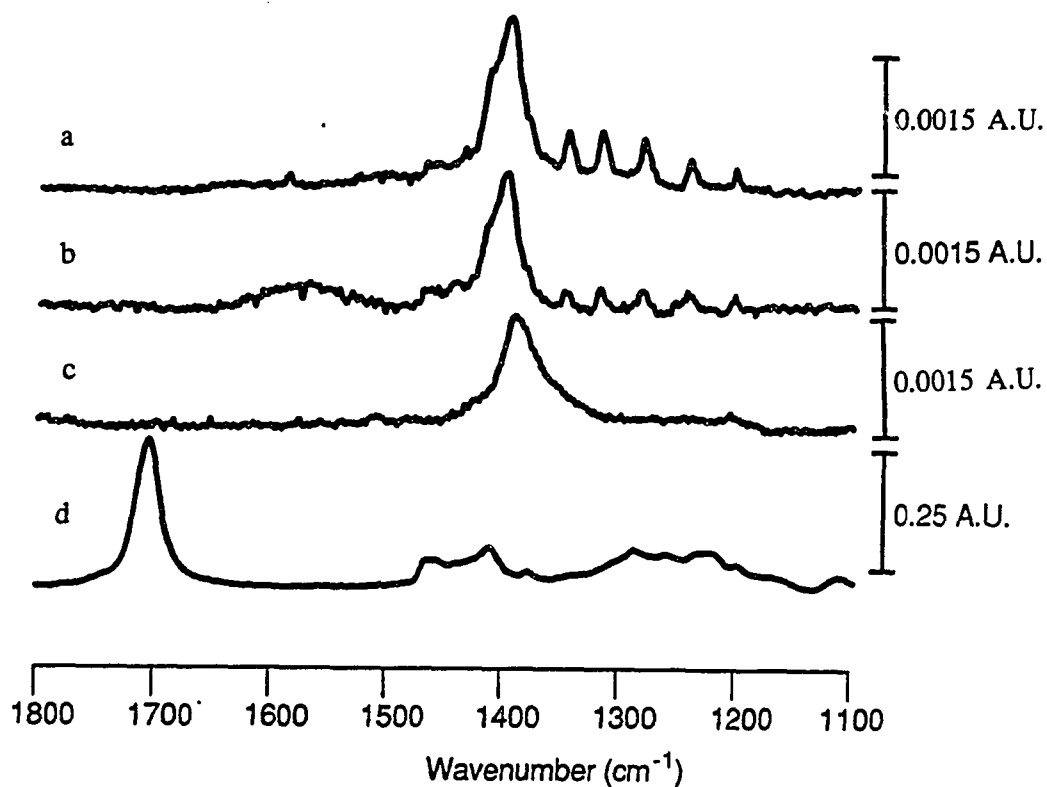


Figure 4. Infrared reflection spectra (low energy region) of (a) nonanoic acid self-assembled from the gas-phase at Ag, (b) nonanoic acid self-assembled from hexadecane solution at Ag, (c) perdeuterated nonanoic acid,  $\text{CD}_3(\text{CD}_2)_7\text{COOH}$ , self-assembled from the gas-phase at Ag, (d) bulk liquid nonanoic acid. The bulk liquid shows localized vibrations associated with short sequences of bonds having a specific conformation<sup>23</sup>.

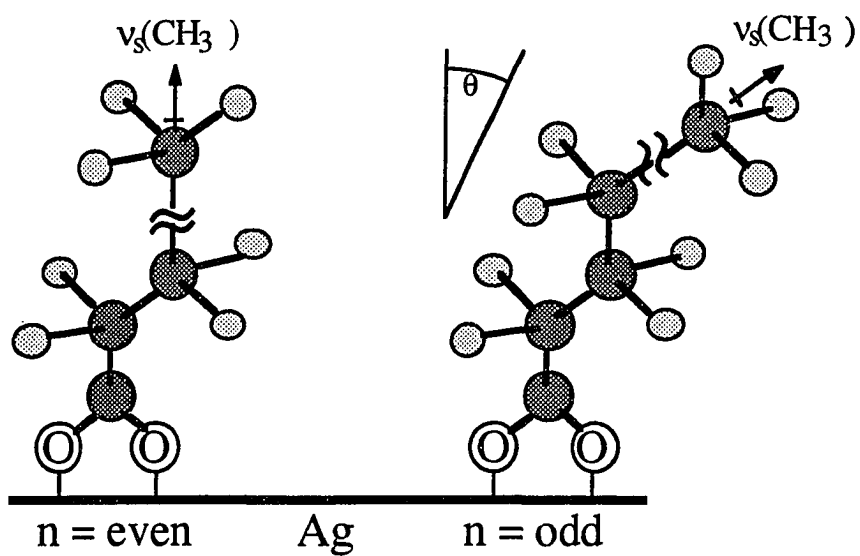


Figure 5. Model of carboxylate monolayers on Ag for chains with an even (right) or odd (left) number of methylene groups, accounting for the odd-even effect in  $v(\text{CH}_3)$  intensities.

proposed for solution phase self-assembled monolayers of alkanolic acids<sup>24</sup>. The energy of the  $\nu_s(\text{COO}^-)$  decreases as the length of the alkyl chain increases, from 1411  $\text{cm}^{-1}$  for acetic acid to 1397  $\text{cm}^{-1}$  for undecanoic acid. This mode appears at 1405  $\text{cm}^{-1}$  for  $\text{CD}_3$ -acetic acid/Ag, and 1393  $\text{cm}^{-1}$  for nonanoic- $\text{d}_{17}$  acid/Ag, indicating that increasing mass of the alkyl chain attached to the carboxylate decreases the energy of the  $\nu_s(\text{COO}^-)$  mode.

### Methyl modes

Insight concerning the orientation of these monolayers near the chain terminus is obtained from methyl stretching modes. As discussed previously<sup>9,18</sup>, the peak at 2963  $\text{cm}^{-1}$  is ascribed to the in-plane asymmetric methyl stretch,  $\nu_a(\text{CH}_3, \text{ip})$ . The peak intensities of the methyl modes exhibit the same odd-even dependence observed in the contact angle data, Figure 6. The spectroscopic origin of this odd-even progression has been discussed in detail<sup>15</sup>. As shown in Figure 5, addition of a methylene unit, which converts an even chain into an odd chain, causes the transition dipole for  $\nu_a(\text{CH}_3, \text{ip})$  to shift towards the surface normal, whereas that of  $\nu_s(\text{CH}_3)$  shifts away from the surface normal. Thus the intensity of the  $\nu_a(\text{CH}_3, \text{ip})$  mode will be greater for the odd chains relative to the even chains, while the intensities of the  $\nu_s(\text{CH}_2, \text{FR}_1)$  and  $\nu_s(\text{CH}_2, \text{FR}_2)$  modes will be greater for the even chains.

These observations of the odd-even effect for the acids self-assembled on Ag from both the gas phase and from solution are striking. The results are the same as for *n*-alkanethiols at Ag from solution, but the effect is offset by one methylene unit for *n*-alkyl thiols at Au (i.e. the odd-even effect is reversed). Taken together, these results demonstrate the influence of the head group-metal substrate interactions on the conformation and structure of the hydrocarbon chain.

Once the polymethylene wagging modes were assigned (see below), we looked for a spectral feature at 1370  $\text{cm}^{-1}$ , which could be assigned to the methyl umbrella mode. The

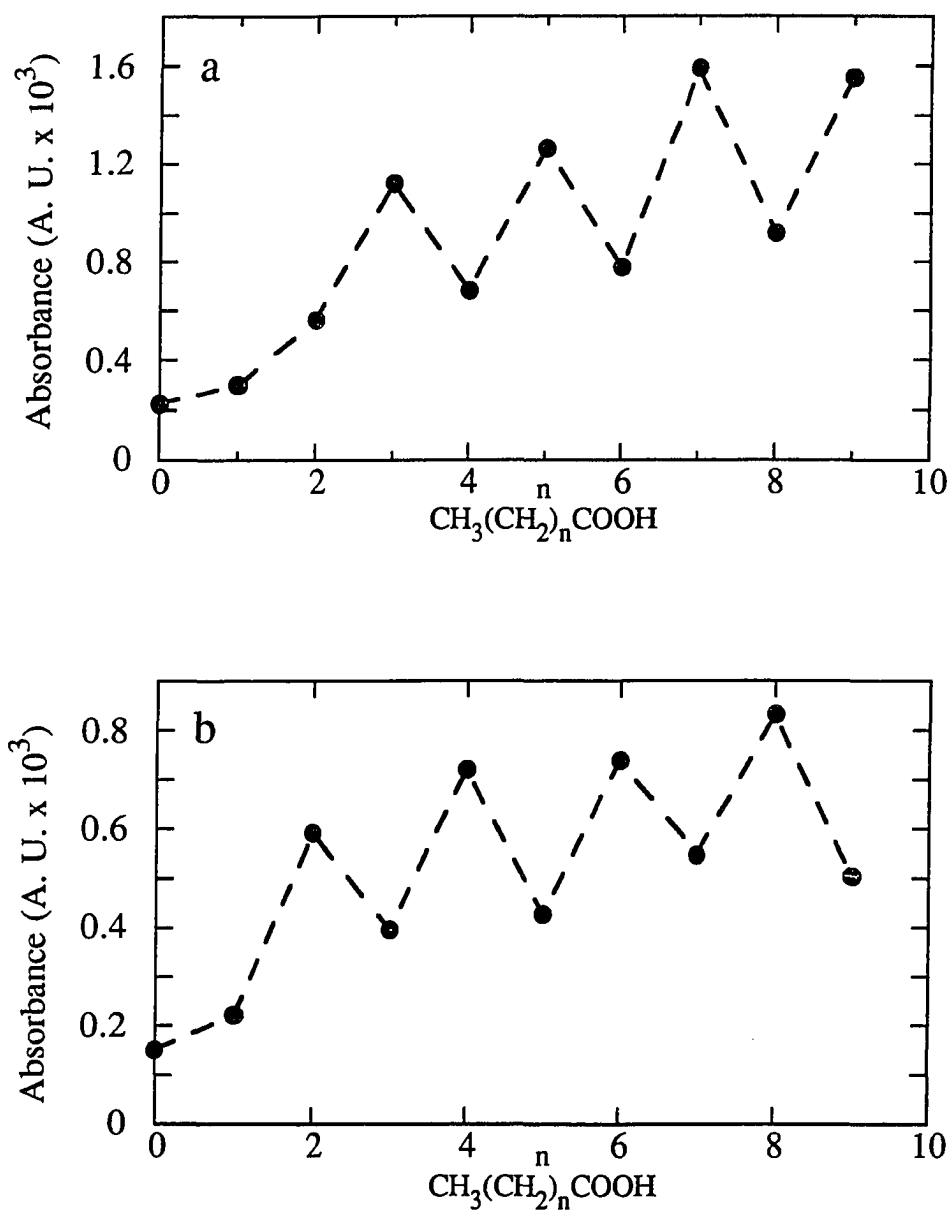


Figure 6. IR peak intensities for monolayers of *n*-alkanoic acids ( $\text{CH}_3(\text{CH}_2)_n\text{COOH}$ ) self-assembled from the gas phase at Ag: (a) intensities of the  $\nu_a(\text{CH}_3, \text{ip})$  mode; (b) intensities of the  $\nu_s(\text{CH}_3, \text{FR}_2)$  mode.

assignment and measurement of this methyl umbrella mode could not be made due to overlap with the very strongly absorbing  $\nu_s(\text{COO}^-)$  and the polymethylene wagging modes.

#### Orientation of the polymethylene chain

The weak intensities of both the  $\nu_a(\text{CH}_2)$  and  $\nu_s(\text{CH}_2)$  stretching modes indicate a near normal orientation to the Ag surface. This conclusion is based on the "surface selection rule"<sup>25</sup>, which causes a preferential excitation of vibrational modes with dipoles normal to highly reflecting metallic surfaces. A chain axis exactly normal to a smooth metallic surface plane with no defects in the polymethylene chain has surface-forbidden (zero intensity) methylene C-H modes. The very low intensities observed for  $\nu_a(\text{CH}_2)$  and  $\nu_s(\text{CH}_2)$  indicate there are very few disordered chains, *i.e.*, most of the monolayer is organized into crystalline domains where the chains have small average tilts. The average orientation of the alkyl chain in organic monolayer films can be determined by consideration of the infrared surface selection rule<sup>25</sup>. This qualitative analysis relies on a comparison of the observed spectrum with that calculated for an isotropic surface layer of comparable density<sup>4,26,27</sup>. The orientation analysis for decanoic acid/Ag and undecanoic acid/Ag indicates that the  $-(\text{CH}_2)-$  spacer groups of the alkyl chains at Ag exhibit respective average tilt (the angle made by the hydrocarbon chain to the surface normal) and twist (the rotation of the hydrocarbon chain on its molecular axis) of  $\sim 14^\circ$  and  $\sim 43^\circ$  respectively. The tilts were calculated for decanoic and undecanoic acid spectra, since these are the only two monolayers whose  $\nu_a(\text{CH}_2)$  and  $\nu_s(\text{CH}_2)$  modes were defined well enough to permit reliable measurement of absorbance intensity.

#### Vibrations of the polymethylene alkyl chain

The spectral feature at  $1467\text{ cm}^{-1}$  in Figure 4 is assigned to the  $\delta(\text{CH}_2)$  or "scissors" mode. The intensity of this mode is weak for a perpendicular surface-chain geometry because the orientation of the transition moment is parallel to the surface (see above). This mode does

have a high intensity for propanoic acid, which may be due to trace hydrocarbon contamination. The spectral feature at 1380-1382  $\text{cm}^{-1}$ , observed only as a shoulder on the  $\nu_s(\text{COO}^-)$  for  $n=1-7$ , is assigned to the polymethylene wagging fundamental<sup>28</sup>. Assignment of this mode and measurement of intensity are difficult due to overlap with the very strong  $\nu_s(\text{COO}^-)$ , especially for  $n=8-9$  for which the  $\nu_s(\text{COO}^-)$  moves to lower energy, obscuring the 1382  $\text{cm}^{-1}$  shoulder. The spectral feature at 1412  $\text{cm}^{-1}$ , observed only as a shoulder on the  $\nu_s(\text{COO}^-)$  for  $n>4$ , is assigned to the  $\alpha\text{-CH}_2$  deformation,  $\delta\text{-CH}_2$ <sup>29</sup>. Assignment of this mode and measurement of intensity are difficult due to overlap with the very strong  $\nu_s(\text{COO}^-)$ , especially for the short chains, for which the  $\nu_s(\text{COO}^-)$  is at its highest energy.

The series of progression bands observed between 1345-1220  $\text{cm}^{-1}$  is characteristic of an alkyl chain fully extended in an all *trans* zig-zag conformation. Thus the series of bands between 1382 and 1200  $\text{cm}^{-1}$  in Figure 4, which are assigned to the  $\omega(\text{CH}_2)$  (wagging) modes, indicates that the monolayer assembly exhibits this extended conformation. Disordered chains would show end gauche or kink modes at 1469  $\text{cm}^{-1}$ , 1366  $\text{cm}^{-1}$ , 1353  $\text{cm}^{-1}$ , 1341  $\text{cm}^{-1}$ , and 1300  $\text{cm}^{-1}$ <sup>23,30,31</sup>; no such peaks were observed. This is reasonable as the concentration of defects approaches zero for short chain alkanes in the bulk<sup>23,31</sup>. There may be some weak bands between 1380-1200  $\text{cm}^{-1}$  due to low concentration of defects, but their detection is precluded by the many wagging modes of the all-*trans* conformer.

Peak positions for individual modes are affected both by end group and chain length. Polar end groups cause both the intensity and energy of the wagging modes to increase. Wagging mode intensity increases as chain length decreases. Also, shorter chains have their first progression band at higher energy. The literature of *n*-alkanoic acid salts contains many examples of this phenomenon. However, one generalization can be made. The C-C stretch is generally misassigned as part of the wagging progression, based on its proximity to the

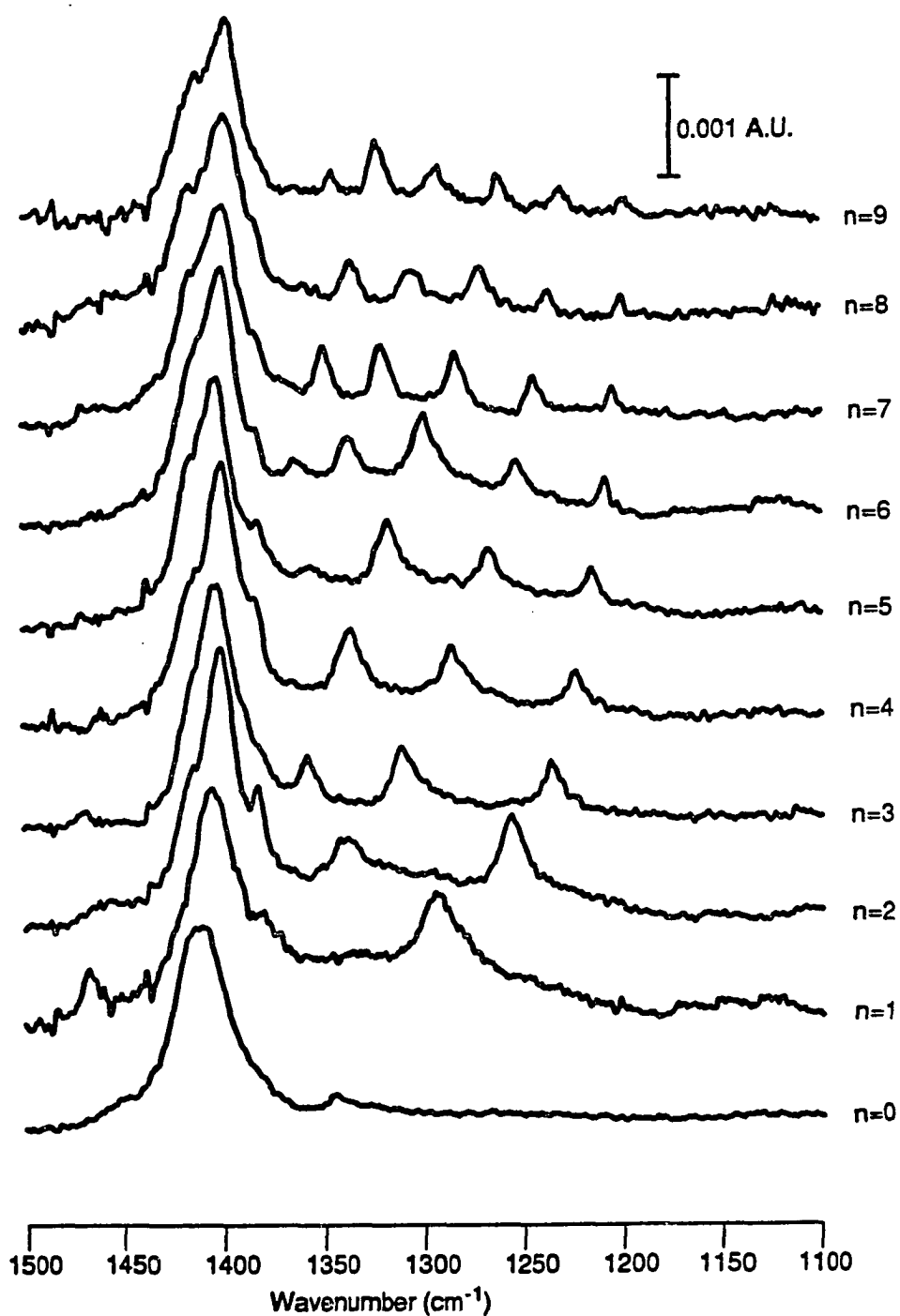


Figure 7. Infrared reflection spectra (low energy region) of  $n$ -alkanoic acids,  $\text{CH}_3(\text{CH}_2)_n\text{COOH}$ , self-assembled from the gas-phase at Ag. For clarity, the spectrum for  $n=0$  is plotted at  $2/3$  intensity.

wagging modes and comparable intensity. As suggested by the spectra in Figure 7, this was not an unreasonable assumption, but it has been disproven in this work. The unprecedented spectral resolution obtained for the gas phase self-assembled monolayers resulted in the complete assignment of the methylene wagging modes (Figure 8). As in the bulk alkane studies<sup>28</sup>, there are still some modes that are difficult to assign due to their low intensities.

The narrowness and intensity of the wagging modes indicates that the chain is free of gauche kinks which tends to broaden these modes. The solution-formed analogs peaks are broader and less intense. This broadening as well as greater tilt from the surface normal has made assignments difficult in other monolayer systems.

We briefly review the selection rules for methylene wagging modes as explained in previous studies of alkyl chains in *n*-paraffins<sup>21</sup> and apply them to surface-bound alkyl chains. These modes can be described by an oscillator function, for which the integer *k* characterizes each normal mode. The tabulation of peak positions for an extensive series of bands allowed us to assign each band to a particular *k* value, based on the monotonic increase in energy as chain length decreases. The results are displayed in Figure 8 for the *n*-alkanoic acids self assembled from the gas phase at Ag. For an alkyl chain which is oriented nearly perpendicular to the surface, only the methylene wagging mode whose dipole has a component parallel to the molecular axis, *i.e.*, perpendicular to the surface, will be observed (surface effect, see above). In the bulk, odd chains have  $(n+1)/2$  wagging modes whose dipole moment is parallel to the molecular axis (*k*-odd), which are therefore observed at a conducting surface such as Ag. There are also  $(n-1)/2$  weaker wagging modes whose dipole moments are perpendicular to the molecular axis (*k*-even) and are therefore not seen at a conducting surface. Even numbered chains have  $n/2$  IR-active wagging modes (for which *k* is odd; the *k*-even modes are not IR active), whose resultant dipole is in the chain of the carbon skeleton, parallel to the axis of the chain. Hence all IR active wagging modes are surface active for the even chains. The result is that for both odd and even chains at a surface, only the *k*-odd modes are observed. For



example, octanoic acid/Ag ( $n=6$ ) has  $6/2 = 3$  modes; nonanoic acid/Ag ( $n=7$ ) has  $(7+1)/2 = 4$  wagging modes observed.

The assignment of the progression bands was greatly aided by the initial assignment of the  $C-C_{k=1}$  stretching mode. This band, the highest energy band of the C-C stretches, is observed at  $1206\text{ cm}^{-1}$  for nonanoic acid/Ag. It is assigned to  $\nu(C-C)$  because it is observed in both the nonanoic acid/Ag and the perdeuterionanoic acid/Ag monolayer spectrum, which has no  $CH_2$  modes. The other monolayer studied which has no  $CH_2$  groups is acetic acid/Ag, which has a single peak at  $1345\text{ cm}^{-1}$ , corresponding exactly to its position as predicted from the trend for  $\nu(C-C)$  as illustrated in Figure 8. The  $C-C_{k=1}$  mode is observed from  $1345\text{ cm}^{-1}$  for  $n=0$  to  $1199$  for  $n=9$ . The trend to increasing energy for the CC mode as chain length decreases is also observed for the  $CC_{k=1}$  mode of *n*-alkyl paraffins<sup>28</sup>.

While the progression of wagging modes arises from the nonlocalized vibrations, i.e., involving the entire chain, this CC mode appears to be localized. Because this CC mode follows the trend all the way down to acetic acid ( $n=0$ ), we believe that this relatively high intensity mode is due to the  $C-CO_2^-$  bond. The band moves to lower energy as the length, i.e., the weight, of the attached alkyl chain increases. As a further proof that this is the  $\nu(C-CO_2^-)$ , no such CC vibration is observed in thiolate monolayers at Ag<sup>15</sup>. The carboxylate is a polar end group to the polymethylene chain, and causes energy and intensity of this mode to increase. Although the spectra suggest other  $\nu(C-C)$  modes at lower energy, these modes are of such weak intensity as to be barely distinguishable from the background; no definite assignments could be made.

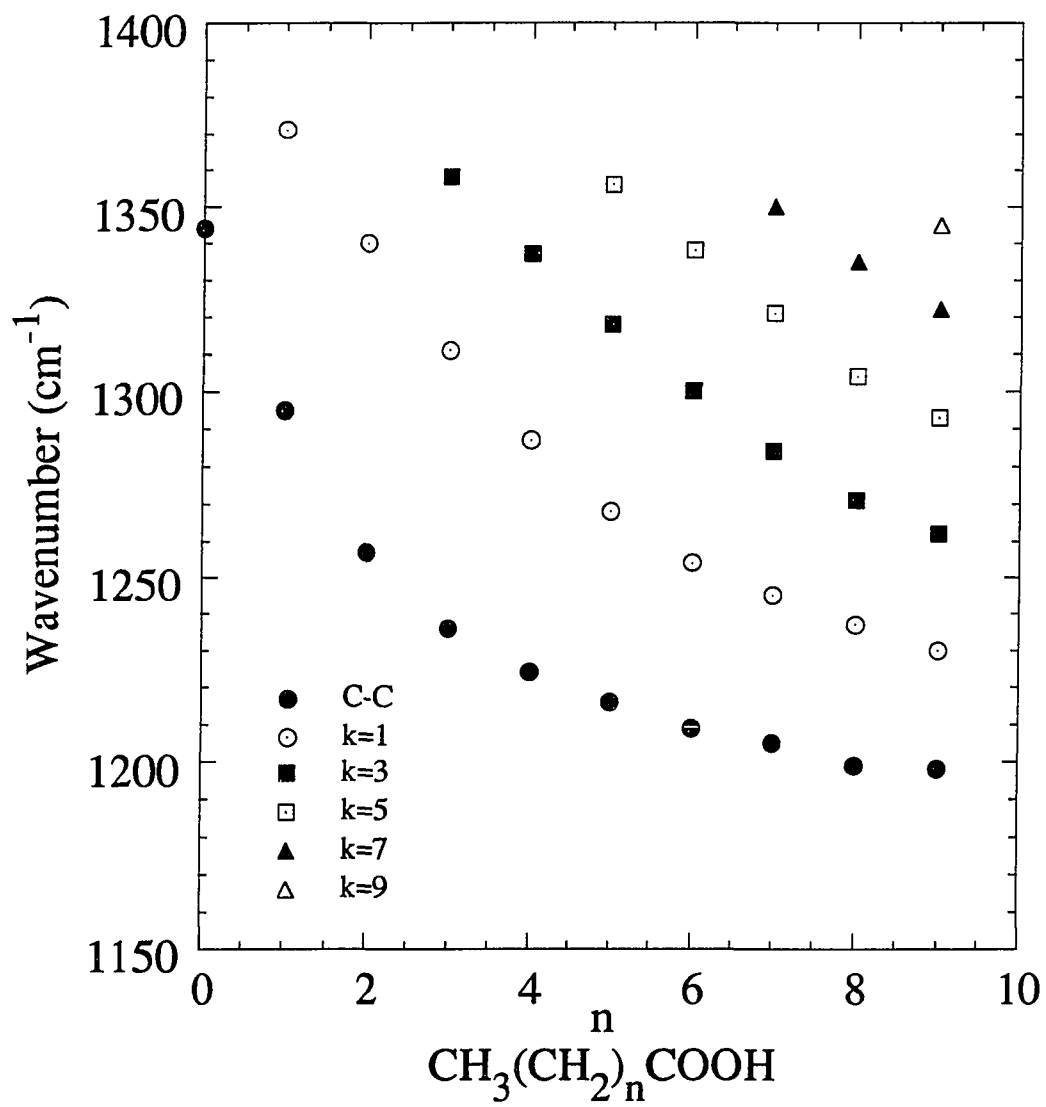


Figure 8. Array of methylene wagging modes and C-C stretching modes for  $n$ -alkanoic acids self-assembled from the gas phase at Ag.

### Discussion of the general utility of the technique

We surveyed a variety of systems to investigate the general utility of gas-phase self-assembly.

#### *n*-Alkylthiols at Ag

The *n*-alkylthiols self-assembled at Ag from the gas phase also produce monolayers. We determined this from ellipsometric thicknesses and IR peak intensities, both of which are comparable to those obtained from solution-assembled monolayers. The thiolate monolayers exhibit the progression bands between 1400-1100 cm<sup>-1</sup>, although bands are liquid-like in the C-H stretching region. Advancing contact angle measurements were comparable to those obtained from solution-assembled monolayers of *n*-alkanethiolate monolayers at silver self-assembled from solution.<sup>15</sup> Receding contact angles were generally higher than the gas phase self-assembled acids at Ag, which is attributed to less dissolution of the monolayer, although values were low compared to the solution analogs. In short, the gas phase self-assembled *n*-alkylthiol monolayers do not exhibit the unusual crystallinity that their acid analogs do.

#### *n*-Alkylthiols at Au

These are the most extensively studied monolayers in both the gas<sup>13</sup> and solution<sup>2,3</sup> phases. The *n*-alkylthiols have been shown by ellipsometry to give mono- and multilayer structures when Au substrates were exposed to purified gas streams of the self-assembly precursors. We previously found that the *n*-alkylthiols give only unstable monolayer films at Au when self-assembled from the gas phase. We attributed this to participation of the solvent in the proton dissociation required for the chemisorption process to occur.

*n*-Alkanoic acids and *n*-alkylthiols at Cu

When allowed to react from the gas phase at the surface of evaporated Cu films, these systems give multilayer films of high order and low wettability, to be discussed in a forthcoming paper<sup>32</sup>. Multilayer formation is attributed to the greater reactivity and diffusivity of Cu atoms compared to Ag and Au.

## CONCLUSIONS

The influence of solvent on monolayer adsorption has been previously demonstrated. In this work, the ramifications of using the gas phase as medium for self-assembly of a variety of monolayer systems have been studied. Infrared reflection spectroscopy and contact angle measurements indicate that *n*-alkanoic acids adsorb from the gas phase to form monolayer films at Ag. The IR spectra indicate that monolayer formation proceeds via a symmetrically bound Ag carboxylate salt, as in solution. The monolayer formed is less complete than that obtained from solution, as evinced by IR intensities for the methyl stretches and receding contact angle (wettability). IRS also shows that the monolayers formed are crystalline and ordered. Advancing contact angle data demonstrate that monomolecular films of short alkyl chains self-assembled from the gas phase have low wettability, comparable to their solution analogs.

These results are novel because, in homogeneous solution, >11 CH<sub>2</sub> units are required to form a crystalline-like monolayer. Here, monolayers formed are crystalline-like when the chain contains as few as 7 CH<sub>2</sub> units, and possibly fewer. This observation is unprecedented in hydrocarbon monolayer formation. The remarkable film structure is also demonstrated by the observation of intense progression bands for all the short alkyl chains, which are characteristic of a highly ordered, crystalline-like chain environment.

The present study provides new insight into the packing and dynamics of film formation, further illustrating the importance of solvent. There may be heretofore unobserved subtle effects of solvent used for self-assembly. Perhaps the alkyl chains initially assume their lowest energy conformation, i.e., all *trans*, but are later disrupted by the immersion and rinsing processes.

For a monolayer film in which the alkyl chain is perpendicular to the surface, IRS provides two probes of the polymethylene chain. The CH stretching region has been well studied in previous work, giving information on orientation, packing, and crystallinity. While

much weaker in intensity, the CH<sub>2</sub> wagging region has been shown here to give comparable information. In addition, the strong dependence on the nature of the end group was observed.

The progression modes arising from the CH<sub>2</sub> wags are weaker for alkyl chains tilted away from the normal. This is because the dipole moment is oriented parallel to the alkyl chain. The  $\omega(\text{CH}_2)$  modes are thus a qualitative indicator of chain tilt. For example, it is extremely difficult to see the individual  $\omega(\text{CH}_2)$  modes for monolayers of alkanethiolate/Au. Another factor causing low intensity is the less polar head group. For highly tilted monolayer films, the surface effect reduces intensities of modes and doubles the number of modes for odd chains as the dipole transitions for *k*-even modes shift toward the surface normal.

Reassignment of the  $\nu(\text{C-COO}^-)$  stretch is an important new finding. In earlier spectroscopic studies of long chain *n*-alkanoate carboxylate salts, this band was repeatedly assigned to a methylene wag, since it follows the spacings of the methylene wagging very well. As far as we know, this is the first time this band has been assigned to a C-C stretch and, more specifically, to  $\nu(\text{C-COO}^-)$ . The complete assignment of wagging mode progression bands was made possible by the isotopic labeling study with *n*-nonanoate/Ag monolayers. It should now be easier to make assignments for other systems in which the  $\omega(\text{CH}_2)$  progression is not as intense or is less well defined, due to chain tilting from the surface normal or to less-polar end-groups. Many unassigned monolayer spectra have been published with excellent progression band resolution, including studies with polar end-groups at both ends of the polymethylene chain<sup>17</sup>.

Studies on gas phase self-assembly are continuing in our laboratory using perfluoroacids and perfluorothiols and *n*-alkanoic acids at Cu. Because perfluoroacids self-assembled from solution have already been demonstrated to bind more strongly than their hydrocarbon analogs to Ag surfaces<sup>33</sup>, these studies may reveal information about the dynamics of organic film formation. Studies using highly crystalline, long-chain compounds at higher temperatures (to enhance their volatility) will be undertaken to see how far this

technique can be used to optimize film formation. We expect these studies will result in improved monolayer characteristics such as higher receding contact angle and better film robustness.

## REFERENCES

- (1) Bigelow, W. C.; Pickett, D. L.; Zisman, W. A. *J. Colloid Interface Sci.* **1946**, *1*, 513-38.
- (2) Whitesides, G. M.; Laibinis, P. E. *Langmuir* **1990**, *6*, 87-96 and references therein.
- (3) Ulman, A. *An Introduction to Ultra-Thin Organic Films From Langmuir-Blodgett to Self-Assembly*; Academic: San Diego, 1991.
- (4) Allara, D. L.; Nuzzo, R. G. *Langmuir* **1985**, *1*, 45-52 and references therein.
- (5) Schneider, T.; Buttry, D. A. *submitted 1992*,
- (6) Smith, E. L.; Franek, J. E.; Porter, M. D. *Langmuir* **1992**, in preparation.
- (7) Bain, E. D.; Whitesides, G. M. *J. Am. Chem. Soc.* **1989**, *111*, 7164-75.
- (8) Laibinis, P. E.; Whitesides, G. M.; Allara, D. L.; Tao, Y.-T.; Parikh, A. N.; Nuzzo, R. G. *J. Am. Chem. Soc.* **1991**, *113*, 7152-7167.
- (9) Porter, M. D.; Bright, T. B.; Allara, D. L.; Chidsey, C. E. D. *J. Am. Chem. Soc.* **1987**, *109*, 3559-68.
- (10) Bowden, F. P.; Moore, A. C. *Trans. Farad. Soc.* **1951**, 900-908.
- (11) Dubois, L. H.; Zegarski, B. R.; Nuzzo, R. G. *Langmuir* **1986**, *2*, 412-7.
- (12) Nuzzo, R. G.; Zegarski, B. R.; Dubois, L. H. *J. Am. Chem. Soc.* **1987**, *109*, 2358.
- (13) Thomas, R. C.; Sun, L.; Crooks, R. M.; Ricco, A. J. *Langmuir* **1991**, *7*, 620-622.
- (14) Cook, H. D.; Ries, H. E. J. *J. Phys. Chem.* **1959**, *63*, 226-230.
- (15) Walczak, M. M.; Chung, C.; Stole, S. M.; Widrig, C. A.; Porter, M. D. *J. Am. Chem. Soc.* **1991**, *113*, 2370-8.
- (16) Stole, S. M.; Porter, M. D. *Appl. Spectrosc.* **1990**, *49*, 1418-20.



- (17) Nuzzo, R. G.; Dubois, L. H.; Allara, D. L. *J. Am. Chem. Soc.* **1990**, *112*, 558-69.
- (18) Nuzzo, R. G.; Allara, D. L. *J. Am. Chem. Soc.* **1983**, *105*, 4481-83.
- (19) Snyder, R. G.; Hsu, S. L.; Krimm, S. *Spectrochim. Acta, Part A* **1978**, *34A*, 395-406.
- (20) Snyder, R. G.; Strauss, H. L.; Elliger, C. A. *J. Phys. Chem.* **1982**, *86*, 5145-50.
- (21) Snyder, R. G. *J. Molecular Spectroscopy* **1960**, *4*, 411-434.
- (22) Schlotter, N. E.; Porter, M. D.; Bright, T. B.; Allara, D. L. *Chem. Phys. Lett.* **1986**, *132*, 93-98.
- (23) Snyder, R. G. *J. Chem. Phys.* **1967**, *47*, 1316.
- (24) Chau, L.-K.; Smith, E. L.; Wolff, K. M.; Porter, M. D. in preparation.
- (25) Greenler, R. G. *J. Chem. Phys.* **1966**, *44*, 310-15.
- (26) Porter, M. D. *Anal. Chem.* **1988**, *60*, 1143A-50A.
- (27) Allara, D. L.; Nuzzo, R. G. *Langmuir* **1985**, *1*, 52-66.
- (28) Snyder, R. G.; Schachtschneider, J. H. *Spectrochimica Acta* **1963**, *19*, 85-116.
- (29) Umemura, J. *J. Chem. Phys.* **1978**, *68*, 42-48.
- (30) Hagemann, H.; Strauss, H. L.; Snyder, R. G. *Macromolecules* **1987**, *20*, 2810-2819.
- (31) Maroncelli, M.; Qi, S. P.; Strauss, H. L.; Snyder, R. G. *J. Am. Chem. Soc.* **1982**, *104*, 6237-6247.
- (32) Smith, E. L.; Porter, M. D. in preparation.
- (33) Chau, L.-K.; Porter, M. D. Unpublished results.

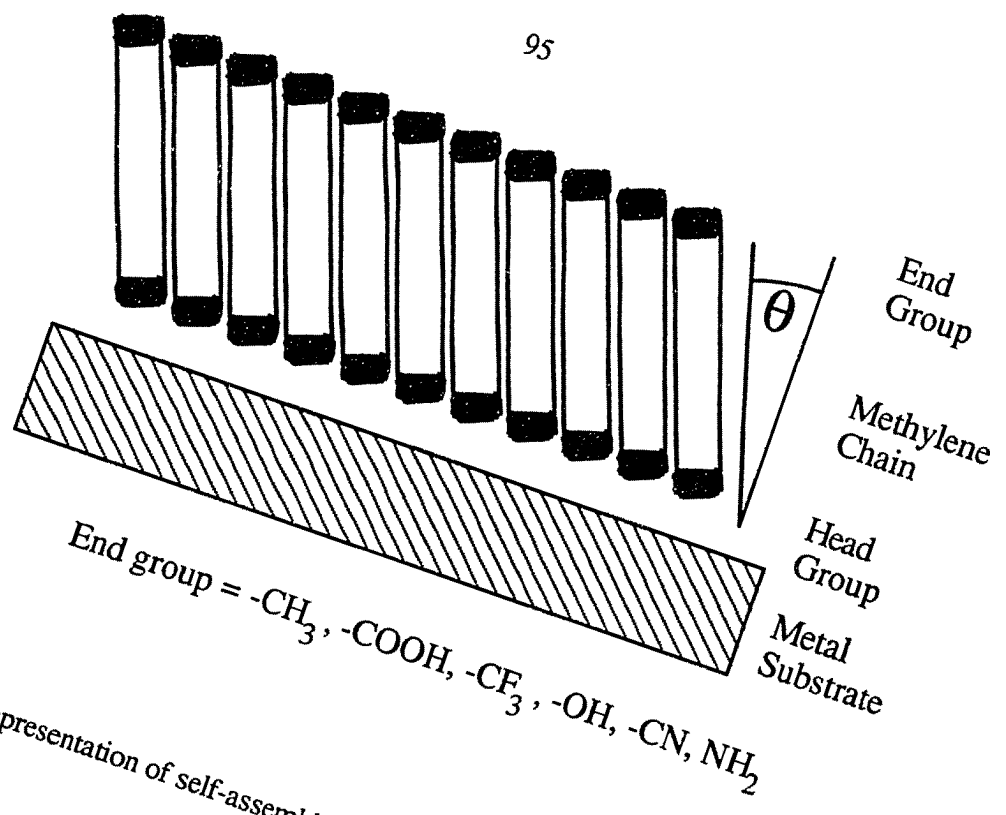
**PAPER IV**

**DEPOSITION OF METAL OVERLAYERS AT END-GROUP  
FUNCTIONALIZED THIOLATE MONOLAYERS ADSORBED AT AU.  
SURFACE AND INTERFACIAL CHEMICAL CHARACTERIZATION OF  
DEPOSITED COPPER OVERLAYERS AT CARBOXYLIC ACID-  
TERMINATED STRUCTURES**

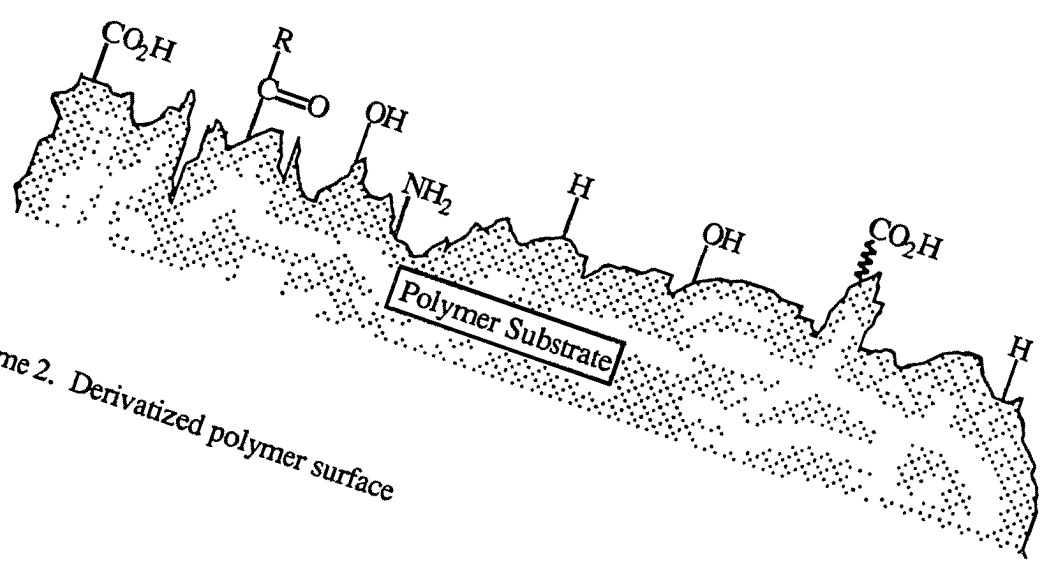
## INTRODUCTION

The construction of organized monolayer films from thiol compounds at Au surfaces provides a unique opportunity for the rational manipulation of the architecture of organic interfaces<sup>1,2</sup>. These films form spontaneously upon immersion of Au substrates into dilute (1 mM) thiol-containing solutions. As shown by Scheme 1, long chain alkanethiols chemisorb as ordered densely packed arrays of Au thiolates<sup>3-5</sup> that have an average tilt ( $\theta$ ) of  $\sim 30^\circ$  from the surface normal<sup>4,6-9</sup>. The separation distance between neighboring adsorbates is  $\sim 0.5$  nm<sup>10-13</sup>, representing a  $(\sqrt{3} \times \sqrt{3})R30^\circ$  adlayer structure at Au(111), the predominant crystalline face of the surface of evaporated Au films<sup>11,12,14,15</sup>. Densely packed layers are also formed when the diameter of the end group is comparable to or smaller than that of the polymethylene spacer group<sup>7</sup>. Because of their structural definition and compositional flexibility, thiolate monolayers at Au have been utilized as models for delineating the structural basis of properties such as wettability<sup>2,7,16,17</sup>, electron-transfer<sup>2,6,18,19</sup>, and adhesive strength<sup>20,21</sup>. Advances in sensor science are also beginning to emerge as a consequence of recent work<sup>22,23</sup>. This paper presents the results of the first in a series of studies aimed at utilizing various end-group derivatized thiolate monolayers as models of the surfaces of polymeric materials that promote the adhesion of a deposited metal overlayer.

It is well recognized that adhesion of metal overlayers at polymeric materials is enhanced by various chemical pretreatments of the polymer surface<sup>24,25</sup>. For example, the peel strengths of silver films deposited at polyethylene that has been pretreated with an oxygen or nitrogen plasma are markedly enhanced with respect to untreated polyethylene<sup>26</sup>. A delineation of the factors that promote the adhesion is, however, complicated because such pretreatments often yield a polymeric surface that is poorly defined both morphologically and compositionally, as depicted in Scheme 2. Thus, as noted recently<sup>20,21</sup>, the structural and compositional



Scheme 1. Schematic representation of self-assembled thiolate at Au



Scheme 2. Derivatized polymer surface

attributes of thiolate monolayers at Au provide an effective starting point for untangling the interactions of fundamental importance to adhesion.

The following sections examine several details of the interfacial structure formed by the vapor deposition of thin (~0.2 and 5 nm) Cu overlayers at carboxylic acid-terminated alkanethiolate monolayers chemisorbed at Au ( $\text{HO}_2\text{C}(\text{CH}_2)_n\text{S}/\text{Au}$ ,  $n = 10$  and  $15$ ). Both the nature of the deposited metallic overlayer and a delineation of possible chemical (*e.g.* bonding) and physical (*e.g.* perturbation of the chain packing) interactions between the metallic overlayer and monolayer are of particular interest. To this end, we have used infrared reflection spectroscopy (IRS), x-ray photoelectron spectroscopy (XPS), and atomic force microscopy (AFM) as principal characterization techniques. The information from IRS and XPS provides insights into the composition and structure of the organic monolayer before and after deposition of the Cu overlayer, as well as the overlayer oxidation state. The surface roughness of the deposited overlayer is probed using AFM. Our findings are also examined within the context of the bonding of monolayers formed from long-chain alkanic acids ( $\text{CH}_3(\text{CH}_2)_n\text{CO}_2\text{H}$ ) which chemisorb as ordered arrays at evaporated Cu substrates<sup>27,28</sup>. The potential application of thiolates at Au to fundamental studies of the adhesion of metal overlayers at surface functionalized polymeric materials is briefly discussed.

## EXPERIMENTAL SECTION

### Sample preparation

The substrates were prepared by the resistive evaporation of 300 nm of Au onto either silicon (Montco Silicon Inc. Royersford, PA) or mica (Asheville-Schoonmaker, Newport News, VA) using an Edwards 306A cryopumped evaporator (Fairfield, CA). The Au-coated silicon substrates were used for IRS, wettability, and optical ellipsometric characterizations, and were prepared by cutting 4 inch Si(100) wafers into 1 x 3 inch rectangular plates. The substrates were rinsed thoroughly with absolute ethanol before loading in the deposition system. The silicon substrates were primed with a ~10 nm adhesive layer of Cr prior to Au deposition. During deposition, the temperature of the Si-supported samples increased to ~50°C because of radiative heating by the evaporation source. The mica substrates were heated to 250°C for ~1 h prior to Au deposition, with this temperature maintained throughout the deposition. The coated mica substrates were allowed to cool to below ~70°C before removing to the atmosphere. The Au films deposited at both substrates are predominantly (111) textured<sup>14</sup>. At a macroscopic level, alkanethiolate monolayers formed at Au on mica or silicon substrates are structurally similar, as judged in other comparative studies<sup>3,15</sup>. However, the films at mica exhibit larger portions of atomically flat crystallites than those at silicon, facilitating a characterization using AFM. The pressure during all depositions was less than  $1 \times 10^{-6}$  torr. The Au and Cr deposition rates were 0.3 and 0.2 nm/s, respectively. Before deposition of the thin Cu overlayers, the monolayer-coated Au samples were held under vacuum ( $< 10^{-6}$  torr) for ~1 h in the evaporator chamber to reduce the level of sorbed contaminants. The Cu overlayers were deposited at a rate of 0.1 - 0.2 nm/s. After Cu deposition, samples were left in the vacuum chamber to cool for 30-45 min, then removed under flowing nitrogen and immediately characterized by IRS. Characterization by XPS was performed within 1-2 days of sample preparation.

Monolayers were formed from 11-mercaptoundecanoic acid ( $\text{HO}_2\text{C}(\text{CH}_2)_{10}\text{SH}$ , abbrev. MUA), 16-mercaptohexadecanoic acid ( $\text{HO}_2\text{C}(\text{CH}_2)_{15}\text{SH}$ , abbrev. MHA), and hexadecanethiol ( $\text{CH}_3(\text{CH}_2)_{15}\text{SH}$ , abbrev. HDT) by the immersion of the Au substrates into 1 mM ethanolic solutions of the mercapto-compound. With the exception of those used in the ellipsometric thickness determinations (see below), the substrates were immersed immediately upon removal from the evaporator. Immersion times were typically 24 h, primarily for convenience. Upon removal from solution, the samples were rinsed thoroughly with ethanol and allowed to dry in the laboratory ambient under a glass cover. The MHA and MUA were synthesized according to an earlier procedure<sup>17</sup>. The HDT was purchased from Aldrich and purified by passage through a neutral alumina (Aldrich) column immediately prior to use. For purposes of clarity, we abbreviate the composition of the multilayer structures by writing their abbreviations with the topmost layer on the left; *e.g.* a vapor deposited layer of Cu onto a MHA monolayer film at Au on silicon is written as Cu/MHA/Au/Si.

## **Instrumentation**

### **Contact angle measurements**

Advancing contact angles ( $\theta_a$ ) were measured in air using a Ramé-Hart Model 100-00 115 goniometer as described previously<sup>9</sup>. Hexadecane and water were used as probe liquids. For these measurements, a 2  $\mu\text{L}$  droplet was formed on the substrate with the needle of the syringe in the droplet. The value of  $\theta_a$  was determined as the volume of the droplet was slowly increased.

### **Ellipsometric measurements of film thickness**

The thicknesses of the monolayers were determined by optical ellipsometry at 632.8 nm in two steps with a computer-interfaced Gaertner Model L-116B ellipsometer as described pre-

viously<sup>9</sup>. After monolayer formation, each sample was again analyzed and the film thickness calculated from a three-phase parallel layer model, using the average complex refractive index of the individual sample and a real refractive index of 1.45 for the film. A value of 1.45, which is representative of the adsorbate precursors<sup>29</sup>, facilitates comparison with thickness data that has been reported for a variety of monolayers<sup>2,5,6,17</sup>.

### Infrared spectroscopy

Infrared spectra were acquired with a Nicolet 740 FT-IR interferometer. Monolayer spectra were obtained using p-polarized light incident at 80° with respect to the surface normal. These spectra are reported as  $-\log(R/R_0)$ , where R is the reflectance of the sample and  $R_0$  is the reflectance of a reference octadecanethiolate-d<sub>37</sub> monolayer at Au. A home-built sample holder was used to position the substrates in the spectrometer<sup>30</sup>. Both sample and reference reflectances are the average of 1024 scans. Spectra of bulk MUA and MHA were obtained by their dispersion in KBr. All spectra were collected at 2 cm<sup>-1</sup> resolution (zero-filled) with Happ-Genzel apodization. Liquid N<sub>2</sub> cooled HgCdTe and InSb detectors were used. The spectrometer and sample chamber were purged with boil-off from liquid N<sub>2</sub>. Further details of these methods as well as the preparation of the reference substrates are given elsewhere<sup>7,9</sup>. We note that Cu films at these thicknesses are IR-transparent primarily because of the formation of islands as opposed to a continuous film<sup>31</sup>.

### X-ray photoelectron spectroscopy

X-ray photoelectron spectra (XPS) were acquired at room temperature with a Physical Electronics Industries 5500 (Eden Prairie, MN) multi-technique surface analysis system. This system, equipped with a hemispherical analyzer, a toroidal monochromator, and a multichannel detector, samples a 2 mm<sup>2</sup> area. A pass-energy of 29.35 eV was used for the high resolution spectra, giving a resolution of 0.8 eV, as estimated from the FWHM of the Au(4f<sub>7/2</sub>) peak.



Monochromatic Al  $K_{\alpha}$ -radiation (1486.6 eV) at 300 W was used for excitation.

Photoelectrons were collected at 45° from the surface normal in a constant transmission mode. Acquisition times were typically ~15 minutes, with no discernible signal degradation over the course of the measurement. The Au(4f<sub>7/2</sub>) emission was monitored as an internal reference to binding energy and sample charging. Small changes ( $\leq 0.2$  eV) in the position of the Au(4f<sub>7/2</sub>) peak during the course of the measurements indicated negligible sample charging. The base pressure of the ion-pumped ultrahigh vacuum (UHV) chamber during analysis was less than  $9 \times 10^{-10}$  torr.

### Atomic force microscopy

All AFM images were acquired using a Digital Instruments Nanoscope II (Santa Barbara, CA). The instrument was equipped with a 0.7  $\mu\text{m}$  scan head. After loading a sample, the instrument was allowed to come to thermal equilibrium, which usually required ~30 min. All images were acquired in air with the tip in contact with the sample in the constant force mode. In this mode, the force between the AFM tip and the sample surface is held constant, and the vertical displacements of the sample needed to maintain the preselected force are recorded as the surface rasters under the tip. Silicon nitride cantilevers (Digital Instruments) with pyramidally shaped tips and a force constant of 0.58 N/m were used. Images were acquired at a force of ~50 nN. The lateral displacement of the tip was calibrated using freshly cleaved mica. Images were smoothed with an eight-point moving average algorithm (*i.e.* the lowpass filter utility of the Nanoscope II).

## RESULTS AND DISCUSSION

The following sections present and discuss the results of a characterization of the interfacial structure of MHA and MUA monolayers at Au (MHA/Au and MUA/Au, respectively) before and after deposition of a thin Cu overlayer (Cu/MHA/Au and Cu/MUA/Au, respectively). The goal is to develop descriptions of the interactions of the overlayer with the end-group functionalized monolayer. The first section describes the results of a study of the structures and interfacial properties of MHA/Au and MUA/Au prior to Cu deposition. This section, presented in the context of earlier studies<sup>7,17,32</sup>, provides a basis for the discussion of the changes in the composition and structure of the monolayers after Cu deposition. The second section examines the interactions of the Cu overlayer with the end group and makes comparisons to structures of monolayers of alkanolic acids adsorbed at Cu surfaces<sup>27,28,33</sup>. We conclude with an assessment of the roughness of the deposited overlayer using the imaging capability of AFM.

### General physical and structural characteristics of MHA/Au and MUA/Au

#### Wettability and ellipsometric thicknesses

Samples were always wetted upon emersion from the MHA- and MUA-containing solutions. Measurements of wettability for MHA/Au and MUA/Au using water and hexadecane as probe liquids gave advancing contact angles of less than 15°, consistent with the formation of a high free energy surface<sup>17,32,34</sup>. These findings were not affected by extended immersion in the thiol-containing solutions.

Optical ellipsometric characterizations gave a film thickness of  $17 \pm 1$  Å for MUA/Au and  $25 \pm 1$  Å for MHA/Au, consistent with the formation of films of one molecular layer. Though slightly larger than theoretically expected for an extended polymethylene chain

structure with an average tilt of  $30^\circ$  from the surface normal, the experimental thicknesses agree with those reported earlier<sup>17,32</sup>. Improvements in the thickness determinations<sup>6,17</sup>, as well as considerations of the effect of an adsorbed contaminant layer at high free energy carboxylic acid surfaces, have been discussed<sup>7,17,32</sup>.

### Infrared spectroscopic characterization

Infrared reflection spectra of the MHA/Au and MUA/Au are shown in the low and high frequency regions in Figures 1 and 2, respectively. The spectrum of MHA dispersed in KBr is included for comparison. Peak positions and mode assignments are given in Table 1. Diagnostic spectral features include the C=O stretching modes ( $\nu(\text{C=O})$ ), and the asymmetric ( $\nu_a(\text{CH}_2)$ ) and symmetric ( $\nu_s(\text{CH}_2)$ ) methylene stretching modes. The presence of these features confirms the formation of the carboxylic acid-terminated monolayers. The absorbances of the methylene modes are comparable to those found in studies of methyl-terminated thiolates<sup>6,7</sup>, consistent with the formation of a film with a thickness of one molecular layer.

Insights into the local environment and spatial arrangement of these layers can be inferred from the peak positions and absorbances of  $\nu_a(\text{CH}_2)$  and  $\nu_s(\text{CH}_2)$ . Earlier spectroscopic studies<sup>35,36</sup> have demonstrated that the peak positions of the methylene stretching modes are qualitative indicators of the packing of the polymethylene chains. For polymethylene chains packed in a crystalline-like phase (*e.g.* MHA in KBr),  $\nu_a(\text{CH}_2)$  and  $\nu_s(\text{CH}_2)$  have peak maxima at  $2918\text{ cm}^{-1}$  and  $2850\text{ cm}^{-1}$ , respectively. In contrast, the peak maxima of these modes for polymethylene chains in a liquid-like environment are  $6\text{--}8\text{ cm}^{-1}$  higher in energy. Thus, the experimentally measured peak positions of MHA/Au are indicative of a densely packed array of polymethylene chains. A comparison of the band widths of the  $\text{CH}_2$  stretching modes for the monolayer and KBr spectra also shows negligible differences,

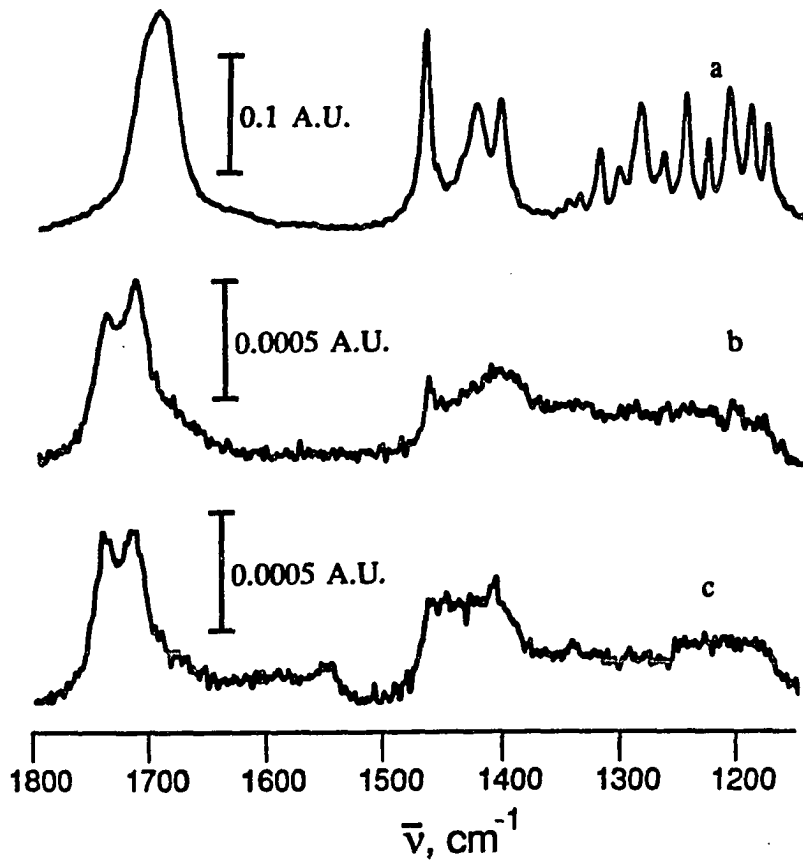


Figure 1. Infrared spectra in the low frequency region for (a) MHA in KBr, (b) MHA/Au/Si, and (c) MUA/Au/Si

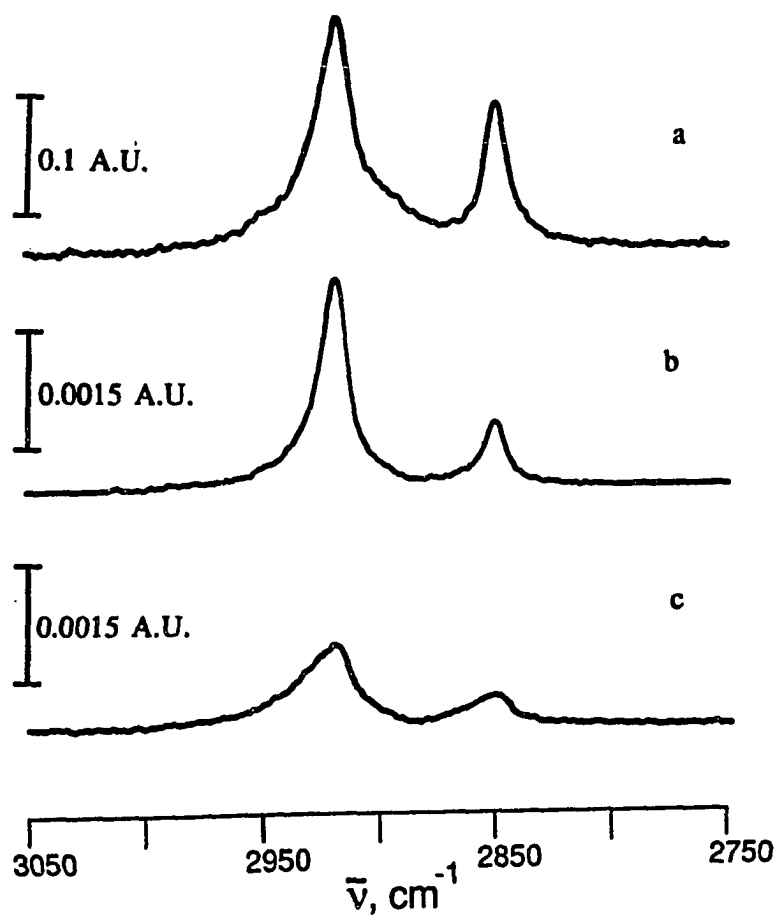


Figure 2. Infrared spectrum in the high frequency region for (a) MHA in KBr, (b) MHA/Au/Si, and (c) MUA/Au/Si.

Table 1. Mode assignments and peak positions ( $\text{cm}^{-1}$ ) for 16-mercaptohexadecanoic acid (MHA) and 11-mercaptoundecanoic acid (MUA) dispersed in KBr, as monolayers at Au, and as monolayers at Au after deposition of  $\sim 5$  nm overlayer of Cu

mode assignment	MHA			MUA	
	KBr	monolayer	Cu overlayer	monolayer	Cu overlayer
$\nu_a(\text{CH}_2)^a$	2918	2918	2920	2919	2922
$\nu_s(\text{CH}_2)^a$	2850	2850	2850	2850	2853
$\nu(\text{C}=\text{O})^b$	1699	1742,1718		1739,1717	
$\nu_a(\text{COO}^-)^c$			1550		1555
$\nu_s(\text{COO}^-)^c$			1423		1430
$\text{CH}_2$ scissors def, $\delta^a$		1471 <sup>b</sup>			
$\alpha\text{-CH}_2$ scissors def, $\delta^a$		1412 <sup>b</sup>			
$\text{CH}_2$ wags <sup>a</sup>		d			

<sup>a</sup>From references 35,36.

<sup>b</sup>Free and hydrogen-bonded acids<sup>37-43</sup>, respectively.

<sup>c</sup>From references 28,44,45.

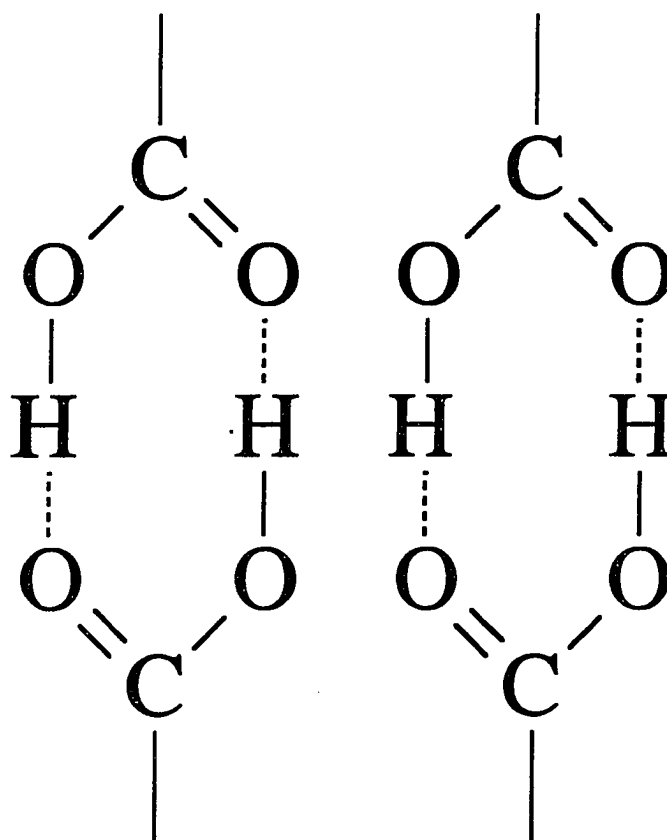
<sup>d</sup>Absorptions attributable to  $\text{CH}_2$  wags should appear between approximately 1200 and  $1360 \text{ cm}^{-1}$ .<sup>46</sup> However, low signal-to-noise does not permit definite assignments for the monolayer spectra.

confirming that the microscopic environments of the polymethylene chains in the monolayers and the bulk compound are similar.

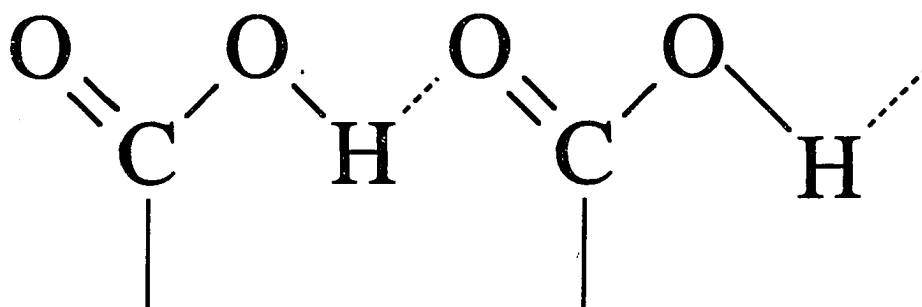
In contrast, extension of the above analysis to MUA/Au reveals a subtle difference in comparison to the packing at MHA/Au. Although the peak positions of both  $\nu_a(\text{CH}_2)$  and  $\nu_s(\text{CH}_2)$  are similar, the bandwidths at MUA/Au are broader than those at MHA/Au. Furthermore, the band broadening is skewed to the high energy side of both modes. We attribute this observation to a portion of the surface phase existing in a packing arrangement resembling that found for polymethylene chains in a liquid-like environment<sup>47</sup>. This is likely a reflection of the differences in the extent of the cohesive interactions between neighboring polymethylene chains in MUA/Au relative to MHA/Au.

The average orientation of organic monolayer films can be determined by consideration of the infrared surface selection rule<sup>48</sup>. The analysis relies on a comparison of the observed spectrum with that calculated for a isotropic surface layer of comparable density<sup>45,49</sup>. In agreement with earlier findings<sup>7</sup>, the analysis for MHA/Au yields an average tilt (the angle made by the hydrocarbon chain to the surface normal) and twist (the rotation of the hydrocarbon chain on its molecular axis) of  $\sim 30^\circ$  and  $\sim 45^\circ$  respectively<sup>34</sup>. The tilt and twist are comparable to that found for methyl-terminated thiolates of similar polymethylene chain length<sup>4,6-9</sup>, arguing that both the size of the carboxylic acid group and hydrogen-bonding (see below) between neighboring end groups have no observable effect on the underlying chain structure. Analysis of the orientation of the polymethylene chains of the MUA/Au monolayer and of the carboxylic acid functionalities is precluded by the lack of an optical function that is representative of the environment of these modes.

Qualitative details concerning the structure at the chain terminus of these monolayers can be developed from the infrared spectroscopy of carboxylic acids (see Table 1). In general, carboxylic acids in the condensed phase are intermolecularly hydrogen-bonded as head-to-head dimeric or linear polymeric structures, as shown in Schemes 3 and 4,



Scheme 3. Dimeric form of hydrogen-bonded carboxylic acids



Scheme 4. Polymeric form of hydrogen-bonded carboxylic acids



respectively. The infrared active modes of the  $\nu(\text{C}=\text{O})$  mode of the dimeric forms for alkanolic acids<sup>37,38</sup> lie between 1703 and 1715  $\text{cm}^{-1}$  and for dimeric  $\beta$ -oxalic acid<sup>39-43</sup> between 1726 and 1732  $\text{cm}^{-1}$ . The polymeric forms have been observed for  $\alpha$ -oxalic and acetic acids<sup>39-43,50,51</sup>, with  $\nu(\text{C}=\text{O})$  modes between 1648 and 1698  $\text{cm}^{-1}$ . By comparison, non-hydrogen-bonded carbonyl modes are generally found between 1735 and 1760  $\text{cm}^{-1}$ . Thus, the high frequency features at 1742  $\text{cm}^{-1}$  for MHA/Au and 1739  $\text{cm}^{-1}$  for MUA/Au are attributed to free non-hydrogen-bonded carboxylic acids while the features at 1718  $\text{cm}^{-1}$  for MHA/Au and 1717  $\text{cm}^{-1}$  for MUA/Au reveal the presence of the dimeric structures usually found in hydrogen-bonded alkanolic acids.

As put forth in an earlier description of the end group structure of MHA/Au<sup>7</sup>, steric constraints in a densely packed monolayer would hinder the formation of face-to-face hydrogen-bonded dimers. An examination of molecular models of the monolayer suggests that the carboxylate groups could, however, form "sideways" dimeric structures by a partial rotation of the carboxylic acid groups about the  $\text{C}_\alpha\text{-C}_{\text{C}=\text{O}}$  bond, as shown in Scheme 5. In such a structure, the barrier to rotation would be compensated by hydrogen-bond formation<sup>52</sup>. This barrier is expected to be relatively small as the enthalpy difference between *cis-trans* isomers of crystalline dodecanoic acid is only  $\sim 0.2$  kcal/mol<sup>38</sup>. Both monolayers are therefore composed of free carboxylic acid groups and hydrogen-bonded dimers.

At the present time, a more detailed assessment of the hydrogen-bonding interactions of these monolayers is problematic. Interestingly, the Scheme 3 dimers have two carbonyl modes: a higher energy IR-active antisymmetric vibration consistent with that observed in Figure 3, and a lower energy IR-forbidden symmetric vibration<sup>41</sup>. Because this symmetric vibration is Raman-active, experiments using Raman spectroscopy may further delineate the nature of these end group interactions.

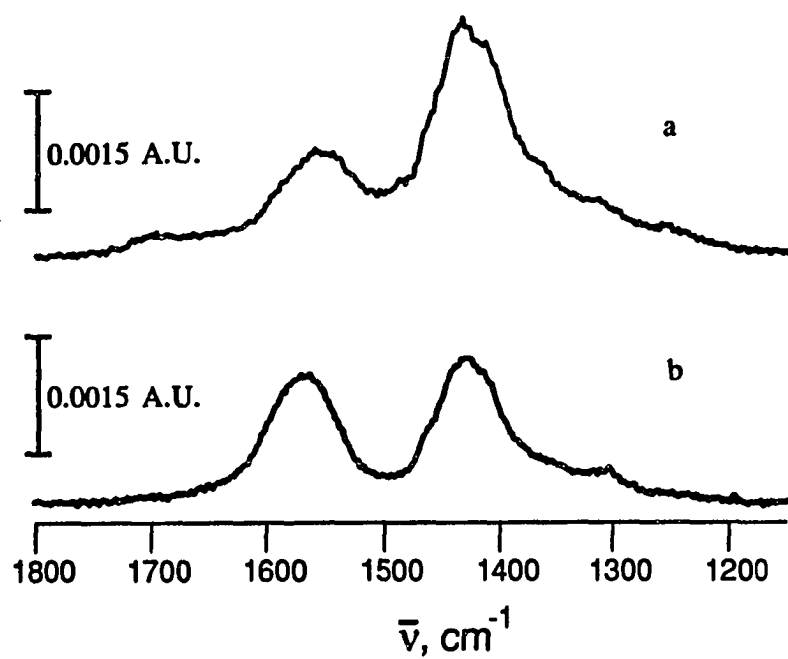
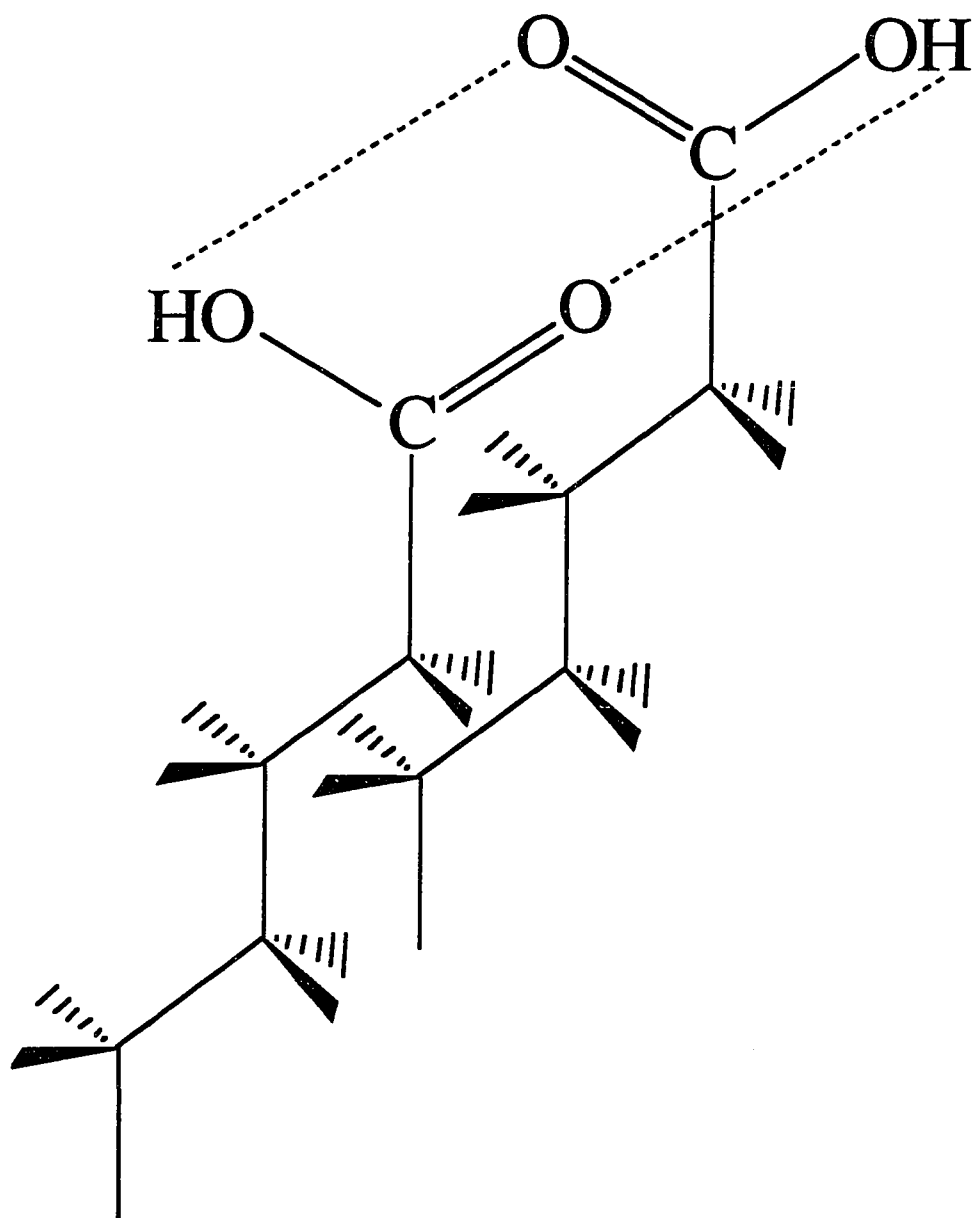


Figure 3. Infrared spectra in the low frequency region after deposition of a 5 nm Cu overlayer. (a) Cu/MHA/Au/Si (b) Cu/MUA/Au/Si .



Scheme 5. Proposed structure of hydrogen-bonding in carboxylic-acid terminated monolayers

## Monolayers of MUA/Au and MHA/Au with Cu overlayers

### Infrared spectroscopic characterization

Representative IRS spectra in the low and high energy regions for MUA/Au and MHA/Au after deposition of a 5 nm Cu overlayer are shown in Figures 3 and 4, respectively. These spectra provide details regarding changes in the composition and structure of the monolayers after Cu deposition. Peak positions and band assignments are given in Table 1. As evidenced by the absence of  $\nu(\text{C}=\text{O})$  in Figure 3, the deposition of the 5 nm overlayer leads to the loss of the acidic functionality of both monolayers. This loss and the appearance of bands at 1544 and 1430  $\text{cm}^{-1}$ , which are assigned to  $\nu_{\text{a}}(\text{COO}^-)$  and  $\nu_{\text{s}}(\text{COO}^-)$  respectively, reveal that the carboxylic acid functionalities are transformed into carboxylate functionalities. In addition, the observation of both  $\nu_{\text{a}}(\text{COO}^-)$  and  $\nu_{\text{s}}(\text{COO}^-)$  indicates that the carboxylate groups of both monolayers are canted relative to the surface normal. A comparison of the relative absorbances of  $\nu_{\text{a}}(\text{COO}^-)$  and  $\nu_{\text{s}}(\text{COO}^-)$  argues that the carboxylate group of Cu/MHA/Au exhibits a larger cant than that of Cu/MUA/Au. The presence of these modes raises the issue of the nature of the interaction between the canted carboxylate and the Cu overlayer. Previous literature findings<sup>28,33,44,45</sup> ascribe the interaction with Cu to a carboxylate, with both oxygen atoms interacting with the metal, or to a pseudo-ester with only one oxygen atom bound to the copper<sup>20</sup>.

As will be elaborated in a forthcoming paper detailing the directly analogous chemistry of monolayers formed from *n*-alkanoic acid monolayers at Cu films<sup>28</sup>, we have formally assigned the end group interactions to a Cu(II) carboxylate salt with the bands at 1544 and 1430  $\text{cm}^{-1}$  assigned to  $\nu_{\text{a}}(\text{COO}^-)$  and  $\nu_{\text{s}}(\text{COO}^-)$  respectively. This assertion is based on literature assignments<sup>44,45</sup> of the IR spectra of bulk Cu(II) *n*-alkanoate salts<sup>28</sup>. Diagnostic IR features of an ester-like species are the positions of the  $\nu(\text{C}=\text{O})$  and  $\nu(\text{C}-\text{O})$ . Pseudo-esters exhibit a  $\nu(\text{C}=\text{O})$  above 1630  $\text{cm}^{-1}$  and a  $\nu(\text{C}-\text{O})$  below 1435  $\text{cm}^{-1}$  as found for

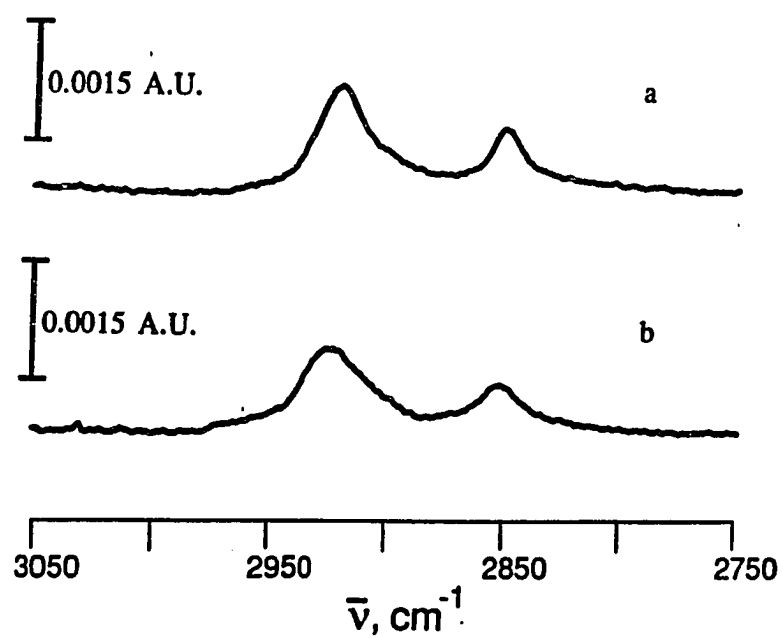


Figure 4. Infrared spectra in the high frequency region after deposition of a 5 nm Cu overlayer. (a) Cu/MHA/Au/Si (b) Cu/MUA/Au/Si.

Cu *bis*  $\beta$ -diketonates and Cu(oxalate)<sub>2</sub><sup>53-55</sup>. Further, the positions of the spectral features in Figure 3 are comparable to those of bulk Cu(II) alkanolate salts<sup>28</sup> which are chelated through both oxygen atoms of the carboxylate. The oxidation state assignment is confirmed by the results of XPS measurements (see below).

Additional insights into the structural changes of the monolayer that occur upon deposition of the Cu overlayer are gained by an examination of the high frequency spectra (Figure 4). The  $\nu_a(\text{CH}_2)$  and  $\nu_s(\text{CH}_2)$  modes are broadened after metal deposition for both MHA/Au and MUA/Au, with the broadening, which is more pronounced for MUA/Au, occurring towards the liquid-like (higher energy) side of the bands. A recent study of Ag overlayers deposited on octadecanethiolate monolayers at Au<sup>56</sup> suggest the evaporated metal may penetrate into the polymethylene structure and contact the underlying Au substrate. Such penetration may also cause the disruption of the chain structure of MUA/Au and MHA/Au. The pronounced broadening of the  $\nu_a(\text{CH}_2)$  and  $\nu_s(\text{CH}_2)$  of Cu/MUA/Au may reflect the enhanced susceptibility to packing disruption of the shorter polymethylene chain structure.

The absorbances of the bands in the CH stretching region were found to decrease somewhat after Cu deposition. Although variable, such a change is most notable by a comparison of the CH stretching region for MHA/Au before and after Cu deposition. The loss in signal may be due to two possibilities: the low transparency of the Cu overlayer and/or the partial desorption of the monolayer from heating during the Cu deposition. Earlier studies<sup>17</sup> have found that alkanethiolate monolayers desorb slowly in solutions above ambient temperatures ( $\geq 70^\circ\text{C}$ ) as well as in air. As a test, Cu/MUA/Au and Cu/MHA/Au samples were subjected to an accelerated process by heating to  $\sim 80^\circ\text{C}$  for about 20 minutes, in air. Characterization of such samples by IRS revealed no detectable hydrocarbon stretching features, consistent with a thermally activated desorption mechanism.

### X-ray photoelectron spectroscopy results

An XPS study was undertaken to gain further insight into the interactions between the Cu overlayer and the monolayer. The XPS results provided both elemental analysis and oxidation state determination of the overlayer structure. A more quantitative analysis of chemical composition was precluded by possible adsorption of trace contaminants and, more importantly, by the Cu overlayers. The O(1s) and C(1s) peaks were especially broadened after deposition of the Cu overlayer. Overlayers can affect both intensities and binding energies of the photoelectrons emitted at the interface<sup>57</sup>. Factors affecting intensities and binding energies for thiolate monolayers at Au have been discussed<sup>17</sup>.

Photoelectron attenuation by the 5 nm Cu overlayers precluded the collection of data pertaining to interactions with the carboxylic acid end group of the monolayer. To reduce attenuation, Cu/MHA/Au samples with much thinner (~0.2 nm) Cu overlayers were prepared. The low-energy IR spectrum for such a sample is shown in Figure 5. The presence of a weak carbonyl mode<sup>58</sup> indicates incomplete conversion of the carboxylic acid end group to the carboxylate. A 0.2 nm Cu overlayer is about 4 Cu atoms per adsorbed MHA (estimated from the electrochemically determined MHA coverage<sup>3,15</sup> and from the bulk<sup>56</sup> density of Cu<sup>29</sup>). This excess of Cu indicates that much more than a monolayer of Cu atoms is required to achieve full reaction of the MHA, consistent with Cu island formation in the first few angstroms of Cu deposited. The detection by XPS (see below) of small amounts of elemental Cu and Cu(I) (probably as Cu<sub>2</sub>O), reveals that not all the Cu present is reacted with the MHA monolayer. Differences in the signal intensity reflect variations in the Cu deposition process and/or the degree of penetration of Cu between the polymethylene chains of the monolayers. The XPS survey spectra for 0.2 nm Cu evaporated onto an MHA monolayer (Cu/MHA/Au) are consistent with the expected composition as summarized in Table 2. Table 2 also presents the results of XPS characterizations of 0.2 nm Cu overlayers at uncoated Au and at a methyl-terminated thiolate monolayer at Au (HDT/Au), both of which

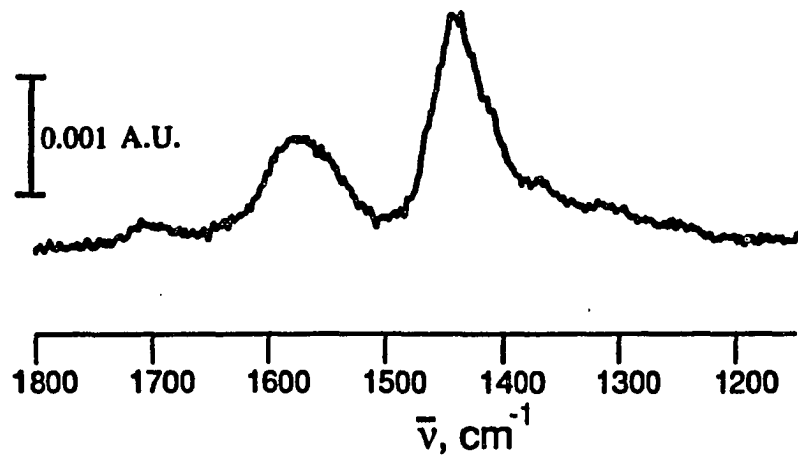


Figure 5. Infrared reflection spectrum of 0.2 nm Cu overlayer at MHA/Au/Si



Table 2. Binding energies (eV) and compositional assignments for XPS spectra of ~0.2 nm Cu overlayers deposited at uncoated Au (Cu/Au), a hexadecanethiolate monolayer at Au (Cu/HDT/Au), and a monolayer of 16-mercaptohexadecanoic acid at Au (Cu/MHA/Au)

	Sample		
	Cu/HDT/Au	Cu/Au	Cu/MHA/Au
Au(4f <sub>7/2</sub> )	83.95	83.75	83.9
S(2p <sub>3/2</sub> )	161.8	-	161.8
S(2p <sub>1/2</sub> )	162.8	-	162.8
C(1s)			
a	284.7	284.7 <sup>c</sup>	284.5
b	-	-	288.3
O(1s)	530.8	531.7	531.7
Cu(2p <sub>3/2</sub> )			
Cu(0) and Cu(I)	932.2	932.3	933.0
Cu(II)			934.8
Cu(II) satellites			938 - 945
Cu(2p <sub>1/2</sub> )			
Cu(0) and Cu(I)	951.8	951.8	953.0
Cu(II)	-	-	954.8
Cu(II) satellites	-	-	~963

<sup>a</sup>Attributed to C bound to hydrogen.

<sup>b</sup>Attributed to C bound to oxygen.

<sup>c</sup>Attributed to adventitious adsorption prior to placement in the XPS chamber.

serve as control samples for comparison to the carboxylic acid-terminated structures. The Cu(2p) spectra of Cu/Au and Cu/HDT/Au have identical peak positions and show a slight shoulder on the 932.3 eV peak, probably from trace amounts of Cu(II) compounds as, for example, CuO<sup>27,59</sup>.

The nature of the chemical interaction between the evaporated Cu and the carboxylate end groups of the MHA/Au can be seen in the Cu(2p) XPS region shown in Figure 6. The same regions for Cu/Au and Cu/HDT/Au are shown for comparison. All three spectra contain features for elemental Cu and/or Cu(I). For Cu/MHA/Au, the presence of Cu(II) is clearly indicated by the Cu(2p<sub>3/2</sub>) peak at 934.8 eV, the Cu(2p<sub>1/2</sub>) peak at 954.8 eV, and the characteristic Cu(II) satellite structure at 938-945 eV and ~963 eV. The satellite structure is only observed in the presence of the open-shell d<sup>9</sup> configuration of Cu(II)<sup>57</sup>. Satellites are not present in XPS spectra of the control samples. These results confirm that interaction between the Cu and the carboxylic acid end group leads to the formation of a Cu(II) carboxylate salt. Our findings contrast with a report of a Cu(I) pseudo-ester observed Cu vapor-deposited onto MUA/Au in UHV<sup>20</sup>. Cu(I) carboxylates are very unstable towards air and moisture<sup>60</sup> but may be stable in UHV.

### AFM characterization

The roughnesses of the evaporated Au/mica, MHA/Au/mica, 5 nm Cu/MHA/Au/mica and 5 nm Cu/MUA/Au/mica were examined using AFM. Representative AFM (0.5 μm x 0.5 μm) images are shown in Figures 7 and 8. Both images are top-view presentations with the lighter portions of the gray vertical scale corresponding to higher regions of the surface and the darker portions to lower regions of the surface. Figure 7 contains an AFM image of Au/mica. These substrates have a roughness factor of  $1.2 \pm 0.2$ , as determined electrochemically by oxidative desorption of iodine<sup>15</sup>, and have been shown using scanning tunnelling microscopy (STM), to be comprised of crystallites that have atomically flat terraces

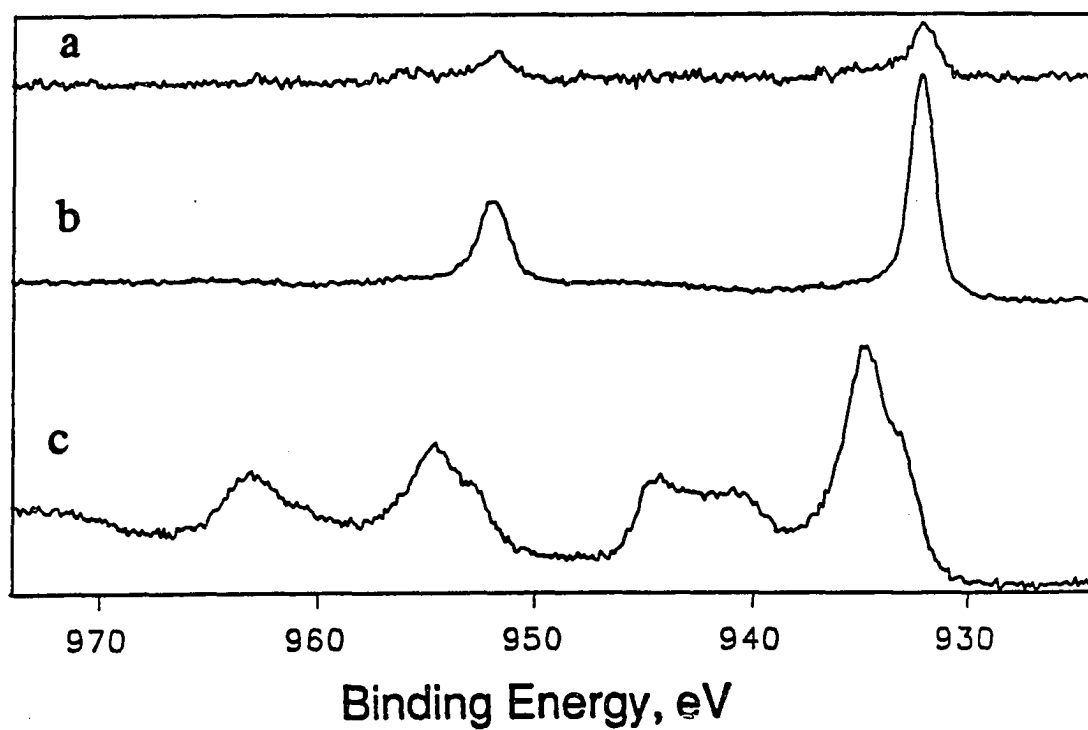


Figure 6. Cu ( $2p_{3/2}$ ,  $2p_{1/2}$ ) photoemission spectra for a 0.2 nm Cu overlayer. (a) Cu/HDT/Au/Si (b) Cu/Au (c) Cu/MHA/Au/Si. The data were not smoothed during or after acquisition; for each sample, the energy region was scanned several times over the course of a measurement to increase signal.

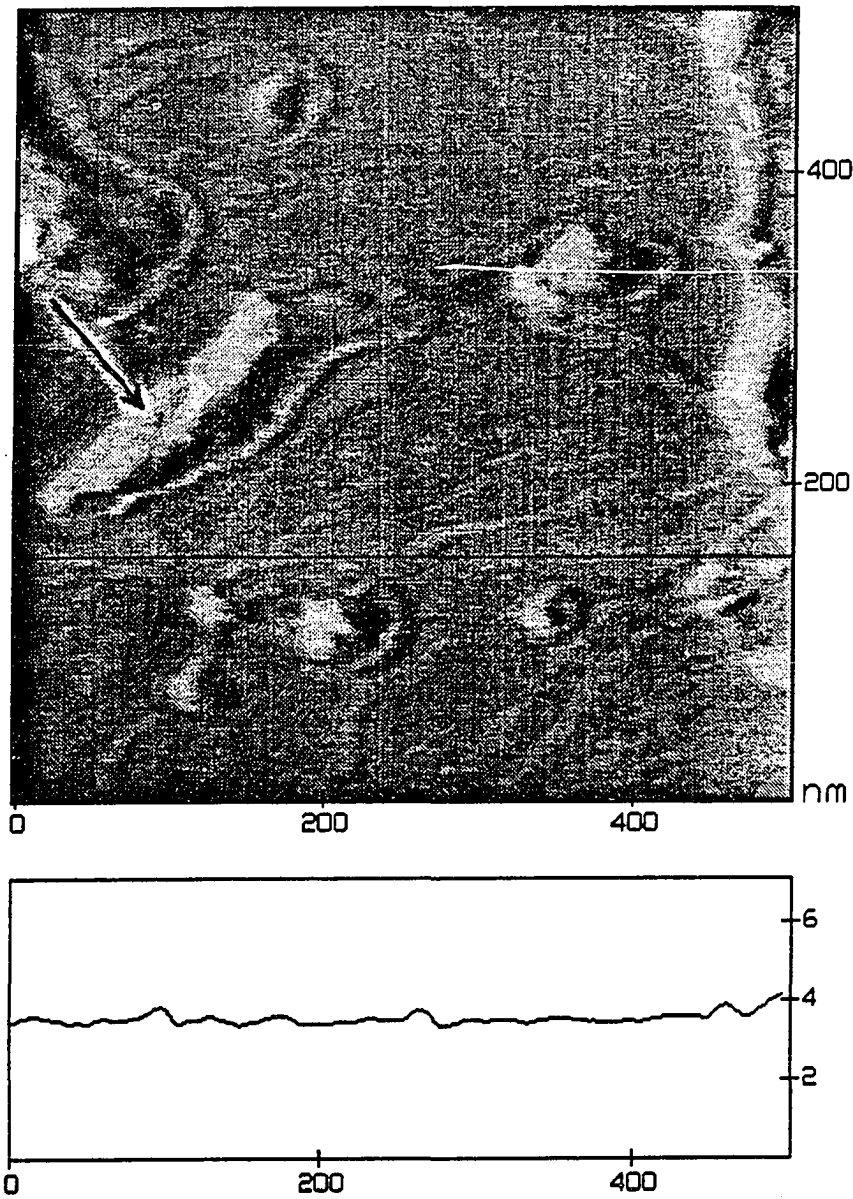


Figure 7. (a) A  $0.5\ \mu\text{m} \times 0.5\ \mu\text{m}$  lowpass filtered AFM image of uncoated Au/mica. The z-range is 5 nm. The arrow points to a grain boundary. (b) A cross-section of the image taken along the black line drawn in (a).

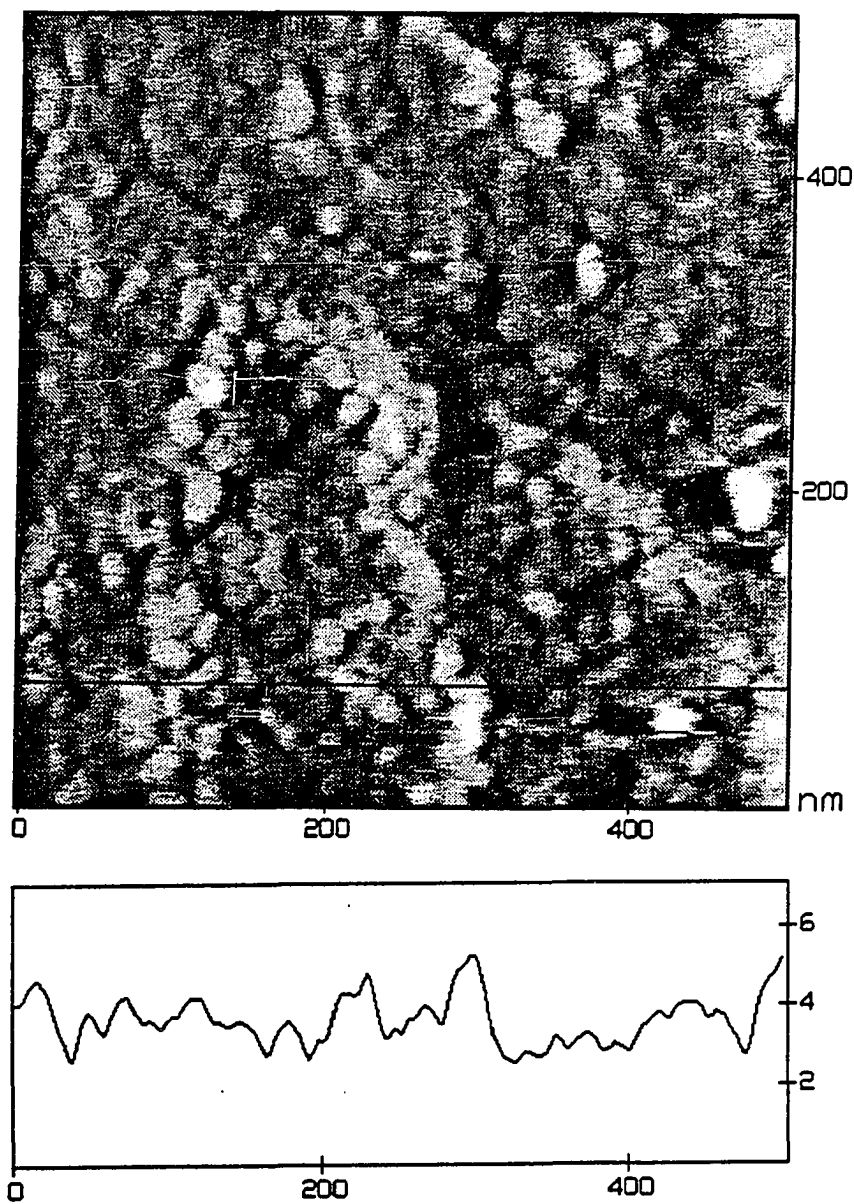


Figure 8. (a) A  $0.5 \mu\text{m} \times 0.5 \mu\text{m}$  lowpass filtered AFM image of Cu/MHA/Au/mica. The z-range is 5 nm. (b) A cross-section of the image taken along the black line drawn in (a).

separated by atomic steps of  $\sim 0.25$  nm<sup>11,14</sup>. The crystallites are several hundred nanometers in size and are separated by grain boundaries of varied width. The arrow in Figure 7A points to one such grain boundary. An accurate topographical assessment of the grain boundaries is limited because of possible interactions between the side of the AFM tip and the sides of the crystallites<sup>61</sup>. The apparent bright region at the left of the indicated grain boundary is most likely due to imaging hysteresis. A cross-section of the surface, as indicated by the line drawn across Figure 7A, is shown in Figure 7B and reveals the flatness of the surface. The topographies at this scale as revealed by AFM for the MHA/Au and MUA/Au are essentially the same as Au/mica.

After deposition of the  $\sim 5$  nm Cu overlayer at MHA/Au, a pronounced change in morphology is observed. Figure 8 shows an image for the  $\sim 5$  nm Cu/MHA/Au/mica. The cross-section in Figure 8B shows the increased roughness of the surface, with Cu crystallites of only  $\sim 20$  nm in size. The morphology of the Cu overlayer is similar to that of a thin (5 nm) Cu film evaporated onto gold-coated mica. This indicates that, although the initial structure of the Cu is chemically bound to the end group of the monolayer, the morphology of the overlayer is not notably different from that of Cu at mica.

## CONCLUSIONS

This section has shown that overlayers of Cu evaporated onto mercaptohexadecanoic and mercaptoundecanoic acid monolayers self-assembled at Au form as the corresponding Cu(II) carboxylate salt. The IRS data further confirm that a 5 nm film of Cu results in the full conversion of the end groups from the acid to the carboxylate. Images from AFM show that the deposited layer is morphologically similar to that of Cu deposited at mica, and reveal increased surface roughness caused by the formation of Cu crystallites on the order of ~20 nm in size. The similarity of the Cu film on the acid-terminated monolayers to that of Cu/mica indicates that the underlying carboxylate terminated monolayer does not influence Cu crystallite formation. Such a finding suggests that studies with these model systems may lead to greater understanding of the interfacial interaction between a metal overlayer and a modified gold surface.

The detection by IR of unreacted carbonyl and by XPS of small amounts of elemental Cu and/or Cu(I) reveals that much more than a monolayer-equivalent of Cu is required for quantitative conversion of the mercaptoacid monolayers to the carboxylate. The presence of an excess of both reactants suggests that the Cu deposits as islands of metal atoms on top of the monolayer, and/or that elemental Cu may be intercalated between the methylene chains. Both possibilities would lead to regions of unreacted Cu and of protonated  $\text{HO}_2\text{C}(\text{CH}_2)_n\text{S}/\text{Au}$ . Efforts to determine if this is a factor are underway using STM and AFM of overlayer films as a function of overlayer film thickness. Thus far, AFM results have only been used for comparisons of crystallite morphology. Studies of the effects of the composition (*e.g.* Ag or Au), thickness, and deposition rate of the overlayer of these and other (*e.g.*  $-\text{CH}_3$ ,  $-\text{CF}_3$ ,  $-\text{OH}$ ,  $-\text{CN}$ , and  $-\text{NH}_2$ ) end group functionalized thiolate monolayers will be used to evaluate the promotion of adhesion of a metal overlayer by organic monolayer films. Of particular interest

is the correlation of the chemical interactions between end group and metal overlayer and physical-mechanical properties such as those measured by peel tests.



## REFERENCES AND NOTES

- (1) Ulman, A. *An Introduction to Ultra-Thin Organic Films From Langmuir-Blodgett to Self-Assembly*; Academic: San Diego, 1991.
- (2) Whitesides, G. M.; Laibinis, P. E. *Langmuir* **1990**, *6*, 87-96 and references therein.
- (3) Widrig, C. A.; Chung, C.; Porter, M. D. *J. Electroanal. Chem.* **1991**, *310*, 335-59.
- (4) Bryant, M. A.; Pemberton, J. E. *J. Am. Chem. Soc.* **1991**, *113*, 8284-93.
- (5) Bain, C. D.; Biebuyck, H. A.; Whitesides, G. M. *Langmuir* **1989**, *5*, 723-7.
- (6) Porter, M. D.; Bright, T. B.; Allara, D. L.; Chidsey, C. E. D. *J. Am. Chem. Soc.* **1987**, *109*, 3559-68.
- (7) Nuzzo, R. G.; Dubois, L. H.; Allara, D. L. *J. Am. Chem. Soc.* **1990**, *112*, 558-69.
- (8) Laibinis, P. E.; Whitesides, G. M.; Allara, D. L.; Tao, Y.-T.; Parikh, A. N.; Nuzzo, R. G. *J. Am. Chem. Soc.* **1991**, *113*, 7152-7167.
- (9) Walczak, M. M.; Chung, C.; Stole, S. M.; Widrig, C. A.; Porter, M. D. *J. Am. Chem. Soc.* **1991**, *113*, 2370-2378.
- (10) Strong, L.; Whitesides, G. M. *Langmuir* **1988**, *4*, 546-58.
- (11) Widrig, C. A.; Alves, C. A.; Porter, M. D. *J. Am. Chem. Soc.* **1991**, *113*, 2805-10.
- (12) Alves, C. A.; Smith, E. L.; Porter, M. D. *J. Am. Chem. Soc.* **1992**, *114*, 1222-7.
- (13) Chidsey, C. E. D.; Liu, G.-Y.; Rowntree, P.; Scoles, G. *J. Chem. Phys.* **1989**, *91*, 4421-3.
- (14) Hallmark, V. M.; Chiang, S.; Rabolt, J. F.; Swalen, J. D.; Wilson, R. J. *Phys. Rev. Lett.* **1987**, *59*, 2879-82.
- (15) Walczak, M. M.; Alves, C. A.; Lamp, B. D.; Deinhammer, R. S.; Porter, M. D. Manuscript in preparation.

- (16) Nuzzo, R. G.; Allara, D. L. *J. Am. Chem. Soc.* **1983**, *105*, 4481-83.
- (17) Bain, C. D.; Troughton, E. B.; Tao, Y.-T.; Evall, J.; Whitesides, G. M.; Nuzzo, R. G. *J. Am. Chem. Soc.* **1989**, *111*, 321-35.
- (18) Li, T. T.-T.; Weaver, M. J. *J. Am. Chem. Soc.* **1984**, *106*, 6107-8.
- (19) Tarlov, M. J.; Bowden, E. F. *J. Am. Chem. Soc.* **1991**, *113*, 1847-9.
- (20) Czanderna, A. W.; King, D. E.; Spaulding, D. J. *Vac. Sci. Technol. A* **1991**, *9*, 2607-13.
- (21) Pale-Grosdemange, C.; Simon, E. S.; Prime, K. L.; Whitesides, G. M. *J. Am. Chem. Soc.* **1991**, *113*, 12-20.
- (22) Nakashima, N.; Taguchi, T.; Takada, Y.; Fujio, K.; Kunitake, M.; Osamu, M. *J. Chem. Soc., Chem. Comm.* **1991**, 232-3.
- (23) Rubinstein, I.; Steinberg, S.; Tor, Y.; Shanzar, A.; Sagiv, J. *Nature* **1988**, *332*, 426-29.
- (24) Mittal, K. L. *J. Vac. Sci. Technol. A* **1976**, *7*, 1-20.
- (25) Burkstrand, J. M. *Surf. Sci.* **1978**, *78*, 513-7.
- (26) Gerenser, L. J. *J. Vac. Sci. Technol. A* **1988**, *6*, 2897-2903.
- (27) Tompkins, H. G.; Allara, D. L. *J. Coll. Interface Science* **1974**, *49*, 410-21.
- (28) Smith, E. L.; Franek, J. E.; Porter, M. D. Manuscript in preparation.
- (29) *CRC Handbook of Chemistry and Physics*; 72nd. ed.; Lide, D. R., Ed.; CRC Press: Boca Raton, FL, 1991.
- (30) Stole, S. M.; Porter, M. D. *Appl. Spectrosc.* **1990**, *49*, 1418-20.
- (31) Sanders, J. V. In *Chemisorption and Reactions on Metallic Films*; J. R. Anderson, Ed.; Academic: London, 1971; Vol. 1; pp 1-39.

- (32) Chidsey, C. E. D.; Loiacono, D. N. *Langmuir* **1990**, *6*, 682-91.
- (33) Dubois, L. H.; Zegarski, B. R.; Nuzzo, R. G. *Langmuir* **1986**, *2*, 412-7.
- (34) Wu, C.-C.; Porter, M. D. Manuscript in preparation.
- (35) Snyder, R. G.; Hsu, S. L.; Krimm, S. *Spectrochim. Acta, Part A* **1978**, *34A*, 395-406.
- (36) Snyder, R. G.; Strauss, H. L.; Elliger, C. A. *J. Phys. Chem.* **1982**, *86*, 5145-50.
- (37) Josien, M.-L.; Lascombe, J.; Vignalou, C. *Compt. Rendu* **1960**, *250*, 4146-47.
- (38) Hayashi, S.; Umemura, J. *J. Chem. Phys.* **1975**, *63*, 1732-40.
- (39) Bellamy, L. J.; Pace, R. J. *Spectrochim. Acta* **1963**, *19*, 435-42.
- (40) Bellamy, L. J.; Lake, R. F.; Pace, R. J. *Spectrochim. Acta* **1963**, *19*, 443-9.
- (41) Bellamy, L. J. *The Infrared Spectra of Complex Molecules*; second ed.; Chapman and Hall: New York, 1980; Vol. II, Advances in Infrared Group Frequencies, pp 176-9 and references therein.
- (42) de Villepin, J.; Novak, A. *Spectrochim. Acta* **1977**, 1009-17.
- (43) de Villepin, J.; Novak, A. *Spectrochim. Acta* **1977**, 1019-24.
- (44) Allara, D. L. In *Vibrational Spectroscopies for Adsorbed Species*; A. T. Bell and M. L. Hair, Ed.; American Chemical Society: Washington, D.C., 1980; Vol. 137; pp 37-49.
- (45) Allara, D. L.; Nuzzo, R. G. *Langmuir* **1985**, *1*, 52-66.
- (46) Smith, E. L.; Porter, M. D. In preparation.
- (47) Parikh, A. N.; Allara, D. L. *J. Chem. Phys.* **1992**, *96*, 927-45.
- (48) Greenler, R. G. *J. Chem. Phys.* **1966**, *44*, 310-15.
- (49) Porter, M. D. *Anal. Chem.* **1988**, *60*, 1143A-50A.

- (50) Krause, P. F.; Katon, J. E.; Rogers, J. M.; Phillips, D. B. *Appl. Spectrosc.* **1977**, *31*, 110-5.
- (51) Teragni, P.; Masetti, G.; Zerbi, G. *Chem. Phys.* **1978**, *28*, 55-72.
- (52) We have attempted to estimate the extent of hydrogen-bonding for the MHA and MUA monolayers. The environment of the carbonyl modes does not greatly affect the extinction coefficient of  $\nu(\text{C=O})$  (Collings, A. J.; Morgan, K. J. *J. Chem. Soc.* **1963**, 3437-40) and we assume similar orientations and absorption cross-sections for both types of carboxylic acid. The relative areas of the absorbances of the features for the free and hydrogen-bonded components of the IR spectra can be calculated by fitting the peaks to a two-peak Lorentzian peak shape<sup>47</sup>. We estimate the proportion of hydrogen-bonded carbonyl groups to be about the same for the odd and even numbered MUA/Au and MHA/Au, about 75-80%, i.e. the majority of the carboxylic acid groups are hydrogen-bonded in a dimeric structure.
- (53) Nakamoto, K. In *Spectroscopy and Structure of Metal Chelate Compounds*; K. Nakamoto and P. J. McCarthy S.J., Ed.; Wiley: 1968; pp 268-275.
- (54) Fujita, J.; Martell, A. E.; Nakamoto, K. *J. Chem. Phys.* **1962**, *36*, 324-31.
- (55) Bellamy, L. J.; Branch, R. F. *J. Chem. Soc.* **1954**, 4491-9.
- (56) Tarlov, M. J. *Langmuir* **1992**, *8*, 80-9.
- (57) *Practical Surface Analysis by Auger and X-ray Photoelectron Spectroscopy*; Briggs, D.; Seah, M. P., Ed.; Wiley: Chichester, 1983.
- (58) We observe the  $\nu(\text{C=O})$  at  $\sim 1698 \text{ cm}^{-1}$  for this disordered hydrogen-bonded carbonyl, which compares with  $1704 \text{ cm}^{-1}$  reported for relatively disordered MUA self-assembled on polished gold foils (Duevel, R. V.; Corn, R. M. *Anal. Chem.* **1992**, *64*, 337-342).
- (59) Johnson, R.; Gardella, J.; Smith, E. L.; Walczak, M. M.; Porter, M. D. Manuscript in preparation.
- (60) Mounts, R. D.; Ogura, T.; Fernando, Q. *Inorg. Chem.* **1974**, *13*, 802-805.

- (61) Because of the pyramidal shape of the AFM tip, it does not provide as highly-resolved crystallite images as does the STM.

## GENERAL SUMMARY

A classic monolayer system is formed by the self-assembly of *n*-alkanoic acids at a variety of metal surfaces. A detailed, self-consistent reexamination by ellipsometry, contact angle and infrared spectroscopy of the self-assembly of  $\text{CH}_3(\text{CH}_2)_n\text{COOH}$  ( $n = 0 - 20$ ) at Cu, along with a detailed examination of the native oxide of Cu, including STM images, revealed that good quality monolayer films consisting of a Cu(II) carboxylate salt are formed. The discovery of gas-phase self-assembled multilayer films of *n*-alkanoic acids and perfluoroalkanoic acids at Cu and their characterization by ellipsometry, contact angle and infrared spectroscopy showed that such films have unusual wettability and crystallinity, and may provide novel interfacial properties. In future, self-assembly of analogous films of alkenoic acids, and their polymerization by ultraviolet irradiation, may provide a more complex system to model adhesion between polymers and metals. In Paper III, the gas phase was shown to be an ideal medium for self-assembly of *n*-alkanoic acids at Ag, resulting in monomolecular films of unusual crystallinity, demonstrating crystalline film formation down to 5  $\text{CH}_2$  units. The full assignment for the first time of the methylene IR wagging modes of *n*-alkyl monolayer films will advance the understanding of IR spectroscopy at surfaces.

In Paper IV, Cu overlayers were deposited at carboxylic acid-terminated *n*-alkanethiolate monolayers at Au to investigate the reactive chemistry of such overlayers; the reactive chemistry was found to be similar to the chemistry obtained for self-assembly of *n*-alkanoate monolayer formation at Cu films. IR reflection spectroscopy and XPS studies determined directly that the Cu-monolayer interaction yielded the Cu(II) salt. It was demonstrated by AFM that a deposited 5 nm film of Cu dictates the microscopic roughness of the surface. Studies of overlayers of other metals such as Ag, and overlayers at monolayers terminated by other functionalities such as alcohols, amines, or electroactive groups, are continuing. The design of such functional group terminated monolayers, and

their characterization, presents many challenging problems. For example, an epoxide-terminated monolayer must be formed *in-situ*, probably from an alkene-terminated monolayer, as it cannot be synthesized as an adsorbate precursor. The effects of such derivatizations on monolayer integrity must also be evaluated.

## ACKNOWLEDGEMENTS

I would like to thank members of the Porter group for many helpful discussions. I am very grateful to Dr. Cindra Widrig for teaching me how to make monolayers in a rigourously correct fashion. Thanks to my conscientious and careful co-authors: Carla Alves who did the AFM, Jim Anderegg the XPS, and Lorraine Siperko for discussions, for Paper IV. Kudos to Joe Franek who did the STM in Paper I. Also, thanks to Carla and John-Bruce Green for many helpful discussions of crystal faces. Thank you to Darwin Popenoe and lately Brian Lamp for keeping the IR spectrometer running well all the time. Thank you to Professor Marc D. Porter for intellectual leadership.

I must express my love and appreciation to my wife, Susannah, for helping me get this done.

This work was supported by IBM Systems Technology. The work was performed at Ames Laboratory. Ames Laboratory is operated for the U. S. Department of Energy by Iowa State University under contract no. W-7405-ENG-82. The United States government has assigned the DOE Report number IS-T-1134 to this dissertation.